The development of a time-resolved confocal microscope for single molecule detection of luminescent polymers

Frances Mc Auley

The Development of a Time-Resolved Confocal Microscope for Single Molecule Detection of Luminescent Polymers

By

Frances Mc Auley

A thesis submitted to the Faculty of Science, The University of Durham, for the degree of Master of Science

Organic Electroactive Materials Group
Department of Physics
University of Durham
January 2007

Abstract

This report details the construction and testing of a confocal microscope for use in single molecule fluorescence spectroscopy. With the prospect of making time-resolved lifetime and spectral measurements of π-conjugated polymers in the condensed phase, the system employs a pulsed 390nm, 65ps diode laser along with compact electronics for time-correlated single photon counting. Following optimisation the microscope records continuous photon arrival times with 100ps resolution, and fluorescence lifetime decays with 40ps resolution.

Isolation of polymer chains has been investigated as a function of dilution by the dispersion of poly[9,9di(ethylhexyl)fluorene] (PF2/6) in a variety of host matrices. Films have been prepared by spin coating from toluene and the emission spectra, confocal lifetime and anisotropy have been investigated. Whilst the choice of host does not show any considerable influence on the spectral characteristics of the luminescent polymer, concentration and spin speed were observed to significantly influence the photophysical properties of the film. Spectral blue shifts in the emission band have been observed as the dilution of the luminescent polymer increases, reaching a maximum shift of 20nm in the most dilute samples. In line with the spectral shift, lifetime measurements show that the fluorescence decay becomes increasingly mono-exponential with dilution. In films exhibiting the maximum spectral blue shift, mono-exponential fluorescence decay was observed, for the oligomer oligo[9,9di(ethylhexyl)fluorene]$_{N=20}$ (OF2/6) in zeonex the lifetime is found to be $\tau = 0.92$ns. The dilution at which this occurs varies from 1×10^{-4} % w/w to 1×10^{-6} % w/w depending on spin speed and host matrix. Significantly longer that the lifetime of OF2/6 in solution, this is thought to be very close to the natural radiative lifetime of the polymer and is taken as a clear indication of chain isolation within the host matrix. Spectral blue shift and progression to mono-exponential fluorescence decay are explained in terms of the decline of low

energy aggregate states and a reduction in non-radiative interchain energy transfer due to increased interchain separation.

Confocal imaging using the specimen scanning technique has been developed using an electronically controlled x-y piezo-stage. By optimising the optical set up the confocal image resolution is currently 0.369nm. The maximum theoretical confocal resolution at 390nm excitation is 0.268nm; the cause of this loss in resolution is thought to originate from slight non-uniformity in the excitation source.

Declaration

The material in this thesis has not been submitted for any other degree or part thereof, at Durham University or any other institution. The material in this thesis is the work of the author except where formally acknowledged by reference.

Acknowledgements

My thanks go to everyone in the OEM group, they have always been ready to help and offer advice; I have very much enjoyed the time I have spent here not least thanks to their good humour and encouragement. My thanks especially go to Andy Monkman who secured the funding that allowed me to do this MSc., not only am I extremely grateful for the opportunity he has given me but also for his support and encouragement throughout the past year. To Lars also, whose help and humour has been invaluable. Those in my office, Helen, my thanks for her wisdom and patience in answering countless questions, to Simon, Carsten Suzi and Chiang, Chien-Jung who have given me many helpful suggestions and practical advice.

Many thanks to Christine Richardson in the biology department for the use of the microtome, for the time and helpful advice she has given to me. Also to Del Atkinson for the use of the optical microscope which was a great help during the final stages of calibrating my experiment.

Thank you to Paul and those in the mechanical workshop who have built and adjusted various experimental pieces and of course to Norman, who has helped me on many occasions.

Finally I thank my family who have always been supportive of everything I do, I am very grateful.

Table of Contents

Table of Figures

Chapter 2-Conjugated Polymers

Chapter 3-Sample Preparation

Chapter 4-Single Molecule Spectroscopic Methods

Chapter 5-Confocal Microscopy

Chapter 6-Time-Domain Lifetime Measurements

Chapter 7-Scanning Imaging

1. Introduction

Scientific research towards the prospect of manipulating and observing matter on an atomic and molecular scale has gathered increasing momentum since its conception by Richard Feynman in the mid twentieth century. Single-molecule observation provides a unique way to characterise molecular dynamics with sensitivity rendered inaccessible by the averaging process inherent in traditional ensemble measurements. It allows the study of exact parameter distributions, an invaluable capability in heterogeneous systems such as crystals, glasses and polymers.

Significant advances to this goal involve the class of scanning probe microscopies, of which scanning tunnelling and atomic force microscopy are the most well known. These highly successful approaches use nanometre scale interactions, bringing a probe tip into close contact with the molecule in order to detect its presence through tunnel currents or deflections in the tip height as the tip is scanned across the relatively flat surface to which the molecule is attached. Optical spectroscopy, on the other hand, offers the advantage of more passive experimentation. This non intrusive method probes single quantum systems leaving them relatively undisturbed in comparison to the intimate nature of scanning probe techniques, though this is often at the cost of spatial resolution. The investigation described here focuses on the optical probing of π-conjugated polymers in the condensed phase, a regime which presents significant challenges as well as exciting opportunities for discovery.

Optical spectroscopy non-invasively monitors molecular environment and conformation through changes in electronic structure. At cryogenic temperatures, spectroscopic studies of the evolution of single molecules under the influence of different external parameters allow precise tests of molecular quantum electrodynamics and microscopic coupling theories. At higher temperatures, they give access to the temporal evolution of different nanodomains of bulk materials in which

single molecules are embedded as reporters of their local environment. Whilst, in biological processes, the development of reliable and versatile fluorescent labelling techniques has made the study of the conformational dynamics of molecular events involving RNA, enzymes and motor proteins accessible to single molecule observation. This diversity of applications has lead to huge developments in the field of single molecule spectroscopy (SMS) which has grown considerably over the past decade from a specialist variety of optical spectroscopy into a versatile technique pervading an ever increasing number of research areas.

Single molecule optical spectroscopy is inevitably complicated by the limitations imposed by diffraction effects and the difficulty of detecting a single entity amongst the interference of background noise. Nonetheless, it does have the potential to open up a wealth of new information into the interactions of single molecules, allowing the detection of rare events that would otherwise be buried under the averaging process of conventional spectroscopic experiments. In practice the results of many single molecules are reported by the construction of a frequency histogram giving the distribution of actual values of an experimental parameter rather than a mean, which, many will agree, is a valuable advantage.

Today, there are several broad groups which define single molecule spectroscopy. They differ in sampling conditions and in the method of excitation; however all share the common need to isolate single molecules for detection. This can involve using low temperature solids to isolate molecules spectroscopically, though more commonly, molecules are spatially isolated by using very dilute samples dispersed in a host matrix. Initial SMS experiments were performed using the low temperature absorption technique and began in 1989 with the detection of a weak absorption signal from pentacene embedded in a host crystal by Moerner and Kador [1]. More recently flow cyclometry has been employed to observe single molecules in solution whilst methods such as

near field scanning optical microscopy, wide-field epi-illumination and far field confocal microscopy have become increasingly popular for solid samples[2].

1.1 Confocal Microscopy

Confocal microscopy has evolved to be one of the most widely used techniques in optical microscopy since the principle was proposed and patented in the late nineteen-fifties. Amongst others, one of the reasons for its tremendous popularity is the relative ease with which extremely high quality images can be produced using specimens prepared for conventional fluorescence microscopy. Characterised by reduced or entirely suppressed background emission from unwanted fluorescence, confocal microscopy has far superior depth discrimination and signal to noise separation than wide field techniques, which suffer significant image degradation from out of focus luminescence.

Unfortunately, the initial development of confocal microscopy was hampered for many years by the lack of high intensity light sources required for imaging, and, by the absence of the sophisticated computer processing required to handle the large amounts of information that confocal systems produce. Consequently the first commercial instruments did not appear until 1987. Despite a slow start, as the twentieth century drew to a close there was a culmination of technological advances: increasing improvements in laser power and stability, the development of high throughput fibre optics, better thin film dielectric coatings and more sensitive detectors, coupled with vastly improved computer processing resources. This revolutionised the capabilities of confocal microscopy and it experienced an explosion in terms of efficiency, accuracy and potential application.

Today, modern confocal microscopes function as entirely integrated electronic systems, with the most advanced configurations coupling numerous detectors to a computer which stores data and displays real time observation of the subject. Several laser excitation sources are often employed with wavelength selection devices and the ability to scan either via the excitation beam or through sample scanning.

Confocal SMS has emerged as an invaluable tool for probing highly heterogeneous semi-conducting nanomaterials of which conjugated polymers form an important group. With the prospect of investigating their interesting photophysical properties this report details the first steps of building and testing a confocal microscope. Methods of isolating polymer chains to produce single molecule films have also been explored and tested using a variety of optical techniques both in ensembles and at a single molecule level. The prototype microscope is based on a single excitation source and detection channel and is designed to provide scanning imaging, lifetime measurements and spectral information. In its current state, the experiment is in fact ready to accept multiple detection channels proposed to study polarisation effects; furthermore wide-field imaging has also been carried out successfully using a cooled CCD camera. The experiment is designed to be an adaptable multi-faceted tool, where by small modifications to the emission or excitation path, different photo-physical parameters may be measured. At this stage the main focus of work has however been directed to optimising the imaging and lifetime capabilities of the microscope, through which it will be possible to confidently assess weather or not the system is running with single molecule detection accuracy. It is hoped that following the work described here, future efforts will be made to expand on and complete the initial steps already made regarding spectral measurements, wide-field images and fluorescence polarisation.

1.2 References

1. Kador, L., D.E. Horne, and W.E. Moerner, *Optical-Detection and Probing of Single Dopant Molecules of Pentacene in a P-Terphenyl Host Crystal by Means of Absorption-Spectroscopy.* Journal of Physical Chemistry, 1990. **94**(4): p. 1237-1248.
2. Bohmer, M. and J. Enderlein, *Fluorescence spectroscopy of single molecules under ambient conditions: Methodology and technology.* Chemphyschem, 2003. **4**(8): p. 793-808.

2. Conjugated Polymers

2.1 Introduction

Polymers have been present in naturally occurring materials such as silk and wood for hundreds of thousands of years. They form a group known as macromolecules, and have a unique chain-like structure made from many small interlinked elements that sets them apart from other materials. In the late 19th century, scientists began to investigate the complex chemical make up of polymers and before long synthetic polymers started to emerge, made by applying small adaptations to naturally occurring materials. The biopolymer cellulose which is found in almost pure form in cotton fibre was one of the first to be modified in this way; being treated with nitric acid to make celluloid, one of the earliest plastic materials.

In the ensuing years great progress was made in synthetic polymer science marking the beginning of a cultural and commercial revolution that would produce a vast array of these flexible, insulating materials. Even with these already dramatic advancements, a further breakthrough was made in the early 1960s when it was discovered that far from being exclusively insulators, some polymers had unique electronic properties. Extensive research into these unusual materials was enthusiastically undertaken in the years that followed and in the 1980s the class of π-conjugated polymers was defined; a new and distinctive group of polymeric materials that would generate unprecedented scientific and commercial interest.

Conjugated polymers have distinctive semi-conducting properties and can be manipulated through doping to have conductivities that rival many metals. With such promising characteristics π-conjugated polymers became the focus of intense scientific interest almost overnight. Not only

were they known to be relatively cheap but they were seen as a new futuristic material with a multitude of potential applications such as field effect transistors, photodiodes, even stealth technology.

Today, conjugated polymers are widely used as active materials in a broad range of electronic devices including organic light emitting diodes (OLEDs) for flat panel display applications, photovoltaic devices, thin film transistors and chemical sensors. Of these, π-conjugated polymer materials have emerged as a major research interest in the field of LEDs. Not only are polymer materials lightweight and flexible but their unique properties mean that they can be electro-optically excited and individually tailored to fluoresce at almost any specific visible wavelength. These characteristics have made polymer LEDs widely regarded as the future of display technology, they have the potential to offer unprecedented colour resolution, and have all the signs of becoming a cheaper, thinner and more efficient replacement to current liquid crystal displays.

2.2 The Physics of Conjugated Polymers

Conjugated polymers derive their semi-conducting properties through delocalized π-electron bonding along the polymer chain, typically formed by a backbone of overlapping orbitals, such as the continuous path of overlapping *p*-orbitals formed by alternating single and double carbon-carbon bonds.

The bonding properties of carbon define the stability of organic polymers. As a group IV element, carbon has four valence electrons, two in the *2s*-orbital and two in the *2p*-orbital. These hybridise to form either *sp*, sp^2 or sp^3 configurations; a bonding mechanism described by molecular orbital theory as linear combinations of atomic orbitals[3].

The three principle hybridisations depend on the number of *p*-orbitals involved. The most common configuration, sp^3 is the saturated carbon sp^3 hybrid which combines the *s*-state with each of the three p_x, p_y and p_z orbitals to produce strong sigma bonds between neighbouring atoms. The resulting four hybrid orbitals form a rigid tetrahedral geometry centred on the carbon nucleus and can be seen in figure 1[2]. Sigma bonded (sp^3) polymers are non-conjugated and exhibit large energy band gaps rendering them electrically insulating and non-absorbing to visible light. In polyethylene for example, which consists of a monomeric repeat unit defined by – (CH_2 – CH_2) –, the energy band gap is 8eV.

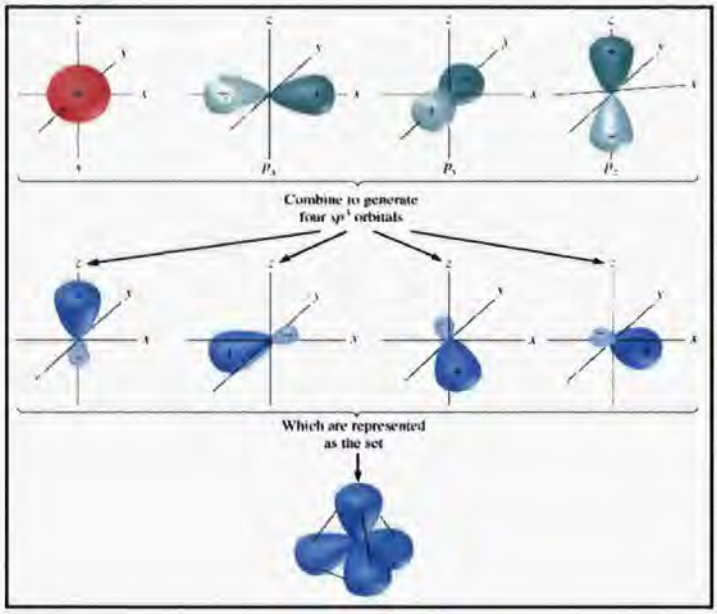

Figure 1: Hybridisation of *s* and *p*-orbital to produce the sp^3 configuration. The *s*-orbital combines with each of the three *p*-orbitals to produce a tetrahedral geometry centred on the carbon nucleus.[2]

In conjugated polymers, hybridisation in the sp^2 configuration is adopted. Here the *s*-orbital hybridises with only two of the *p*-orbitals which as in the sp^3 configuration create strong sigma bonds between neighbouring atoms. These σ-bonds effectively form the backbone of the polymer chain, whilst symmetrical combinations of adjacent unpaired electrons in the remaining *p*-orbital form bonding or anti-bonding π or π* states. Delocalisation is illustrated for the case of ethylene in figure 2. The loss of two hydrogen atoms from ethylene facilitates the formation double bonds and polymerisation into the conjugated polyacetylene – (CH=CH) – the first π-conjugated polymer to be discovered[4]. Continuous networks of adjacent unsaturated carbon atoms create sequences of *p*-orbitals which tend to exhibit π-overlap between nearest neighbours. Realistically

this continuity is limited by structural defects and twist in the chain, though it nonetheless leads to the formation of delocalised π-states along the polymer group[5, 6].

The essential property of the π-electron system that differentiates a typical conjugated polymer from a conventional polymer with σ-bands lies in the electronic band gap. Whilst large energy gaps between σ-σ^* states makes them accessible only through high energy interaction, electronic interactions between the π-π^* orbitals are typically in the range of 1-4eV leading to semiconductor behaviour and low-energy electronic excitations in the UV-visible range.

The nature of charge carrying species in conjugated polymers has been the subject of extensive review in the decades since their discovery. As quasi one-dimensional systems, is now thought that the charge carrying species they produce are unusual in comparison with other materials. Far from the model of free electrons or holes it is now commonly accepted that the charged species of conjugated polymers consist of several types of well defined quasi-particles each made up of a coupled charge-lattice deformation; a model initially proposed by Bassler et al.[7] Although complex, the dynamics of excited state species can be broadly described in terms of intrachain and interchain interactions which respectively account for the microscopic and macroscopic conductivities of conjugated polymer materials. Prompted by local disorder, intrachain interactions account for the majority of charge migration, whilst interchain charge hopping is much less probable. Unravelling the intricate heterogeneous kinetics of these species is a notoriously difficult task, though even from a fundamental point of view, the understanding of excited state species and charge transfer mechanisms is a key requirement to understanding the optical properties of conjugated systems. Detailed investigations to this end can be found throughout literature[8-11] though it is not the focus of this report. The following paragraphs will give a description of the relevant photophysical phenomena and processes involved in photo-excitation spectroscopy.

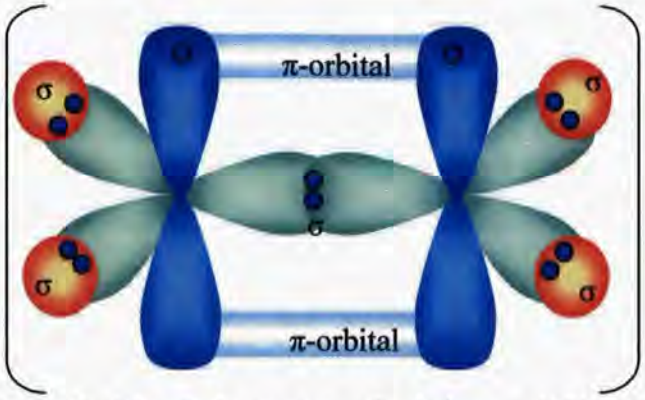

Figure 2: Chemical structure of ethylene – (CH_2=CH_2) – Carbon-Hydrogen bonds are formed by overlap of the C atom sp^2 hybrid orbitals with H atom 1s orbitals. The σ-bond between C atoms arises from overlap of sp^2 orbitals. Carbon-carbon π-bond is formed by overlap of un-hybridised *2p* orbitals from each atom.

2.3 Photophysics

2.3.1 Optical Properties of Conjugated Polymers

Spectroscopic investigation into the associated phenomena of absorption and emission are well established as a method of probing structure on a microscopic scale and provide the backbone of research into conjugated polymers. In conjugated polymers, excitation of delocalised electrons between the π and π* bands can be stimulated either electrically, or optically using light in the UV / visible region. The effect is to produce an exciton which decays over time back to the ground state releasing energy either radiatively via luminescence, or non-radiatively via heat or molecular vibrations. Here, the physical processes behind absorption and both radiative and non-radiative decay will be described in order to give a background for the phenomena observed within this investigation.

2.3.2 Molecular Energy Levels

Molecular energy levels are quantized into discrete levels of electronic, vibrational and rotational energy. Each electronic energy level has a number of associated vibronics, whose frequency and amplitude are governed by the mass of the atoms and the strength of the chemical bonds between them. The diatomic model describes these vibrational states as bound by the potential energy characteristics of the electronic energy level, as can be seen in figure 3. Following a Morse potential, molecules experience a sharp rise in potential as the internuclear separation becomes small, whilst at large separations nuclei escape their attractive potential and disassociate.

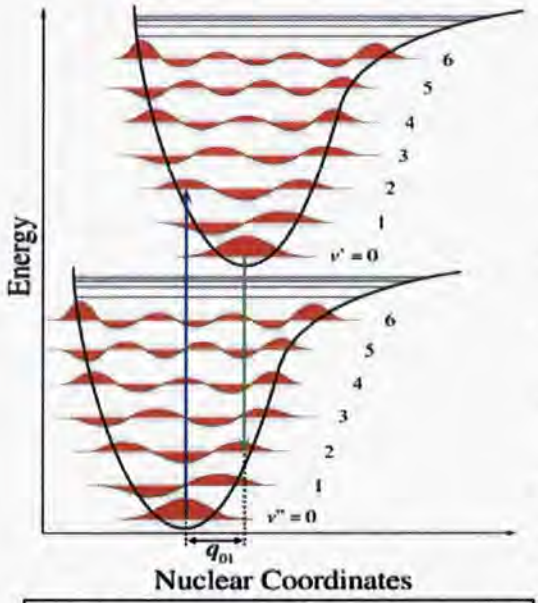

Figure 3: Molecular potential curve for a typical fluorophore. The distribution of occupied vibrational and rotational states is described by the Boltzmann distribution. Electronic potential increases sharply as inter-nuclear separation decreases.[1]

The equilibrium separation in the excited state is greater than the ground state and as a result, excitation from S_0 to S_1 has the greatest probability not between the lowest vibronics but the between vibronic levels with similar equilibrium separations. This phenomenon is described by the Frank-Condon Principle which defines that because excitation occurs faster than the nuclear vibration, the transition occurs without adjustment of the nuclei[12], explaining the vertical transition in figure 3.

Once in the excited state, the molecule decays on a sub-picosecond timescale to the lowest energy level of the excited state, releasing the excess energy as heat to the surrounding molecules, a process known as internal conversion. The molecule may then decay non-radiatively back to the S_0 state or alternatively, radiative emission

may bring the molecule down vertically to a vibrationally excited sub-level of the ground state, where it undergoes further internal conversion to the final low energy configuration[13].

A consequence of the Frank-Condon Principle is that the wavelength of emission is always longer than the wavelength of absorption due to the non-radiative internal conversion process[12]. This energy loss through non-radiative relaxation whilst in the excited state is measured by the Stokes shift which is characterised by the energy difference between the absorption edge and the onset of fluorescence. It is an important physical effect which allows separation of the excitation and emission radiation in many photophysical experiments and not least in the confocal set-up.

The energy spacing and symmetry of the available energy states determine the characteristics of the molecule, with the transitions between different vibrational levels producing characteristic peaks in the absorption and emission spectra known as the vibronic fine structure. At high temperature this vibronic fine structure is homogeneously broadened such that the absorption and emission spectra appear as broad energy bands rather than a series of discrete vibronic peaks. Homogeneous broadening is reduced at low temperature; as the molecule cools the thermal population of upper vibronics reduces causing a narrowing of the absorption line and increased resolution in the emission spectrum. This effect is noticeable in figure 10 chapter 3.4 which compares the emission of a film of oligofluorene 2/6 dispersed in a PMMA matrix both at room temperature and at 77K; inhomogeneous broadening caused by the host at room temperature is evident and the emission intensity at 77K is significantly increased due to a reduction in non-radiative decay.

2.3.3 Absorption

Absorption in polymers often occurs not simply at a specific wavelength but over a broad range of energies corresponding to the vibrational and rotational fine structure of the molecule. As a result, rather than specifying a single absorption probability it is more informative to integrate the range of absorption probabilities over the region where absorption occurs. This integrated absorption probability is called the oscillator strength, *f*:

$$f = \left(\frac{4m_e c\varepsilon_o}{N_A e^2} \right) A \qquad \text{Equation 1}$$

Where:

m_e: *mass of the electron*

c: speed of light

e: charge on the electron

A: integrated area of the absorption peak

N_A: *is Avogadro's constant*

ε_o: *permittivity of free space.*

The oscillator strength is governed by quantum mechanical selection rules for symmetry, parity momentum and spin; it has a maximum value of 1 per electron, which corresponds to strong absorption and a minimum value of 0 whereby transition is forbidden.

When an incident photon is absorbed, the energy state of the molecule is increased by exactly the energy of the photon by means of annihilation in a dipole-dipole interaction mechanism[14]. For visible light, the energy of a photon (equation 2) is of the order of $3\times10^{-19} \le E \le 5\times10^{-19} J$

which is sufficient to stimulate the π - π^* transition in a typical fluorescent polymer making them particularly accessible to optical spectroscopy.

$$E = hv = \frac{hc}{\lambda} \qquad \text{Equation 2}$$

Where:

h: Planck's constant

v: frequency

In absorbing media, the fractional transmission of light through the material can be described by the Beer-Lambert law, so that for a substance of concentration C and an excitation intensity I_0 the emerging intensity, I, is

$$I = I_o \exp\left(-\frac{\sigma N_A C l}{1\times10^3}\right) \qquad \text{Equation 3}$$

The molecular absorption cross section, σ, represents the probability per unit time of absorption of a fluorophore for a photon flux of unity. It is strongly dependant on the type of molecule and wavelength of excitation and is a useful replacement for the molar absorption coefficient, ε, when specification of the concentration of chromophores is difficult or inappropriate to define.

2.3.4 Emission

Once the excited molecule has undergone internal conversion to the lowest lying level of the excited state it can emit a photon to dissipate its excess energy. The probability of emission is dependant on the type of molecule and is generally different from but closely related to the absorption probability. The molecule can in principle use photon emission to decay to any sub-

level within the ground state providing that selection rules are obeyed and that the transition is vertical (figure 3). Each possible transition has an associated energy corresponding to the band gap, and so the emission spectrum is not simply made up of light at one wavelength but is homogeneously broadened by the discrete subset of wavelengths corresponding to the rotational fine-structure of the molecule. Thermal effects then cause further inhomogeneous broadening of these closely spaced bands making them overlap, and a broad single emission peak is observed.

The possible relaxation pathways for an excited fluorescent molecule are summarised in figure 4. Internal conversion dominates rotational and vibrational relaxation within the excited state, fluorescence is described above. Phosphorescence is another form of radiative decay but with a reduced probability. It occurs when the exciton undergoes intersystem crossing from the singlet to the triplet state, and requires a flip in spin before decaying to the singlet ground state[15]. The other possibilities are bleaching and long range energy transfer, which are described in more detail in the following paragraphs.

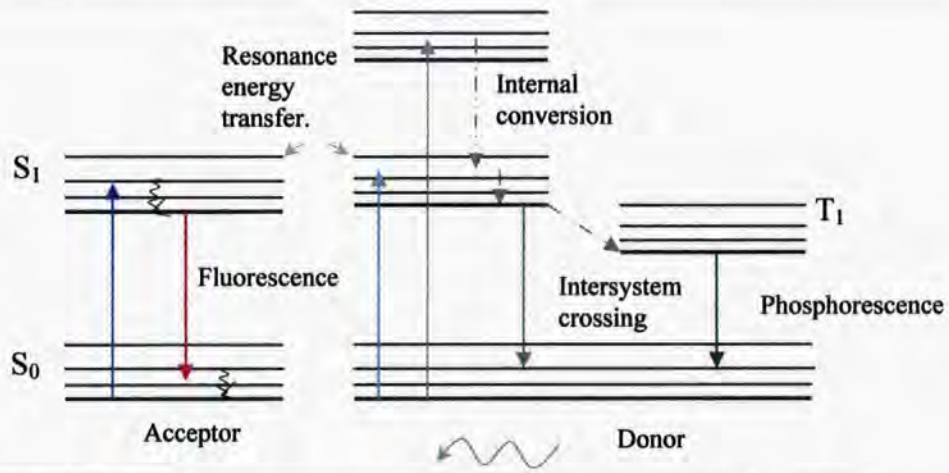

Figure 4: *Relaxation pathways in a fluorescent molecule.* Relaxation is usually achieved through a combination of radiative and non-radiative pathways. Fluorescence is the most common radiative decay, which typically follows internal conversion from an excited vibrational sublevel in the excited state. Phosphorescence also has a finite probability dependant on a flip in electron spin prior to photon emission. Förster energy transfer can occur between neighbouring molecules through a dipole-dipole interaction, alternatively the molecule can photobleach in which case its fluorescent properties are destroyed.

2.4 Energy Transfer and Quenching

Although conjugated polymers have significant advantages over many inorganic materials, one of their principle shortcomings is a large degree of energetic and positional disorder caused by entanglement of extended polymer chains and the presence of structural defects. Such disorder results in the formation of potential minima in the energy profile leading to strongly dispersive charge carrier motion and exciton diffusion. It has been shown[16] that the creation of photo-excitons in conjugated polymers is frequently followed by incoherent migration processes between localized sites along the conjugated chain segments. Excitons formed in the high-energy region of the density of states undergo rapid diffusion towards longer chain segments until the absence of lower energy chain segments leads to localisation. At low temperatures it is believed that this type of exciton migration is suppressed by site selective excitation, producing low-mobility excitons by exciting the low-energy tail of the inhomogeneous distribution of states.

Although this investigation does not propose to study energy transfer and quenching mechanisms specifically, observation of these phenomena does provide useful insight into solvent and concentration effects for the purposes of sample preparation. Here an account will be given of quenching and energy transfer processes so that they may be used as indicators to changes molecular environment.

2.4.1 Förster Transfer

The theory of resonance energy transfer was developed by Professor Theodor Förster, at the Max Planck Institute for Physical Chemistry in Göttingen. Otherwise known as Fluorescence Resonance Energy Transfer (FRET), Förster transfer describes the non-radiative transfer of excitation energy from the excited molecule to a nearby acceptor molecule. The energy transfer

between donor and acceptor molecules is the result of long-range dipole-dipole-interactions and occurs with an efficiency defined by their spatial separation[17]. The distance at which RET is 50% efficient is called the Förster distance. The expression for the Förster distance consists of a number of physical constants, which can be reduced down to equation 4, taking wavelength in nanometers and giving the Förster distance in angstroms[12]:

$$R_0 = 0.211\left(\kappa^2 n^{-4} Q_D J(\lambda)\right)^{1/6} \qquad \text{Equation 4}$$

Förster Distance (Å)

Where:

$J(\lambda)$: the overlap integral, this expresses the degree of spectral overlap between the donor emission and the acceptor absorption.

κ^2: describes the relative spatial orientation of the donor and acceptor transition dipoles, the typical value is assumed to be $\frac{2}{3}$

Q_D: the quantum yield of the donor in the absence of the acceptor.

n: the refractive index of the medium.

Once R_0 is known the rate of energy transfer can be calculated using:

$$R_0 = \left(\tau_D \kappa_T(r)\right)^{1/6} r \qquad \text{Equation 5}$$

Where:

τ_D is the lifetime of the donor in the absence of energy transfer.

Within the point-dipole approximation the rate of energy transfer κ_T, between the donor and acceptor molecules is inversely proportional to the sixth power of the donor-acceptor separation, r, making the observation of energy transfer a useful tool for studying proximity. Förster transfer

depends on the spectral overlap of the donor emission and the guest absorption reflecting the necessity of energetic resonance during transfer. Investigations into FRET show that the Förster distance is typically in the range of 40 to 70 Å[18]

2.4.2 Electron Exchange and Dexter Transfer

If the interchain separation between donor and acceptor is small enough to cause overlapping of orbitals, resonance is no longer required to facilitate energy transfer. This only occurs over very short distances of between 10-15Å and effectively makes it possible for electrons to exchange taking either excitation energy or spin with them[19].

2.4.3 Exciton Migration

Exciton migration is a spatial phenomenon that involves sequential movement of the exciton between neighbouring sites. This is in contrast to energy transfer which refers to a donor-acceptor system. Exciton migration consists in a hopping between sites of either the triplet or singlet exciton, though in conjugated polymers the singlet case is more dominant. Exitons migrate to neighbouring sites of lower energy until the final low energy configuration is reached. The rate of exciton migration is dependant on the distribution of sites and most importantly on the energy difference between them. The most commonly accepted description of the rate of exciton migration is defined by Richert[20] et al using an exponential dependence of the energy difference which does not allow for uphill migration.

2.4.4 Quenching and Temperature Effects

Quenching is a general description for any process that reduces the emission intensity of luminescence. In any form, quenching is most commonly associated with molecular contact between the fluorophore and the quencher and so is largely governed by diffusion[21], making quenching a useful indicator of isolation in dilute polymer films where it is expected that large intermolecular separations will significantly reduce diffusion mechanisms.

Quenching can result from fluorophore interaction with a wide variety of substances. One of the most significant of these is oxygen, which quenches almost all known fluorophores. Photo-oxidation can be reduced through using vacuum storage and/or by sealing samples in an inert host matrix to reduce the amount of oxygen they are exposed to giving increased emission longevity. Temperature effects also strongly influence quenching, at low temperature the reduced mobility of excitons and quenchers inhibits diffusion; furthermore, the number of thermal and vibrational phonons is reduced resulting in fewer non-radiative losses and greater radiative decay. Low temperature also enhances vibrational resolution in the emission spectrum. Due to the energy dependence of relaxation, high energy excitons have a larger probability to relax through energy transfer than low energy excitons, hence at low temperature there is usually significant spectral narrowing of the energy distribution[22].

Though quenching is most commonly observed during ensemble measurements it is also an important phenomenon in single molecule spectroscopy. In single-molecule fluorescence, two important quantities must be maximised, namely the rate of fluorescence and the number of photons that a molecule can emit on average. In the case of organic molecules, triplet bottlenecks, a term that describes the situation where excitons become trapped in 'dark' states, such as the triplet state, result in significant reduction of the emission rate. This should be taken into careful

consideration when selecting materials for single molecule spectroscopy; efficient fluorophores have low rates of intersystem crossing or short dark state lifetimes, which reduces the trapping probability and makes them the most simple to detect.

Concerning photo-destruction, at room temperature, exciton interaction with defect states limits the total amount of fluorescence to approximately 10^6 photons per molecule[23]. At cryogenic temperatures however, as mentioned above, the photodecomposition channels that result in quenching are often suppressed, and small reactive molecules such as oxygen or water cannot diffuse. In this case, the amount of fluorescence is only limited by sudden conformational changes of the host-guest system, which shift the absorption line of the molecule away from resonance with the laser, and so at low temperature, significantly increased luminescence is observed.

2.4.5 Bleaching

Photo-degradation is a major problem in confocal microscopy. Bleaching is an irreversible photochemical reaction that modifies the fluorophore so that it no longer fluoresces[24]. It is thought to be associated to the excited triplet state which populates via intersystem crossing from the singlet excited state. Although the probability of intersystem crossing is typically quite small, because the transition to the ground state from the triplet state requires the electron to change spin, the triplet lifetime is considerably longer than the singlet lifetime and has been observed by Romanovskii et al. to be as long as a second[25]. Once the exciton is in the triplet state therefore, the fluorophore becomes particularly prone to bleaching effects. Whilst the probability of intersystem crossing varies from fluorophore to fluorophore, the intense fluorophore specific nature of confocal excitation means that this process often occurs within seconds of excitation as the fluorophore constantly cycles between absorption and emission. Although bleaching is not

entirely understood it has been frequently associated with the interaction of the polymer with ultraviolet radiation and singlet oxygen, if the specimen permits the use of protective agents such as propyl gallate, hydroquinone etc..[26] or special products which act as anti-oxidants or triplet quenchers can reduce the problem of bleaching. Failing this sealing the polymer in a host matrix and taking precautions such as vacuum storage will also help to slow the bleaching process.

2.5 References

1. http://www.raunvis.hi.is/~agust/ee3morsef.htm, *Morse Potential*. 2005.
2. http://wps.prenhall.com/wps/media/objects/602/616516/Chapter_07.html, *Covalent Bonds and Molecular Structure*. 2006.
3. Bruice, P.Y., *Organic Chemistry*. 1995, New Jersey: Prentice Hall.
4. Shirakawa, H., et al., *Synthesis of Electrically Conducting Organic Polymers - Halogen Derivatives of Polyacetylene, (Ch)X.* Journal of the Chemical Society-Chemical Communications, 1977(16): p. 578-580.
5. Kishino, S., et al., *Estimate of the effective conjugation length of polythiophene from its chi((3))(omega;omega,omega,-omega spectrum at excitonic resonance.* Physical Review B, 1998. **58**(20): p. 13430-13433.
6. Meier, H., U. Stalmach, and H. Kolshorn, *Effective conjugation length and UV/vis spectra of oligomers.* Acta Polymerica, 1997. **48**(9): p. 379-384.
7. Bassler, H., *Charge Transport in Polymers Studied by Combining Optical and Electrical Techniques.* Makromolekulare Chemie-Macromolecular Symposia, 1990. **37**: p. 1-16.
8. Werst, M., et al., *Energy-Transfer and Trapping in the Photosystem-I Core Antenna - a Temperature Study.* Biophysical Journal, 1992. **61**(4): p. 868-878.

9. Lu, H.P. and X.S. Xie, *Single-molecule kinetics of interfacial electron transfer.* Journal of Physical Chemistry B, 1997. **101**(15): p. 2753-2757.

10. Jia, Y.W., et al., *Simulations of the Temperature-Dependence of Energy-Transfer in the Psi Core Antenna.* Biophysical Journal, 1992. **63**(1): p. 259-273.

11. Cho, E.H. and S.J. Lockett, *Calibration and standardization of the emission light path of confocal microscopes.* Journal of Microscopy-Oxford, 2006. **223**: p. 15-25.

12. Lakowicz, J.R., *Principles of Fluorescence Spectroscopy.* 2nd Edition ed. 1999, New York: Kluwer Academic/Plenum Publishers.

13. Müller, M., *Introduction to confocal fluorescence microscopy.* 2006, Washington: SPIE- The International Society of Optical Engineering. 42-49.

14. Schubert, M. and B. Wilhelmi, *Non-linear Opticas and Quantum Electronics.* 1986, New York: John Wiley and Sons.

15. Song, L., *Photobleaching kinetics of fluorescein in quantitative fluroescence microscopy.* 1996, University of Leiden.

16. Kersting, R., et al., *Femtosecond Energy Relaxation in Pi-Conjugated Polymers.* Physical Review Letters, 1993. **70**(24): p. 3820-3823.

17. Forster, T.H. in *10th Spiers Memorial Lecture.* 1959.

18. Cerullo, G., et al., *Ultrafast Forster transfer dynamics in tetraphenylporphyrin doped poly(9,9-dioctylfluorene).* Chemical Physics Letters, 2001. **335**(1-2): p. 27-33.

19. Dexter, D.L., *A Theory of Sensitized Luminescence in Solids.* Journal of Chemical Physics, 1953. **21**(5): p. 836-850.

20. Richert, R., *Analysis of Non-Exponential 1st-Order Reactions.* Chemical Physics Letters, 1985. **118**(5): p. 534-538.

21. Jakubiak, R., et al., *Aggregation quenching of luminescence in electroluminescent conjugated polymers.* Journal of Physical Chemistry A, 1999. **103**(14): p. 2394-2398.

22. Meskers, S.C.J., et al., *Dispersive relaxation dynamics of photoexcitations in a polyfluorene film involving energy transfer: Experiment and Monte Carlo simulations.* Journal of Physical Chemistry B, 2001. **105**(38): p. 9139-9149.

23. Becker, W., *Advanced Time-Correlated Single Photon Counting Techniques.*, J.W. Castleman, J.P. Toennies, and W. Zinth, Editors. 2005, Springer. p. 193-196.

24. Lindquist, L., *A flash photolysis study of fluorscein.* Arkiv för Kemi, 1960. **16**(8): p. 79-138.

25. Romanovskii, Y.V., et al., *Phosphorescence of pi-conjugated oligomers and polymers.* Physical Review Letters, 2000. **84**(5): p. 1027-1030.

26. Tsien, R.Y. and A. Waggoner, *Handbook for Biological Confocal Microscopy*, ed. J.B. Pawley. 1995, New York: Plenum Press. 267-279.

3. Sample Preparation

3.1 Introduction

Without the assurance of samples that contain isolated molecules rather than entire or partial aggregates, it becomes difficult to build an experiment capable of reliable single molecule detection. Paradoxically, without an experiment capable of single molecule detection, it is difficult to detect with certainty whether a film is isolated or not. A considerable focus of this work has been devoted to the isolation of polymer chains to produce samples to be used in the confocal experiment. In the absence of direct fluorescence imaging of the film, alternative photo-physical observations such as emission spectra, anisotropy and the (confocal) fluorescence lifetime, have instead been used to probe the local environments of polymer films.

Due to the relative size and flexibility of conjugated polymers, they frequently aggregate where possible to lower their overall energy. Such aggregation effects are particularly notable in films whereas in dilute solutions they are largely absent. Several groups have observed this effect for PPV derivatives: in dilute solutions where the polymer chains are presumed to be isolated, stimulated emission, photoluminescence and absorption decay dynamics are seen to be identical with a characteristic relaxation time[1]. Nonetheless, in films, stimulated emission has been seen to vary significantly from photoluminescence and absorption[2] . Rothberg et al. have reported wavelength-dependant absorption dynamics along with the presence of a small long-lived tail in MEH PPV leading them to conclude that in addition to the intrachain excitons found in solution, films contain interchain electronic species, which have been postulated to constitute upwards of 90% of the excitons.

There is some debate as to the nature of exciton migration within films, however seemingly conflicting evidence found in literature can be mostly resolved if it is considered that the conformation of polymer chains in solution can influence the chain morphology, and hence the interchain photophysics in films cast from different solvents. The yield of interchain species remains a subject of study, but there is emerging consensus that the strong variation in luminescence characteristics of polymer films results from film preparation.

Studies on MEH-PPV suggest that the degree of interchain interaction and aggregation is directly related to the choice of solvent and the concentration of the spinning solution[3]. In the following experiments it is expected that in aggregated systems, delocalisation of excitons over a number of chains will result in a change in the band shape and position of the emission spectrum. In this section the effect of the optically inert host matrix and luminescent polymer concentration are studied. The spectroscopic properties of films cast from a polyfluorene-toluene solution are investigated with respect to concentration and are compared in different host matrices of PMMA, Zeonex, Polystyrene and Pentacosane. It is expected that as the polymer chains become increasingly isolated within the host matrix there will be evidence of emission at higher energy accompanied by longer mono-exponential lifetimes indicative of reduced exciton migration and energy transfer.

3.2 Experimental

3.2.1 Luminescent Polymers.

Initial assays were carried out using methyl-substituted poly-phenylene MeL-PPP. MeL-PPP is a well-characterized fluorescent polymer, which has been intensively studied as an emitter in polymer LEDs [4]. As a soluble conjugated polymer, MeL-PPP is an interesting material for

electro-optical applications as its band gap lies in the blue region of the visible spectrum. The structure of MeL-PPP is shown in scheme 1, the rod like geometry of the molecule makes it susceptible to ordered chain packing which has previously been attributed to interchain interactions[5, 6]. Evidently such characteristics are disadvantageous for investigations in the single molecule domain and in view of this, the majority of investigations described within this report have been conducted using the homopolymer poly[9,9-di(ethylhexyl)fluorene] (PF 2/6) synthesised by Ulli Scherf (Wuppertal) the structure of which is shown below. Polyfluorene has become a particularly promising candidate for use in display applications over the past decade. Not only has it demonstrated high quantum yields, efficient blue emission and good thermal stability, its solubility encompasses a variety of solvents and doping with appropriate long wavelength fluorophores has made it possible to produce emission over the entire visible spectrum[7, 8]. To increase solubility and reduce the risk of chain aggregation during the film making process, the oligomer OF 2/6 N=20 has been used in the following investigations.

Scheme 1

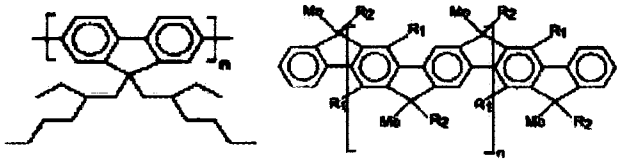

PF2/6 **MeL-PPP**

3.2.2 Pentacosane Host

Before investigating samples prepared by spin coating - the most common method of sample preparation for single molecule spectroscopy, an alternative method of sample preparation with a much faster solvent-solid transition time than spin casting was investigated. For this purpose pentacosane was chosen as the host matrix. Pentacosane is an alkane hydrocarbon of 23 repeat

units with a boiling point of 53°C; its physical characteristics are similar to those of candle wax. The use of pentacosane was intended to inhibit aggregation during the liquid-solid transition due to its high viscosity in the liquid phase. Having a relatively low melting point, polyfluorene is easily dissolved into the liquid wax without damaging the polymer chains through heating. Dilute solutions of OF2/6 in toluene (*Romil)* were prepared at 0.1%, 10^{-3}%, 10^{-5}%, 10^{-7}% by weight by stirring OF 2/6 in toluene over several hours at room temperature. The OF/Toluene solution was then dissolved into molten pentacosane at 60°C and stirred for 2hrs (at 60°C) to allow the toluene to evaporate. The resulting pentacosane-polyfluorene matrix was then coated onto sapphire discs and quenched in liquid nitrogen with the intended effect of freezing the polymer chains in their solvent isolated state.

The emission spectrum of pentacosane-OF2/6 samples was measured using a Jobin Yvon Fluoromax-3 fluorospectrometer – figure 1. Initial spectral analysis shows a blue shift in the low concentration spectra. The emission from the lowest, 10^{-7}%, concentration film was too weak to be detected by the spectrometer. At dilutions less than 0.1%, the position of maximum emission has shifted to shorter wavelength by 8nm. Changes in the emission peak are accompanied by a change in the shape of the emission band at low concentration. Interestingly in the potentially aggregated state the second vibronic is much more dominant than in dilute films

The dilution dependant spectral changes are attributed to the diminishing effects of aggregation. From the difference in peak position between the high and low concentration samples it is thought that the contribution of intermolecular interaction is considerable in the most concentrated film and less important in the more dilute samples. In the highest concentration the emission is red shifted in comparison to the dilute films; this lowering of emission energy is ascribed to intermolecular interaction leading to the existence of delocalised electronic states. Concerning the band shape, in dilute films it is thought that through increasing chain separation

non-radiative decay is reduced leading to the reduction in the 0-1 vibronic peak. Furthermore the dominance of the 0-1 mode accompanied by a slightly narrower emission peak at high concentration is indicative of self-absorption of the blue end of the emission spectrum.

Lifetime measurements of pentacosane films were made using the confocal time-resolved single photon counting module described in chapter 5 to measure the effects of concentration on fluorescence lifetime.

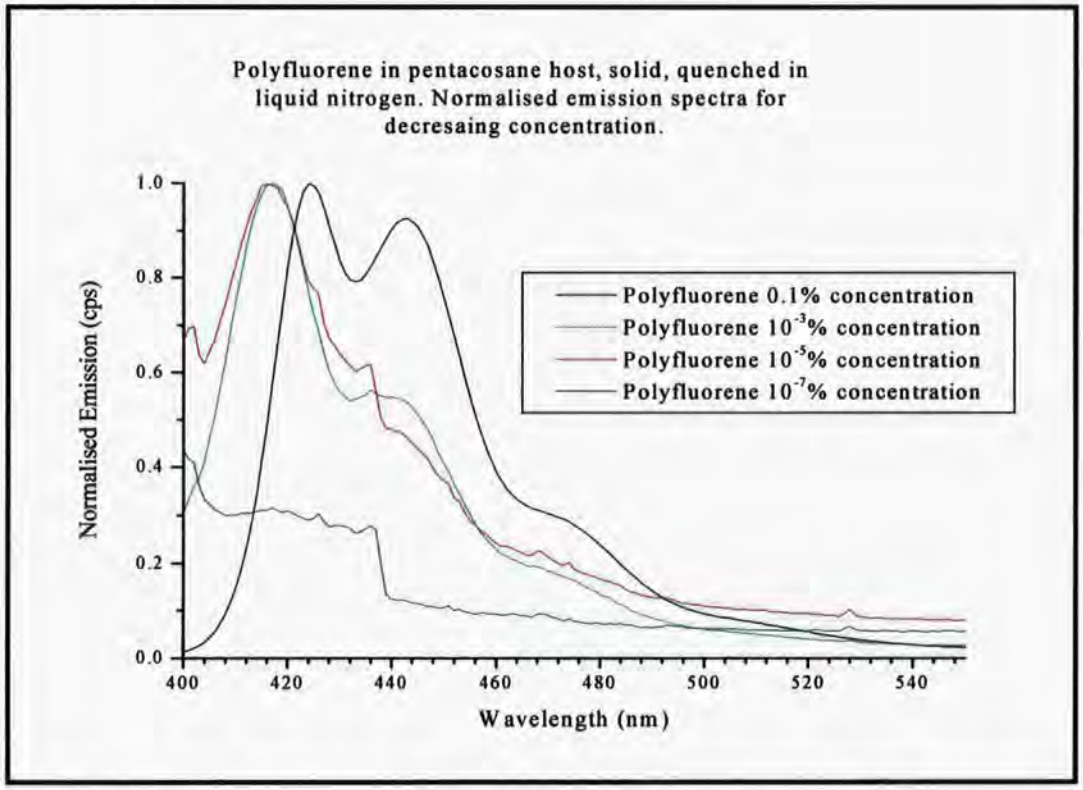

Figure 1: Emission spectra for decreasing concentrations of Polyfluorene in Pentacosane solid matrix. Lower concentrations show clear blue shift in the primary peak along with a reduction in the secondary decay mode.

Figure 2 shows the fluorescence decay curves for OF2/6 at 0.1% and 10^{-3}% concentration at room temperature. Although spectra have been presented for film concentrations down to 1 x 10^{-5}% w/w, unfortunately at the time of measurements it was not possible to measure fluorescence lifetime of the lowest concentrations on the confocal system which was still under development. Specifically the experiment had no means of protecting the detection units from external light such that insufficient background exclusion lead to poor signal to noise; a particular problem at

low concentrations where the long integration times left the system unable to discriminate between sample emission and background noise.

The decays presented here are representative of numerous time decays taken for the higher concentration samples; they are displayed in logarithmic form in order to emphasize the various decay modes present and have been deconvolved from the excitation pulse using global analysis. The shift in time between the decays is due to a slight alteration in the TAC parameters and is not representative of any photophysical processes.

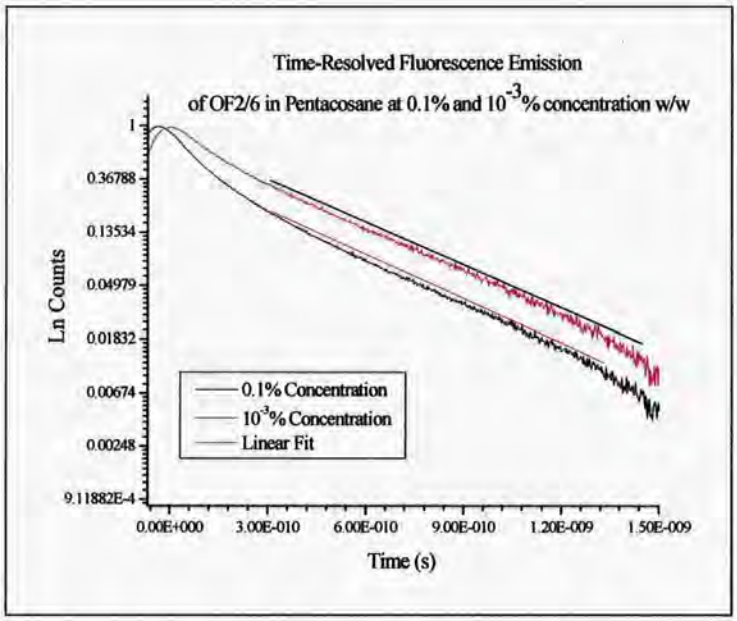

Figure 2: Lifetime decays taken on the confocal system of OF2/6 in pentacosane, 0.1% and 0.001% concentration. The higher concentration films shows a larger region of fast decay which is attributed to a higher level of interchain exciton migration than in the lower concentration brought about by a larger mean chain separation at low concentration. The lifetime of the linear regions of both curves is 361ps.

It can be seen from figure 2 that neither of the kinetics follow the predicted mono-exponential model of isolated molecules; up to four decay regimes are evident in the high concentration and three are obvious in the low concentration. Despite the multi-exponential nature of the lifetime decays, there are two obvious regions of interest in both curves. Initially both decays exhibit a fast component that extends from 7ps to 300ps in the 0.1% concentration, and from 8ps to 200ps in the 10^{-3}% concentration, phenomena attributed to rapid initial migration to defect sites. It is interesting to note that the fast component is significantly lower in the more dilute sample suggesting that there are fewer accessible pathways to the low energy sites. Following the initial fast decay both

fluorescence traces converge towards a common long lived single exponential decay. This regime is accessed more rapidly in the dilute film, within 272ps as opposed to 380ps in the concentrated film; it is thought that this occurs again as a result of increased interchain separation which typically means that there are fewer migration pathways available to excitons leading to a reduction in quenching. This is in good agreement with resonant energy transfer theories whereby the rate of transfer between a donor-acceptor system is inversely proportional to the 6th power of donor-acceptor separation. In the absence of more dilute samples with which to compare the 0.01% film at this stage it should also not be ruled out that the initial fast decay component may be caused by rapid intrachain migration to quenching sites along the polymer such as ketone groups[9]. Although chain defects are less common amongst oligomers it is certainly a possibility especially considering the comparatively long N=20 chain under investigation.

A linear fit has been made to the exponential region of the graph:

If the fluorescence emission decays according to $f(x) = A\exp^{-\frac{x}{\tau}}$ where A is the amplitude, x is time and τ is lifetime, then $\ln(f(x)) = \ln A - \frac{1}{\tau}x$. This gives the gradient of figure 2 as the reciprocal lifetime. Using *Microfocal Origin*, the linear fit has been calculated:

$$\ln(f(x)) = -0.74669 + 2.76917 \times 10^{9} x$$

$$\tau = 3.61 \text{x} 10^{-10} \text{s}$$

The lifetime of 361ps is in agreement with that of polyfluorene in solution[10] and is considerably longer than the fast lifetime observed for high concentration polyfluorene films. It is unusual to see this component in film lifetimes and although it is clear from the presence of the fast decay components that the molecules are not isolated, it is thought that the molecules are becoming

increasingly separated, perhaps into isolated clusters of aggregates. Hence what is observed here is an intermediate phase on the way to more defined isolation. Alternatively it could be that chains are no longer entangled and hence are spatially isolated, though perhaps not sufficiently to stop all interchain energy transfer processes. A major contributor to transfer in this case would be FRET, and given that FRET distances are typically on the order of angstroms these distances would still not be great enough for diffraction limited optical probing of single molecules.

Following lifetime measurements of OF2/6 in pentacosane it was evident that the SMS system required light-proofing in order to be used for single molecule investigations. To this effect a compartmentalised light exclusion box was designed and is described in more detail in the experimental section of chapter 5. During the construction of the exterior box, further sample investigations focussed on the physical characteristics of pentacosane films.

A very clear disadvantage of pentacosane is its poor optical characteristic. A number of samples are shown in figure 3 prepared as previously described; they are pentacosane doped with polyfluorene at the bottom of the image and doped with MeL-PPP at the top. Whilst at an ensemble level the transparency of the films is not a major drawback since the emission signal is in general considerably greater than distorting background effects such as scattering, at single molecule level thick, opaque films pose a significant problem; the excitation beam is scattered and wave-guided through the sample negating all the benefits of small excitation volumes and low background emission that define confocal microscopy. Further, the uneven topography of the pentacosane samples causes significant problems for scanning imaging, where

Figure 3: Polyfluorene and MeL-PPP in pentacosane. Polymer is dissolved into pentacosane in the liquid phase at 60°C then wiped onto sapphire discs before rapid quenching liquid nitrogen. Samples are uneven, thick and have low transparency.

very homogeneous, flat films are required to keep the image in focus (see section 5.3.2). Changes in thickness have implications for refraction of the excitation beam whilst air bubbles also make the films unreliable.

In order to overcome this issue, different methods of producing the film were investigated, including sandwiching the polymer host complex between the quartz disk and silicon before quenching and also allowing a slower cooling process to remove air bubbles. Without quenching there was no noticeable change in spectral properties compared to quenched samples of the same concentration, attributed to the high viscosity of the molten wax impeding movement of the polymer chains even on the longer time scale of cooling using iced water. The samples prepared by squashing the molten complex between silicon and quartz did show improved flatness and transparency, however they were still too opaque for confocal imaging and still had an uneven topography when examined under an optical microscope.

As a final attempt to prepare the pentacosane samples for confocal imaging, the use of a microtome was investigated to slice the samples into micron thin strips. Attempts were made with the kind help of Christine Richardson in the biology department to slice the wax samples however they were too brittle for slicing. In view of these limitations the pentacosane host was seen to be unsuitable for use in the confocal single molecule system and the main focus of sample preparation was moved to spin coating.

3.2.3 Spun Samples

OF2/6 N=20 mass averaged molecular weight M_w = 15 000 g/mol. was dissolved in toluene with a concentration of 0.1% w/w by heating and stirring at 50 °C for 1hr then stirring at room temperature overnight. From this more dilute solutions were made by sequentially diluting and

mixing until the lowest concentration was reached. All dilutions were stirred into the solvent for 12hours before the next dilution was made.

The host polymers used were PMMA M_w = 15 000, Polystyrene M_w = 280 000, Zeonex M_w 480 000 Host polymers were prepared by dissolving PMMA, Zeonex and Polystyrene in toluene at 2%, 0.2%, 0.25% concentration by weight respectively. The solutions were then stirred and heated at ~60 °C for 3hrs then stirred overnight at room temperature.

PF/Host solutions were made at different concentrations by adding a drop of the relevant PF/Toluene solution to the appropriate weight of the host solution. In this way, concentrations between 0.1% and 1 x 10^{-6} % PF: Host by weight were made. These solutions were then stirred overnight to ensure that the polymer was completely dissolved into the host. Films were made by spin coating a drop of each solution onto 12mm quartz or sapphire discs at 2500rpm for 60s.

All preparation was carried out in a clean room environment with yellow light. Sample substrates were cleaned overnight in nitric acid then sonicated in acetone and isopropranol. Before spin coating the substrates were put into a UV – Ozone cleaner for 10 minutes on each side. To minimize any degradation effects investigations were carried out using freshly prepared films where possible, solutions were stored in sealed vials in the dark when not in use to minimise the effects of photo-degradation.

3.3 Results and Discussion

Photo-induced emission experiments were conducted using a Jobin-Yvon Fluorolog fluorospectrometer with an angle of 90° between the emission and excitation ports (L-format). The emission spectra of OF 2/6 films were taken using an excitation wavelength of 370nm and a

step width of 1nm. In the more dilute films where emission is weak, longer integration times are used; up to 5s in the most dilute sample, the minimum integration time used was 1s.

In figure 5 the peak emission wavelengths for each host at each concentration are compared whilst in figure 4 the emission spectra of dilutions of OF2/6 in PMMA are displayed to illustrate band shape characteristics. The emission spectra in figure 4 are typical of all the guest-host samples. In figure 5 the emission peaks of OF2/6 in pentacosane are displayed for comparison.

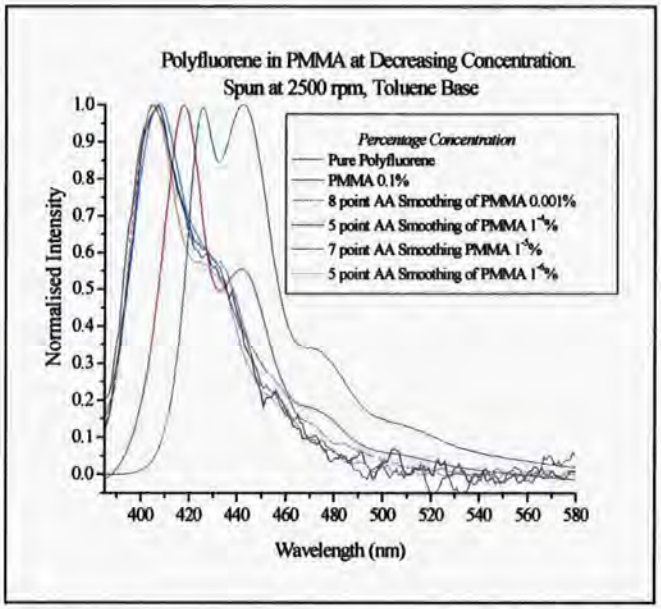

Figure 4: Emission spectra of OF2/6 in PMMA at decreasing concentration; excitation wavelength 370nm. Spectra are normalized for comparison.
As concentration decreases a spectral blue shift is apparent accompanied by a reduction in the 0-1 mode.

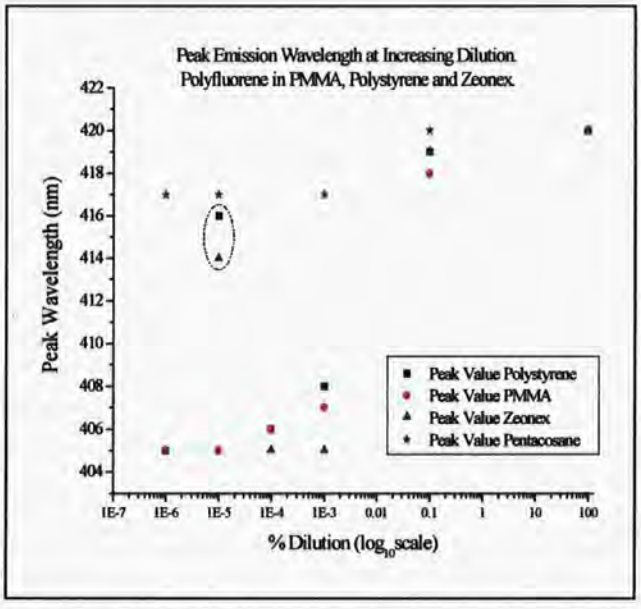

Figure 5: Peak emission wavelength of OF2/6 in PMMA, Polystyrene and Zeonex at decreasing concentration. Apart from anomalous values for Zeonex and Polystyrene hosts at 10^{-5}%, all samples shift towards the blue as dilution increases reaching a minimum of 405nm.

As in the pentacosane host the emission maximum shifts to shorter wavelength at lower concentration, though it is now clear that much greater blue shifts are accessible in the spun cast films. Although spectral shifting occurs at different rates depending on the host, a plateau is reached at 405nm in all cases. Both the Zeonex and Polystyrene films show anomalous spectral positions at 10^{-5}% concentration. The reason for this is unclear although it could be attributed to a contamination during film preparation, perhaps during spin coating or it could be a consequence of a problem within the Fluorolog; excitation intensity variation for example. In any

case at 10^{-6}% the trend is re-established for polystyrene although in zeonex the emission at this level was too weak to discern the peak accurately.

The shift in the emission maxima (figure 5) in more dilute films is consistent with decreased interchain interaction and delocalisation of electronically excited states. This effect is immediately noticeable as the pure polyfluorene 425nm emission peak shifts by 5nm to give a markedly more energetic emission in the 0.1% film. At 0.001% there is a sharp drop in the peak emission wavelength in all films from where it continues to decrease at different rates depending on the host. Such behaviour is attributed to the effect of increasing chain separation which gradually cuts off exciton migration routes, reduces non-radiative decay and hence increases the final emission energy. The reason that this occurs much faster in the Zeonex films is thought to be due to increased solubility of the oligomer in the host compared to polystyrene and PMMA. Problems of emission in the most dilute polystyrene and zeonex films are thought to be a result of variation in the viscosity of the initial solutions which in turn has caused the polystyrene and zeonex films to be thinner and therefore less emissive overall than the PMMA based samples.

Further evidence for increasing interchain separation can be drawn from changes in the band shape, the 0-0 mode becomes much broader at low concentration and the contribution from the 0-1 mode in the in the blue shifted films becomes less. Reduction in the 0-1 mode is attributed to reduced vibrational relaxation, and in consideration of the spectral broadening of the 0-0 mode at low concentration it is also clear that self-absorption is contributing to the dominance of the 0-1 mode in the most concentrated sample.

Concerning the band shape, the dominance of the 0-1 mode in the pure film is explained by disorder and the predominance of delocalised states. It is thought that in the disordered system, vibronic coupling between neighbouring molecules plays a greater part in luminescent decay

than the less aggregated dilute films. At high concentration, excitons relax through energy transfer between localised states to a final low energy configuration where the probability of radiative decay is low. As a result, the vibronic coupling mechanism becomes increasingly important in stimulating radiative decay, giving rise to the high relative intensity of the 0-1 transition in the concentrated sample[11]. Self-absorption is also attributed to the dominance of the 0-1 mode at high concentration. Due to the spectral overlap of the 0-0 transition emission band and the absorption band, self absorption occurs and the emission peak corresponding to the 0-0 transition band is decreased, leaving the 0-1 and 0-2 transition bands with increased relative intensity. This effect is clearly illustrated in figure 4 where the 0-0 mode becomes narrower as concentration increases corresponding to the absorption of the blue emission tail.

Notably the 0-1 mode reaches a plateau in relative intensity at and below 0.001% of 55%, this is high compared to polymers such as the ladder type MeL-PPV where the rigidity of the polymer chain prevents conformational relaxation in the excited state leading to dominance of the 0-0 mode. Here therefore it seems that there is still some degree of flexibility in the OF2/6 even at the lowest concentrations suggesting that the host matrix has little effect on the conformational flexibility as concentration decreases.

The origin of aggregation in highly concentrated films is thought to lie at the point of spin casting. Investigations of aggregation in solution have found that aggregation is only prevalent in solutions where the weight to volume ratio exceeds 1% [3] whereby phase segregation of the luminescent and host polymer becomes increasingly probable. The solutions used to spin cast the films investigated here are well below that limit and so the polymer chains are presumed to be isolated whilst in solvent. During spin coating, aggregation is thought to occur when in more concentrated films the slow evaporation of toluene, which has a relatively high boiling point, allows time for interchain interactions to cause the polymer to extend its conformation.

Nonetheless at lower concentration the mean intermolecular separation is thought to be significantly large to inhibit the formation of aggregated states even on the relatively long time scale of the solvent evaporation.

Fluorescence lifetime measurements provide further support for the interpretation of spectral blue-shifting and changes in the band shape as indicators towards chain isolation. Figure 6 shows the lifetime measurements of pure and 0.001% polyfluorene in zeonex, taken on the confocal TCSPM before the experiment was light-proofed whilst in figure 7 following the completion of the box the most dilute sample are displayed. In both cases, for the pure film luminescence is dominated by rapid decay, this is consistent with exciton migration to low lying states that have previously been noted in the red shifted emission peak at high concentration. In the 0.001% film an initial fast decay component is evident though it is significantly shorter lived than that seen in pure polyfluorene, and is followed by a long lived tail. This behaviour is consistent with the blue shift observed in the emission characteristics, interpreted as the reduced availability of the non-radiative pathways. As such initial rapid decay within localised aggregate groups quickly

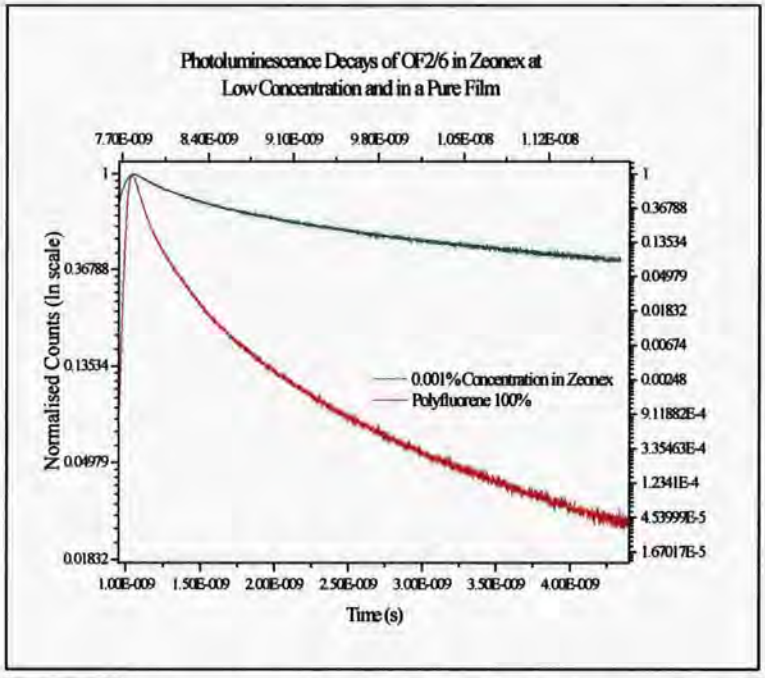

Figure 6: Fluorescence decay of polyfluorene spun in a Zeonex Matrix at 0.001% and in a pure film. The difference in time scales is due to different TAC settings on the TCSPC module and is not representative of a change in sample characteristics; the range for each scale is comparable. In the dilute sample, the decay time is significantly longer than the pure film. Although the dilute sample cannot be described using a single exponential decay, it has fewer decay modes and a shorter fast initial decay component compared with the concentrated sample. This is consistent with reduced exciton migration and non-radiative decay.

becomes localised in relatively high lying excited states which give rise to the bluer emission peak at 0.001% seen in figures 4&5.

The final isolated configuration is clear in figure 7, where at 10^{-4}% and 10^{-5}% concentration decays are perfectly mono-exponential with no initial period of rapid decay. Interestingly a sample of 10^{-4}% made mistakenly at a lower spin speed of 1200rpm is seen to have a less linear decay trace than the identical solution spun at the speed of 2500rpm, which suggests some degree of energy transfer and hence interchain interaction, supporting the argument given for aggregation during solvent evaporation in the spin casting process. The absence of a fast decay mode in the two low dilution films gives compelling evidence for chain isolation, where large interchain separations exclude all energy transfer between chains. This is strongly supported by the high energy emission spectra at low concentration seen in figures 4 & 5.

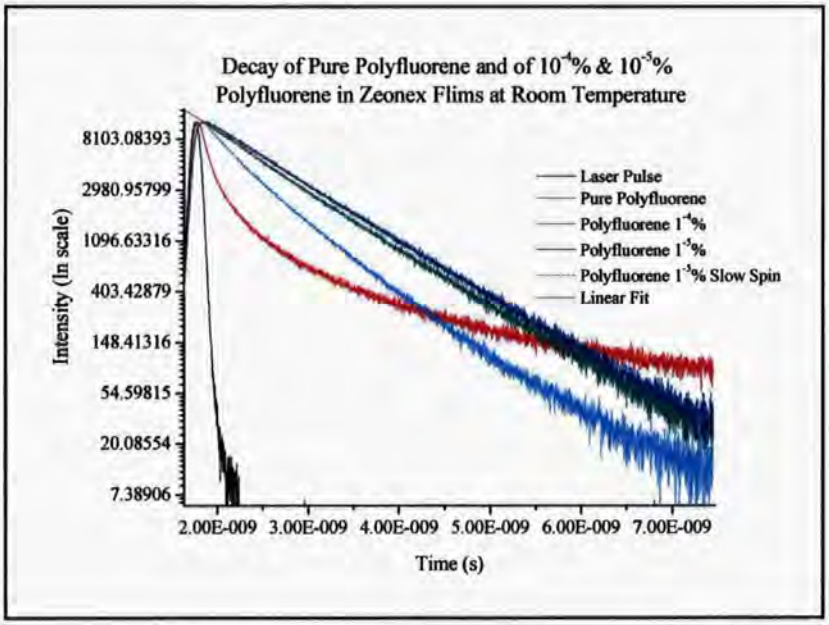

Figure 7: Fluorescence decays of OF2/6 in Zeonex at 10^{-4}% and 10^{-5}% w/w concentration. Pure Polyfluorene film is shown for comparison. The fast decay is absent in the most dilute samples indicating the absence of non-radiative decay pathways. The decays are exponential with a lifetime τ =0.92ns.

The decay lifetime in the 10^{-4}% and 10^{-5}% films are identical, with τ = 0.92ns suggesting emission from a common high energy excited state population. Increase in the fluorescence

lifetime is commonly attributed to a decrease in non-radiative decay, equation 3a chapter 4. Decay of 0.92ns is significantly longer than the solution lifetime of 564ps measured for OF2/6 in MCH[12]. This can be explained largely by the difference in phase between film and solution which leads to less non-radiative decay pathways; whereas generally speaking molecules in dilute solution have a high degree of mobility for rotational and diffusional relaxation, the spun cast molecules are in a quasi-frozen state on the substrate hence rotational and diffusional relaxation pathways are largely absent leading to the observed increase in lifetime.

Spectral blue shift and mono-exponential decay characteristics strongly suggest isolation at 10^{-4} % and 10^{-5} % concentration. A point for concern however is the intensity of the photoluminescence curves of figure 7, which are notably higher than the emission expected from a single fluorophore raising the question not of isolation but as to if the data represents a single molecule or an ensemble of single molecules, brought about perhaps through poor focussing for example. Investigations into single molecule luminescence elsewhere report that molecules undergo irreversible photobleaching after several minutes[13]. The luminescence traces of figure 7 were integrated for considerably longer than this suggesting quite clearly that they are in fact ensemble measurements of single molecules. Until the experiment can image single molecules successfully it will be difficult to resolve this question, though any problem obviously lies firmly with the experimental side and not in sample preparation, where the photophysical evidence for isolation is strong. The implications are for the accuracy of the focal point suggesting the need for a more accurate focussing technique; this is discussed in greater detail later. A further point to note is that since the solvent, toluene, and the host polymer, zeonex, are non-polar, solvo-chromatic effects are not thought to significantly influence the fluorescence lifetime.

The spectral information coupled with the promising results of lifetime measurements detailed in this chapter are beginning to suggest that the most dilute films have been successful in isolating

the polyfluorene chains. As the confocal system is not able to take more precise spectral measurements or produce images of suspected single molecules at this stage, it is proposed to carry out one further bulk measurement on the polyfluorene films. If the films at low dilution do contain well isolated molecules as the lifetime information suggests, it is expected that measurements of the polarisation anisotropy in these films will yield a very high value close to the maximum, 0.4 as interchain interaction, which is largely attributed to be the cause of loss of polarisation, is proposed to be absent in this regime. This will be discussed in the following section.

3.4 Anisotropy Measurements

Anisotropy measurements are based on the principle of photo-selective excitation of fluorophores by polarized light; by restricting the excitation beam through polarisation, fluorophores may be selectively excited according to the orientation of their transition moment. This selection works on the principle that the probability of absorption is greatest if the electric field vector of the incident photon is parallel to the transition moment of the target fluorophore. Consequently, polarised excitation results in a partially orientated excited population leading to partially polarized emission.

The anisotropy describes the average angular displacement of the fluorophore that occurs between absorption and emission of a photon and is defined in equation 1. There are a number of phenomena which can decrease the measured anisotropy, in solution depolarisation effects are typically a result of rotational diffusion whereas in solids interchain energy transfer is thought to by largely responsible for loss of polarisation. In this section the anisotropy has been measured for samples identified by spectral analysis to contain polyfluorene that is isolated rather than aggregated. If these samples are well isolated it is expected that there will be a significant

increase in anisotropy when compared to a sample at high concentration due to a significant reduction in available pathways for interchain energy transfer.

3.4.1 Anisotropy [14]

Anisotropy is a dimensionless quantity that is independent of the total intensity of the sample:

$$\langle r \rangle = \frac{I_v - I_H}{I_V + 2I_H} \qquad \textbf{Equation 1}$$

Steady State Anisotropy

Measurements of the fluorescence anisotropy of polyfluorene films were taken using a Jobin Yvon fluorometer. The fluorometer is configured for anisotropy measurements in the L-format, observing perpendicular and parallel emission sequentially through a single channel.

Because of the idiosyncrasies of this configuration there are a number of factors which should be included in the anisotropy calculations in order to produce accurate results. Particularly important is the transmission function of the monochromator inside the fluorometer since on rotation of the emission polariser from vertical to horizontal it is usual to see a change in the measured intensity of light even if the emission is entirely unpolarised. To measure intensity accurately a term called the G-factor is introduced into the anisotropy equation. The G factor gives a relative sensitivity of the system to vertically and horizontally polarised excitation.

$$I_{VV} = kS_V I_{\parallel} \qquad \text{Equation 2}$$

$$I_{VH} = kS_H I_{\perp} \qquad \text{Equation 3}$$

Equations 2 and 3 represent the intensity observed with the excitation and emission polarisers at vertical, I_{VV}, and the intensity observed with the excitation polariser vertical and emission polariser horizontal, I_{VH}. Taking the ratio of the parallel and perpendicular intensities the G factor is defined as:

$$G = \frac{S_V}{S_H} \qquad \text{Equation 4}$$

where:

k : is a factor of proportionality that accounts for factors such as the quantum yield of the fluorophore and other instrumental factors, equations 2 and 3.

S_V: the sensitivity of the emission channel in the vertical component.

S_H: the sensitivity of the emission channel in the horizontal component.

Empirically the G-factor is measured using horizontally polarised excitation. In this configuration, the excited state distribution is orientated along the observation axis. Consequently both channels measure equal perpendicular components and any variation in I_{HV} and I_{HH} can be attributed specifically to the detection system. The G factor is the ratio of the parallel and perpendicular orientations.

$$G = \frac{I_{HV}}{I_{HH}} \qquad \textbf{Equation 5}$$

By substituting the G-factor into equations 2 and 3 it can be expressed in terms of $I_{||}$ and $I_{\perp}$ and applied to the anisotropy equation 1. The anisotropy as measured with an L-format fluorometer is then given by:

$$r = \frac{I_{VV} - GI_{VH}}{I_{VV} + 2GI_{VH}} \qquad \textbf{Equation 6}$$

Anisotropy (L-format)

When the transition dipole moment of emission is exactly parallel to the absorption dipole an anisotropy maximum r = 0.4 is observed, whilst if the emission and absorption dipole moments are perpendicular, the minimum anisotropy value r = -0.2 results[14].

Loss in anisotropy is generally due to conformational relaxation or exciton migration, which causes a change in the angle between the absorption and emission dipoles. It is also possible to see anisotropy measurements which exceed the maximum value of 0.4; these are almost certainly the result of scattered light, which has an anisotropy close to 1.0, entering the emission detector. Scattering can severely affect anisotropy measurements and should be removed with the use of appropriate emission filters if necessary.

3.4.2 Results and Discussion

The anisotropy of polyfluorene in PMMA was measured using an excitation wavelength of 370nm. The sample under investigation is the same PF in PMMA at 10^{-6} % dilution by weight seen in the emission spectra of the previous section.

An error estimate has been made for anisotropy measurements by taking 12 successive measurements of the same film of polyfluorene in PMMA at 0.1% concentration w/w. During this process there was specifically no interference to the system between readings, that is to say the sample was not moved, the fluorometer was not turned off and the readings were taken in quick succession to avoid any possible effects of sample degradation between readings. The results are shown in figure 8, where the anisotropy has been recorded for each measurement set at different wavelengths in the emission spectrum. It can be seen from the results that whilst in the region of the peak emission $420 < \lambda < 440$ the anisotropy is quite constant, the deviation from the mean becomes greater at less emissive wavelengths. This can be attributed to the increasing

dominance of noise at the tails of the emission spectrum. To achieve the best estimate of the anisotropy, therefore, values have been taken over the peak emission wavelengths, which from previous findings are frequently blue-shifted in comparison to the concentrated sample of figure 8.

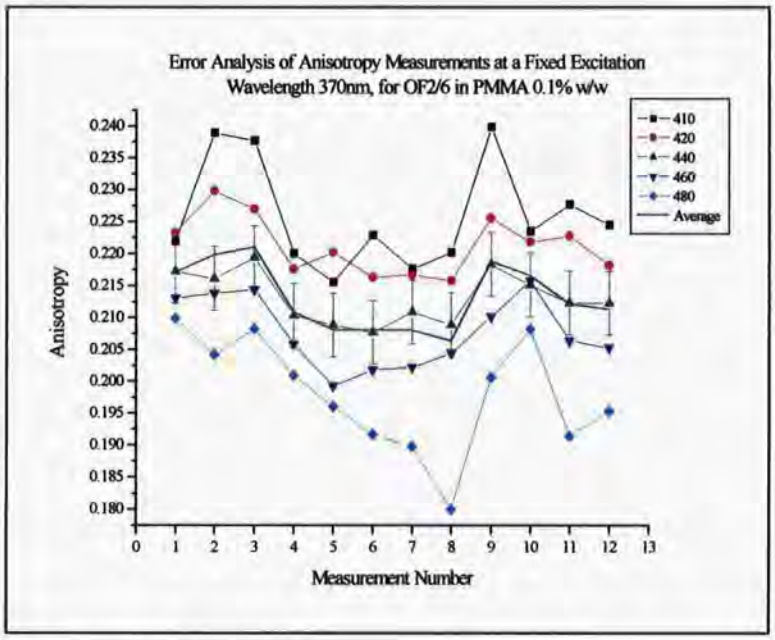

Figure 8: Estimating the error for anisotropy measurements in films. Each line represents the anisotropy measured for each measurement set at a different area of the emission spectrum between 410nm and 480. Whilst the regions of maximum emission show little variation across the measurement set, the 410nm and 480nm lines are more varied. This effect is attributed to random noise dominating the less emissive wavelengths.

Using the average of the 420,440 and 460 nanometre anisotropies for all measurement sets, the standard error for the anisotropy taken over the central emission region in films has been calculated. For an excitation wavelength of 370nm, the standard error of OF2/6 in PMMA α_{370} is:

$$\alpha_{370} = 0.211 \pm 0.00136$$

In figure 9 the anisotropy measurements of figure 8 are displayed as the average anisotropy at each emission wavelength. As mentioned the measurement error increases at the far red and far blue emission wavelengths corresponding to the less emissive regions of fluorescence. What is more interesting perhaps is the general trend to a loss of polarisation at redder wavelengths. Though it is expected that some anisotropy is lost as a result of intrachain exciton migration, it is suggested that the most significant cause for the loss in anisotropy at the red end of the emission spectrum is that here emission emanates increasingly from excitons which have undergone interchain migration to low-lying aggregate or defect

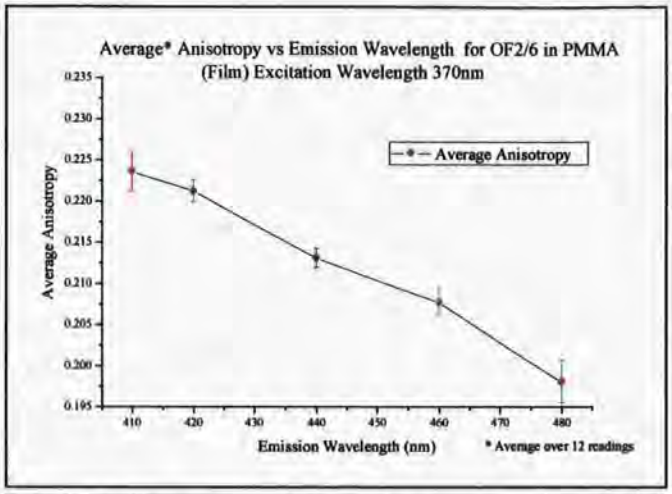

Figure 9: The progression of average anisotropy with emission wavelength, as in figure 8 the wavelengths of least error lie between 420nm and 440nm. There is a clear general trend to lower anisotropy as the emission wavelength increases.

states, in which case the orientation of the emission dipole is likely to alter in relation to the absorption dipole, hence giving a loss in polarisation anisotropy.

Initial attempts to measure the anisotropy at room temperature were severely hampered by poor signal from the sample with the result that no anisotropy value could be extracted from the data due to low SNR. To improve emission, the sample was placed inside a cryostat and cooled to 77K using liquid nitrogen. As can be seen in figure 10, signal was significantly increased and there is clear evidence of spectral narrowing when the normalised spectra are compared (inset).

The increase in signal is thought to be a consequence of the reduced availability of non-radiative pathways such as thermal and vibrational energy transfer resulting in an increase in PLQY. Furthermore at low temperature, dampening of molecular vibration causes the mean bond length to be lower; according to the Frank-Condon principle this results in fewer transitions to high lying vibrational states and so greater spectral resolution is observed. Although an increase in emission is compatible with theory, the scale of the increase is in fact rather large, even after accounting for the effects of reduced non-radiative decay etc... This issue will be discussed in more detail presently, though it is thought that small alterations in the sample position can give rise to widely varying amounts of light falling on the detection slits.

The spectra seen in figure 10 have been divided by the variation in lamp background in order to remove any spectral distortion due to inconsistencies in excitation intensity. This correction

increases the apparent intensity by a factor of ~ 1000. With this in mind it is clear that even the low temperature signal is relatively weak and consequently the integration time was set at 10s per nanometre for anisotropy measurements.

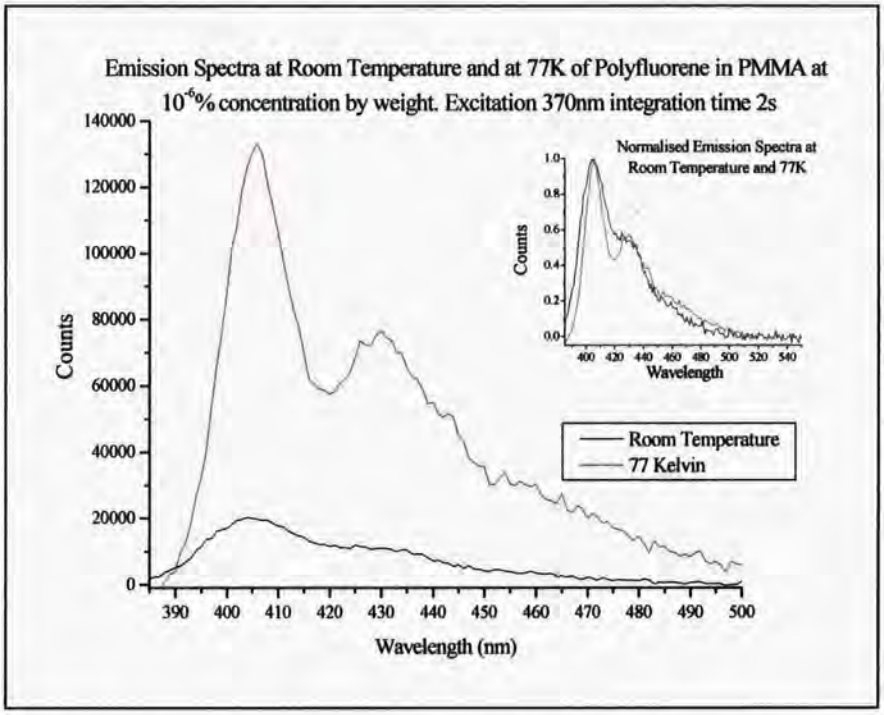

Figure 10: *Emission spectra of PF in PMMA at room temperature (black) and at 77K (red).* The emission at peak is greater at low temperature than at room temperature due to a reduction in non-radiative emission through thermal and vibrational pathways. The inset shows the effects of spectral broadening at higher temperatures; at low temperature, better resolution of the vibronic structure is evident.

Figure 11 displays the measured anisotropy taken at 77K, with an excitation wavelength of 370nm, integration time 10s and step width 1nm. Although the result is noisy, there is a clearly defined region between 400nm and 430nm where the anisotropy is flat. From comparison with figure 10 it can be seen that this region corresponds to the emission wavelengths of the primary and secondary intensity peaks. Beyond 430nm the anisotropy is increasingly dominated by noise and is unreliable for extracting information on the sample, this is thought to be a result of diminishing intensity along the tail of the emission spectrum.

The mean anisotropy between 400nm and 427nm is:

$$\langle r \rangle = 0.34 \pm 0.02$$

Since the error of the averaging process is greater than the systematic error calculated earlier, it is stated here and is attributed to the increased noise at low intensity, an issue noted in the original error calculations.

The experimental anisotropy is large suggesting a highly isolated system with negligible migration. This is unusual in the solid state, where low or zero anisotropy is common, often attributed to interchain charge transfer between closely packed polymer chains. The absence of such depolarisation effects suggests that intrachain migration has been inhibited as result of large chain separation at low concentration, which again gives very clear evidence towards isolation.

In order to establish a trend in the anisotropy with dilution, a batch of samples at each concentration was made and the anisotropy measurements were taken, in the cryostat at 77K and at room temperature. It was expected that as dilution decreased, the anisotropy would tend to the value found for the 10^{-6}% concentration. Nonetheless this line of investigation encountered a number of problems with some interesting implications.

A problem that became clear very quickly was that although using the cryostat allows signal to be increased, the way that the samples are mounted inside the cryostat is not easily repeatable. Samples are mounted at the end of a long arm which can rotate to position the sample at the desired angle to the two monochromators inside the Fluorolog; this makes the repeated positioning of each sample at precisely the same angle very difficult. This is not such a great problem when using highly concentrated samples with good emission but at low intensities, accurate positioning of the sample becomes increasingly important, up to the point that unless the sample is at exactly the right angle, little emission reaches the detection slits. In this situation the signal collected is so weak that the anisotropy measurement becomes dominated by noise.

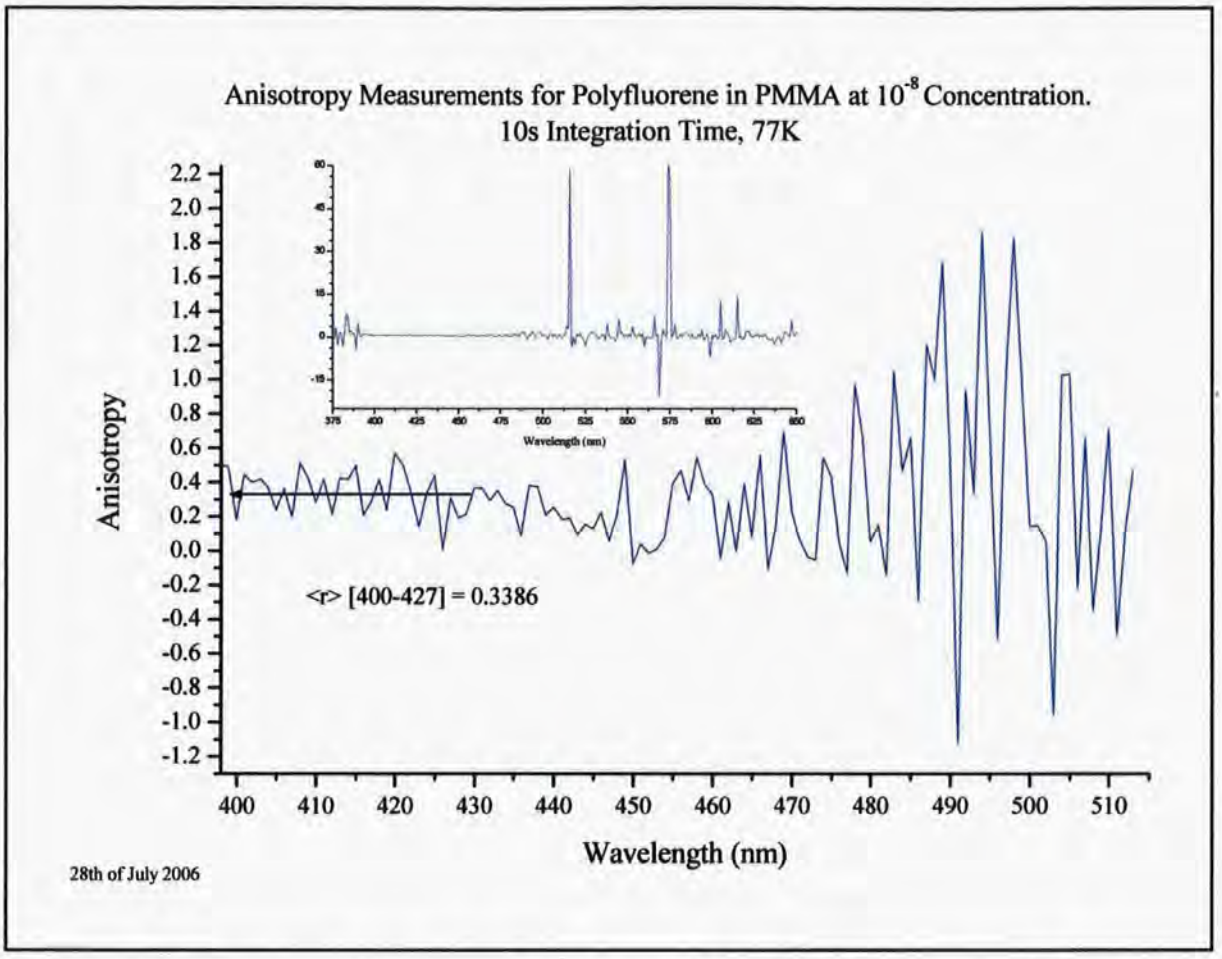

Figure 11: Fluorescence Anisotropy of OF2/6 in PMMA at 10^{-6} % concentration by weight. Anisotropy measured over the peak emission wavelengths gives an average anisotropy of r = 0.3386. Beyond $\lambda = 430$ the low emission intensity results in a poor signal to noise ratio.

The problem is further compounded by the fact that the arm can also move forwards and backwards and side to side inside the cryostat whilst it is being rotated. This combined difficulty of getting the perfect sample position inside the cryostat means that getting the sample in place to be read can take hours if not the whole day, and in some cases it was just not possible even at the best position that could be found to get a successful anisotropy reading from low concentration samples.

Despite these difficulties anisotropy measurements were persevered with, two dilutions were spun at a time and investigated leaving the other solutions stirring under yellow light to reduce photo-degradation. Because of the difficult alignment requirements and the low emission of the samples it typically took two to three days to get an anisotropy reading from both films. When

the anisotropy measurements that had been collected were analysed and compared (not all concentrations were possible due to the cryostat arm issue) they displayed a trend of decreasing anisotropy with increasing dilution, an effect that was unexpected because it suggests increasing interchain transfer with molecular separation. Furthermore there were contradictory trends in the effects of temperature on anisotropy with both the 0.1% and 0.01% having higher anisotropies at 77K but the 10^{-3} % having a higher anisotropy at room temperature. The results are shown in figure 12. Haphazard results of this nature point toward the contribution of another parameter affecting events.

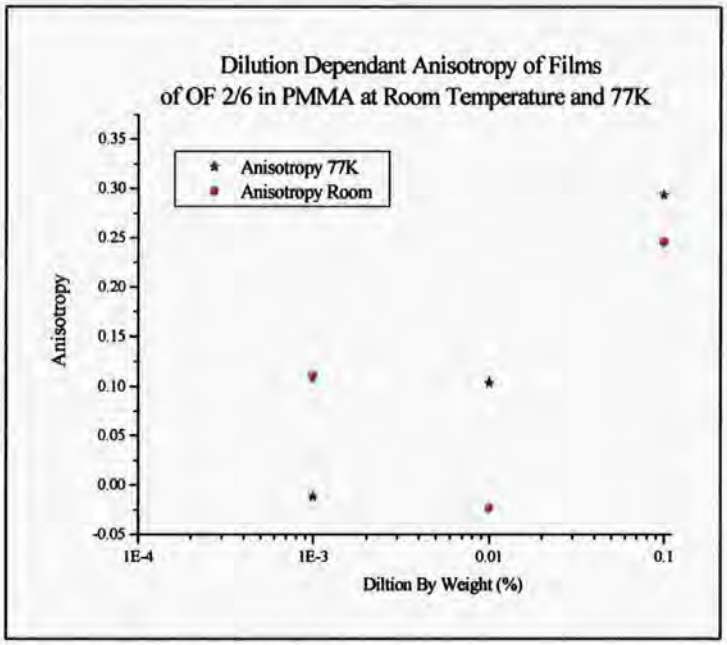

Figure 12: Inconsistencies in anisotropy readings over a range of dilutions at room temperature and at 77K. Although it is expected that anisotropy would increase as dilution decreases, the trend observed is the opposite with anisotropy falling to 0 in the 0.01% concentration film. Additional anomalies lie in the temperature dependence, which has no obvious effect on the anisotropy increasing it in two samples and lowering it in another.

Scattering within the cryostat was eliminated as a cause when similar results were obtained for room temperature measurements in a standard open film holder. With scattering effects ruled out, the only variable factors between films were identified as their age and of the exact position of on the film where the anisotropy is measured. These effects were investigated by taking one set concentration, OF2/6 in PMMA 0.1%, chosen for its good emission and because it is the simplest solution to make. A fresh sample was made using an identical preparation method to previous samples: OF2/6 was dissolved in toluene by mixing for 12 hours then the final solution was made by adding the required amount of the OF/Tol solution into a solution of PMMA in toluene. This was stirred for a further 12 hours before it was spun onto a

quartz substrate at 2500 rpm. Each day for 1 week a sample was spun from this solution and its anisotropy was measured whilst keeping all other experimental parameters constant. Unused solution was left stirring under yellow light to minimise UV degradation and photo-oxidisation.

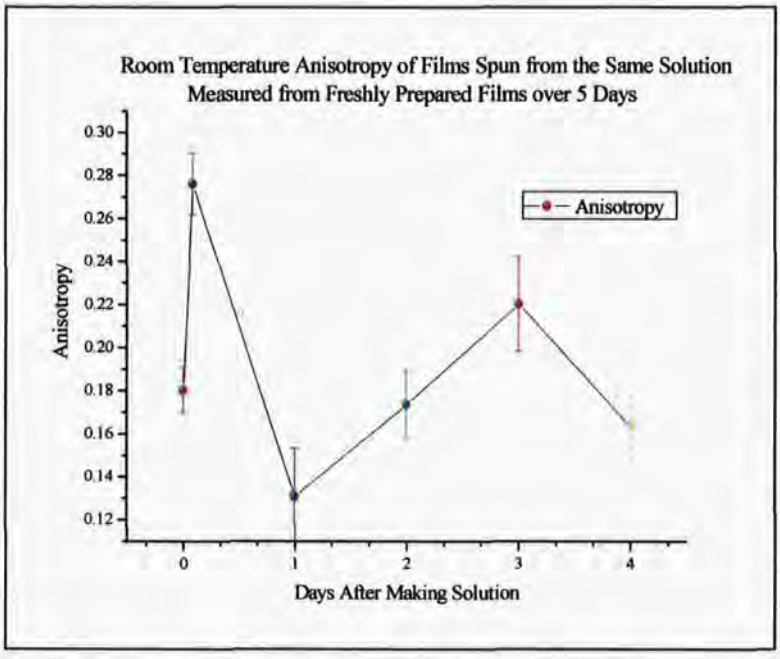

Figure 13: Variation of anisotropy with the age of the spinning solution. There is no obvious correlation between age of solution and the anisotropy, leaving the only explanation as inhomogenaity across the film.

As can be seen from figure 13 there appears to be no firm relationship between the anisotropy and the age of the base solution. Error bars used are the standard error of averaging the anisotropy over the peak wavelengths or the calculated system error denoted earlier, whichever is largest. Whilst the 0, 1, 2 and 4 day old samples are in agreement to within this error, the 2hr old and 3day old are significantly higher. The only explanation for this observation is that the anisotropy is not homogeneous across the film. This theory was verified by measuring the anisotropy of the 2 day old film 10 times under identical conditions, the sample was then removed and replaced (to alter the excitation position slightly) and a further 10 anisotropy measurements were taken. In this way the effect of small changes in position, common to all samples was probed with the additional safeguard of repeated measurements at each point. The results explain the anomalies of the previous anisotropy measurements, whilst the error calculated by the 10 point average was the same before and after the sample was moved, the anisotropy was not, changing by up to 0.095 on the same film at different positions, to double check that time had no role in this change the film was measured, left untouched for a day and

then measured again. These results were the same to within the error of the system calculated earlier. These results strongly imply that the anisotropy is in fact inhomogeneously distributed across the film. Possible reasons for this variation include for example poor substrate quality: scratches on the substrate surface causing uneven surface tension during spinning leading to clumps of polymer molecules. Or, it could be that whilst the solution is left stirring segregation occurs between the PMMA and polyfluorene molecules leading to uneven distributions of the polymer within the film. More simply, it could be that the orientations of polyfluorene chains in the film, which are assumed to be random, give rise to different absorption characteristics depending on the area of excitation. It is clearly a subject that requires further investigation however this will not be carried out in this report, since the primary focus here is that of designing and building a confocal system for single molecule spectroscopy.

3.5 Sample Preparation Conclusions

The effects of varying the host matrix have been investigated for spun films of different concentrations of OF2/6 $N_{=20}$ in PMMA, Zeonex, Polystyrene and Pentacosane. Although spectral analysis of the emission properties of OF2/6 in pentacosane showed initial promise at low concentration, the optical properties of pentacosane were found to be a major drawback. It is a highly opaque substance which is seen to pose problems of scattering and beam distortion during confocal excitation. To improve the characteristics of pentacosane films means of producing very thin samples were investigated by sandwiching drops of the OF-Pentacosane mix in the liquid phase between silicon and sapphire and by using a microtome to produce micron thick slices of the wax. These, amongst other assays, were unsuccessful – sandwiching did not make thin enough layers and the microtome failed because the wax was too brittle to cut. In view of this it was decided that spin coating films was a more suitable means of sample preparation.

Investigations of spin coated films in PMMA, Polystyrene and Zeonex host indicate that as dilution increases, polymer chains become increasingly isolated within the film. Although the isolation can not be confirmed categorically, the results of spectral analysis, lifetime analysis and anisotropy measurements all point towards isolation. At low concentration the peak emission shifts to increasingly higher energy appearing to reach a maximum value at 405nm in the lowest concentrations measured; 1 x $10^{-4,5,6}$ % w/w. The gradual increase in emission energy as dilution increases is attributed to greater chain separation closing off many migration pathways that act to lower emission energy and broaden the emission peaks in more concentrated samples. This proposal is backed further by lifetime measurements taken on the confocal system. These show that as dilution increases, the lifetime approaches a mono-exponential decay. Fast initial decay dominates samples at high concentration whilst as the dilution increases it accounts for a diminishing proportion of the fluorescence implying that excitons become more and more localised following excitation. In concentrations below $1x10^{-4}$% in zeonex the fast component is completely absent whilst in PMMA the mono-exponential decay is only observed in the lowest $1x10^{-6}$ % concentration, examination of the emission spectra for both films, particularly the concentration dependant blue-shift resolves this apparent difference showing that the mono-exponential decay is reached in both cases when emission at 405nm is achieved. The fact that this takes greater dilution in the PMMA is attributed to different solubility of the luminescent polymer in the two hosts. In view of this emission at 405nm is attributed to the initial excited state energy in the absence of energy transfer which in turn implicates spatial isolation of molecules. As dilution increases, increasing molecular separation causes interchain energy transfer to fall, showing intermediate stages of reduced transfer until molecules behave as isolated entities where interchain energy transfer is absent. The mono-exponential lifetime measured for dilute samples of OF2/6 is found to be: $\tau = 0.92$ns a value considerably longer than the lifetime in solution of 564ps. This is in good agreement with theory, where in the absence of

interchain energy transfer the reduced degree of freedom in the condensed phase is expected to increase the fluorescence lifetime.

The band shape of the fluorescence spectrum at high concentration is consistent with that expected for strongly delocalised excitons. In the pure OF2/6 film the 0-1 transition is the dominant mode though below 0.1% concentration the 0-0 peak is the most intense. This phenomenon is clear in both the spun films and in the quenched pentacosane samples. Dominance of the 0-1 vibronic at high concentration is attributed to efficient exciton migration to low lying excited states due to the high concentration of polymer chains. In these levels the low probability of luminescent decay compared to higher lying states means that the effects of molecular vibration, which act to increase the radiative decay probability, become increasingly apparent, leading to the dominance of the vibronic modes in the emission spectrum. This effect has been noted by Meskers et al in investigations into the relaxation of excitons in films of PPV derivatives[11]. At low concentration where interchain separation in greater the importance of vibrational modes becomes less important as fewer excitons are able to migrate to low-energy defect states and so the 0-0 mode grows relative to the 0-1 transition. Self-absorption is also attributed to significant changes in the band shape of the emission spectra. In the most concentrated samples the 0-1 mode approaches a similar intensity to the 0-0 mode and the 0-0 mode is narrow compared to more the emission spectra of more dilute samples. From this it is suggested that the blue emission tail is being re-absorbed thus narrowing and reducing the relative height of the 0-0 emission band.

Anisotropy measurements have been less conclusive. The anisotropy of the most dilute film was recorded. In agreement with the implications of lifetime and spectral analysis, the value was high, almost the maximum indicating that that sample is well aligned and inferring the absence of energy transfer, which is commonly attributed to loss in polarisation. Attempts to establish a

trend in anisotropy with dilution have been unsuccessful and instead produced evidence of inhomogeneous patches of anisotropy across the 0.1% w/w film. It is also expected that solutions of OF2/6 in the host may degrade over time. The causes of this are put forward as a suggestion for further research though not for the purposes of this investigation. In view of these finding anisotropy has been identified as an unreliable measurement for dilute samples; < 0.1% w/w having little scientific confidence, though on a purely empirical level it may be noted that the anisotropy measured at low concentration does support the suggestion of isolation proposed by lifetime and spectral analysis.

A general finding of ensemble measurements of dilute films is that it is often very difficult to make accurate measurements using equipment designed for experiments on concentrated samples. Low emission, characteristic of dilute films approaching isolation, made the use of a cryostat impractical and has raised the need for specific repeatable and accurate sample positioning within the fluorospectrometer. This is particularly necessary for anisotropy measurements where by using polarisers emission was reduced below useful levels unless alignment within the machine was perfect. This made repeated and comprehensive investigations of the anisotropy of dilute samples impractical on the grounds of time.

The accuracy required for the investigation of very dilute samples clearly calls for more specific instrumentation, which is the very focus of this report. Concerning sample preparation it is suggested that specific equipment is designated for SMS studies, impurities are very significant at SMS sample dilutions whereas they are unimportant in more concentrated samples prepared for other applications. Items of general use in the group such as glassware, tweezers, spin coaters and significantly spectrometer sample holders have been the source of frequent contamination of samples or their emission spectra. This makes identification of spectral trends very difficult and leads to much time being spent unproductively cleaning municipal equipment and remaking

contaminated samples. It is therefore recommended that an area be set aside for sample preparation of single molecule films.

The combined findings of high anisotropy, large spectral blue shift and mono-exponential lifetime in the 1x $10^{-4,5,6}$ % concentration films (depending on host) are compelling, suggesting that isolation has been achieved. Bulk measurements have been taken as far as is practical and at this stage it is considered that the work carried out into sample preparation has successfully defined the methodology required to produce films of isolated molecules for SMS.

3.6 References

1. Smilowitz, L., et al., *Time-Resolved Photoluminescence from Poly 2-Methoxy, 5-(2'-Ethyl-Hexyloxy)-P-Phenylene-Vinylene - Solutions, Gels, Films, and Blends.* Journal of Chemical Physics, 1993. **98**(8): p. 6504-6509.
2. Rothberg, L.J., et al., *Photophysics of phenylenevinylene polymers.* Synthetic Metals, 1996. **80**(1): p. 41-58.
3. Nguyen, T.Q., V. Doan, and B.J. Schwartz, *Conjugated polymer aggregates in solution: Control of interchain interactions.* Journal of Chemical Physics, 1999. **110**(8): p. 4068-4078.
4. Bliznyuk, V., et al., *Self-assembled nanocomposite polymer light-emitting diodes with improved efficiency and luminance.* Advanced Materials, 1999. **11**(15): p. 1257-1261.
5. Setayesh, S., et al., *Polyfluorenes with polyphenylene dendron side chains: Toward non-aggregating, light-emitting polymers.* Journal of the American Chemical Society, 2001. **123**(5): p. 946-953.

6. Jakubiak, R., Z. Bao, and L. Rothberg, *Dendritic sidegroups as three-dimensional barriers to aggregation quenching of conjugated polymer fluorescence.* Synthetic Metals, 2000. **114**(1): p. 61-64.

7. Higgins, R.W.T., et al., *Effects of singlet and triplet energy transfer to molecular dopants in polymer light-emitting diodes and their usefulness in chromaticity tuning.* Applied Physics Letters, 2001. **79**(6): p. 857-859.

8. Cerullo, G., et al., *Ultrafast Forster transfer dynamics in tetraphenylporphyrin doped poly(9,9-dioctylfluorene).* Chemical Physics Letters, 2001. **335**(1-2): p. 27-33.

9. List, E.J.W., et al., *The effect of keto defect sites on the emission properties of polyfluorene-type materials.* Advanced Materials, 2002. **14**(5): p. 374-378.

10. Dias, F.B., et al., *Picosecond conformational relaxation of singlet excited polyfluorene in solution.* Journal of Chemical Physics, 2003. **118**(15): p. 7119-7126.

11. Meskers, S.C.J., et al., *Relaxation of photo-excitations in films of oligo- and poly(para-phenylene vinylene) derivatives.* Chemical Physics, 2000. **260**(3): p. 415-439.

12. Dias, F.B., et al., *Fast and slow time regimes of fluorescence quenching in conjugated polyfluorene-fluorenone random copolymers: The role of exciton hopping and dexter transfer along the polymer backbone.* Macromolecules, 2006. **39**(4): p. 1598-1606.

13. Moerner, W.E. and D.P. Fromm, *Methods of single-molecule fluorescence spectroscopy and microscopy.* Review of Scientific Instruments, 2003. **74**(8): p. 3597-3619.

14. Lakowicz, J.R., *Principles of Fluorescence Spectroscopy.* 2nd Edition ed. 1999, New York: Kluwer Academic/Plenum Publishers.

4. Single Molecule Spectroscopic Methods

4.1 Single Molecule Fluorescence Spectroscopy

The complex task of detecting a single molecule amongst trillions of ostensibly transparent matrix molecules requires two deceptively simple steps: isolating a single molecule inside the excitation volume, and ensuring that the signal from that molecule dominates any interfering background emission. These considerations must be carefully met through well-chosen fluorophores and meticulous sample preparation, coupled with the construction and implementation of a robust and reliable experimental method.

In order to detect a single molecule successfully through its fluorescence, the subject fluorophore must have suitable photo-physical characteristics. Both the emission and absorption spectrum of the molecule should be considered along with its absorption cross section, fluorescence quantum yield, excited state lifetime and photo stability. Well chosen compounds are essential if the signal is to be discerned from the noise, similarly close attention should be given to minimising background influences such as laser shot noise, reflectance or out of focus fluorescence emission.

4.1.1 Signal Size

To optimise signal-to-noise, probe molecules should have strongly allowed absorption transitions and a high fluorescence quantum yield. The efficiency of absorption is described by the absorption cross section of the molecule which effectively relates to the area available for photon capture. Equation 1 describes this parameter and it can be seen that apart from the

inherent characteristics of the molecule, the absorption cross section is also strongly influenced by the wavelength of the excitation source, being higher at longer wavelengths.

$$\sigma = 2\pi\left(\frac{\lambda}{2\pi}\right)^2\left(\frac{\gamma_r}{\Gamma_{tot}}\right) \qquad \textbf{Equation 1}$$

Where:

λ: excitation wavelength

γ: spontaneous fluorescence rate

Γ_{tot}: total frequency width of absorption.

Another useful expression for the cross section is expressed in terms of the molecular extinction coefficient ε, and Avogadro's number shown in equation 2.

$$\sigma = \frac{2.303\varepsilon}{N_A} \qquad \text{Equation 2}$$

Regardless of the description, aside from the excitation wavelength, those molecules that exhibit large values of σ are those with strongly allowed electric dipole transitions. In these cases the value of σ approaches the molecular size which is typically of the order of angstroms[2][1, 2].

As excitation power increases so does the rate of photon emission until the transition becomes optically saturated. The saturated state places a limit on the maximum value of the absorption cross section and occurs when the average time between successive photon absorption becomes comparable with the excited state lifetime. In this situation, the rate of absorption becomes so high that there is insufficient time for the molecule to decay back to the ground state before the arrival of the next incident photon, resulting in a bottleneck and reduction in

absorption efficiency, which destroys the otherwise linear relationship between excitation intensity and fluorescence.

Optical saturation intensity scales inversely proportionally with the fluorescence lifetime, therefore for a typical fluorescence lifetime of the order of nanoseconds, optical saturation only becomes problematic at frequencies above 100 MHz[2]. Unfortunately however, intensity is often additionally limited by intersystem crossing into dark states such as the triplet state[3]. Occupation of the triplet state changes the luminescence properties of the fluorophore and reduces the maximum repetition rate to $\frac{1}{(2+k_{ISC}\tau_{triplet})}$, where k_{ISC} is the rate of intersystem crossing and $\tau_{triplet}$ is the lifetime of the triplet state. This places a further restriction on the maximum absorption cross section of the molecule and makes molecules with weak triplet bottlenecks preferable candidates for SMS to those where intersystem crossing is high.

As mentioned earlier, the fluorescence quantum yield is another important quantity to consider in maximising signal characteristics. The fluorescence quantum yield describes the probability of radiative decay per excitation event. It can be expressed either in terms of radiative and non-radiative decay rates: k_{rad} and $k_{non\text{-}rad}$ respectively, or in terms of the ratio of fluorescence lifetime to radiative lifetime.

$$Q = \frac{k_{rad}}{k_{rad} + k_{non-rad}} \qquad \text{Equation 3a} \qquad Q = \frac{\tau_F}{\tau_{rad}} \qquad \text{Equation 3b}$$

For many fluorescent molecules, radiative transition competes with many other non-radiative pathways where the energy of the excited state is transferred to the embedding medium via collisional interactions or through other electronic energy transfer routes. The fluorophores

with characteristically high photoluminescence quantum yields (PLQYs) are those with relatively rigid structures, this configuration prevents decay routes via rotation, vibration etc... leaving radiative decay as the primary path for relaxation[4].

A factor which affects both quantum yield and absorption is the photostability of the molecule. Photostability is arguably the most restrictive factor in any single molecule experiment, defining the maximum number of photons that can be detected. It describes the number of excitation cycles that a molecule can withstand before irreversible chemical changes alter the molecule so that its fluorescent properties are destroyed. This typically occurs after the emission of 10^6 photons[5] though this number can vary widely and is strongly dependent on the embedding medium. In many cases photo-destruction is associated with photo-oxidation of the fluorophore[6], an effect that can be reduced by operating in a vacuum or flooding the sample with an inert gas such as argon or nitrogen to displace any oxygenic molecules.

In view of these photophysical parameters the expected emission from a relaxing fluorescent molecule can be defined in terms of the excitation power, P and frequency υ, along with the detection efficiency of the system such that[7]:

$$s = \frac{DQ\sigma P}{Ah\upsilon} \qquad \textbf{Equation 4}$$

Where:

D is the collection efficiency of the detection path

h is Plank's constant.

A is the cross-sectional area of the focussed excitation beam.

Q is the fluorescence quantum yield.

σ is the absorption cross section.

ν is the excitation frequency.

4.1.2 Background

Whilst choosing a molecule with good photophysical properties is an important consideration in SMS, it only represents one side to the successful detection of a single molecule. Reduction of background signal is undisputedly the most important aim of most single molecule experiments: detecting fluorescence from a single molecule is not difficult; the difficulty lies in *not* detecting anything else. Even tiny amounts of stray excitation light or external scattering are more than enough to completely swamp a single molecule emission and careful planning should be made to reduce its destructive effects.

In single molecule investigations, noise and background arise from a variety of physical and mechanical sources. In any experiment, there are various contributions such as dark counts and cosmic events which are inevitable though they are generally low and fairly constant. Fundamentally, problems in detection are attributed to background which fluctuates; whereas constant noise sources are easily subtracted from the emission signal, variable background emission can easily obscure single molecule fluorescence. The main sources of constant background offsets are DC offset and dark counts and can often be reduced by the choice of a high quality detection system. A DC offset is often present in charged couple devices and results in counts despite zero-light and zero-dark count conditions, while dark counts are electronic in origin and scale linearly with integration time. Detectors that are either cooled of have very small active areas are particularly successful in reducing these sources of noise. Another source of inevitable noise is Poisson noise, which is inherent in any experiment

which relies on integrated detection; it can only be reduced by statistical methods. So, with these factors aside, the main concern of those designing and implementing SMS are those sources which originate either in the detail of the experimental set-up, or from physical phenomena within the sample itself, factors which can be significantly reduced by careful optimisation of the spectroscopic and microscopic system. With regard to this, the two main categories of background emissions will now be discussed; emission resulting from experimental limitations: optics and lasers, and emissions arising from within the sample itself.

Rayleigh scattering of the excitation beam, residual fluorescence from optical parts and residual excitation emission from the red-shifted spectral range (a particular problem in diode lasers) can in the most part be suppressed by the use of highly efficient notch filters and dichroic optics to spectrally discriminate fluorescence from scattered light. The transmission functions of the emission and filter and dichroic beamsplitter used in this investigation are shown in Figure 1. These high quality filters have been chosen by taking into account a number of significant factors. Particularly important in the choice of filter, besides careful wavelength selection to suit the laser and polymer, is the edge function. Ideally vertical edge functions provide the most accurate filtering allowing a sharply defined transmission range, with minimum transmission from wavelengths situated at the filter boundary. This is particularly important in the confocal set-up as the Stokes shift between excitation and fluorescence light is often small, requiring careful separation of the two different modes. Another important issue is that of transmission, clearly in single molecule investigations emission levels are characteristically very low, consequently, care should be taken to choose filters with the highest possible transmission functions, as well as carefully optimised deep blocking of the transmission pass-bands for maximum signal to noise ratios. It can be seen

from figure 1 that the transmission function of the filters used in this investigation are greater than 90% allowing the detection of as much emission as possible.

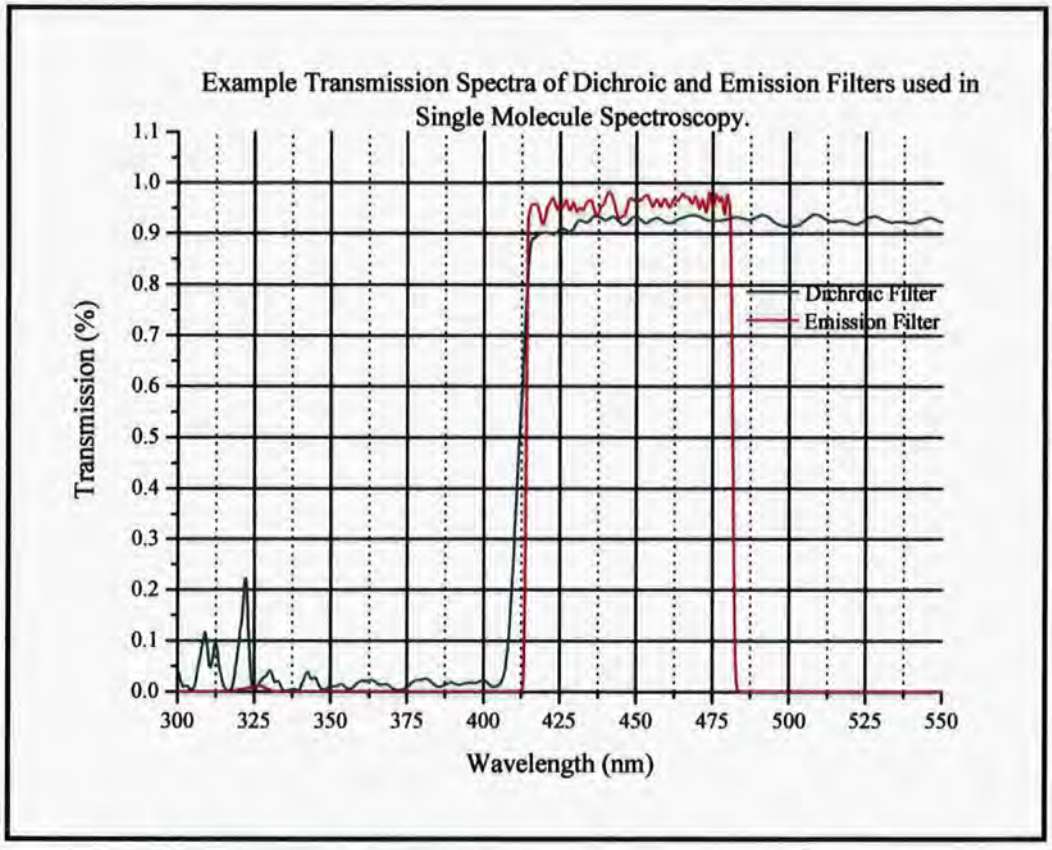

Figure 1: *Transmission spectra for Semrock Brightline dichroic and emission filters, Laser 2000.* The dichroic filter is used to reflect light in the emission band and transmit light in the excitation band. The emission filter is typically a notch or bandpass filter designed to block all external light sources, particularly the excitation beam, and pass only the narrow range of wavelengths associated with the sample fluorescence.

Raman scattering along with other background emissions from within the sample itself are often more difficult to suppress due to spectral overlap with the fluorescence emission. As far as impurities and molecular defects are concerned, careful sample preparations using high quality, high purity materials and ultra-pure solvents are the key to achieving minimum levels of interference. Raman scattering from the host matrix, the influence of impurities and background fluorescence are all directly proportional to the illumination volume, and so the most effective way of reducing their contribution is to produce thin dilute films and probe

them using a diffraction limited excitation beam. This demand has lead to the development of various optical designs to minimise the excitation volume and maximise fluorescence collection, of which total internal reflection[8] and epifluorescence[9] have become increasingly well known. In order to collect as much fluorescence as possible, both techniques rely on a wide collection angle, often achieved either through using parabolic mirrors or microscope objectives with high numerical apertures. This investigation adopts the confocal approach, a branch of epifluorescence in which the objective lens that focuses the excitation beam is also used to collect the fluorescence.

Though it is not always possible to be selective regarding the choice of sample, it should be noted that non-resonant scattering intensity decreases approximately with the fourth power of excitation wavelength. As a result fluorophores with absorption peaks in the near infrared region are clearly superior candidates to those which require higher energy excitation, for example, doubling the excitation wavelength increases background scattering by sixteen-fold.

Combining these discussions into a qualitative description, the signal-noise characteristics of the system is described in equation 5[7].

$$SNR = \frac{\frac{DPQ\sigma}{Ah\upsilon}t}{\sqrt{\left(\frac{DPQ\sigma}{Ah\upsilon}+\left(C_bP+N_d\right)t\right)}} \qquad \textbf{Equation 5}$$

Where:

C_b: background count rate per watt of excitation power.

t: integration time.

The considerations for optimising the parameters in this expression have all been previously discussed, with the exception of the detection efficiency D. In practice, the detection efficiency is not solely dependant on the quality of the detector but is affected by the fraction of the total emission collected by the optics, the fraction of emission which passes thorough the filters, and finally the fractional transmission through all other optics. With complex optical parts in use such as objective lenses, this parameter is often difficult to define, though at the least it should be noted that unnecessary optics should be avoided and that those used should be clean (and cleanable).

4.2 References

1. Moerner, W.E. and D.P. Fromm, *Methods of single-molecule fluorescence spectroscopy and microscopy.* Review of Scientific Instruments, 2003. **74**(8): p. 3597-3619.
2. Becker, W., *Advanced Time-Correlated Single Photon Counting Techniques.* 1st ed, ed. J.W. Castleman, J.P. Toennies, and W. Zinth. 2005: Springer.
3. Dittrich, P.S. and P. Schwille, *Photobleaching and stabilization of fluorophores used for single-molecule analysis with one- and two-photon excitation.* Applied Physics B-Lasers and Optics, 2001. **73**(8): p. 829-837.
4. Tammer, M., et al., *Effect of chain rigidity and effective conjugation length on the structural and photophysical properties of pyridine-based luminescent polymers.* Advanced Functional Materials, 2002. **12**(6-7): p. 447-454.
5. Bohmer, M. and J. Enderlein, *Fluorescence spectroscopy of single molecules under ambient conditions: Methodology and technology.* Chemphyschem, 2003. **4**(8): p. 793-808.

6. Singh, S., et al., *Solid-state polymeric dye lasers.* Journal of Luminescence, 2003. **101**(4): p. 285-291.

7. Michalet, X. and S. Weiss, *Single-molecule spectroscopy and microscopy.* Comptes Rendus Physique, 2002. **3**(5): p. 619-644.

8. Funatsu, T., et al., *Imaging of Single Fluorescent Molecules and Individual Atp Turnovers by Single Myosin Molecules in Aqueous-Solution.* Nature, 1995. **374**(6522): p. 555-559.

9. Lang, E., J. Baier, and J. Kohler, *Epifluorescence, confocal and total internal reflection microscopy for single-molecule experiments: a quantitative comparison.* Journal of Microscopy-Oxford, 2006. **222**: p. 118-123.

5. Confocal Microscopy

5.1 Principles of Confocal Microscopy

Confocal Microscopy is one of the most effective methods of maximising sample emission whilst minimising background effects. In conventional fluorescence microscopy, fluorescence is separated from the excitation source by means of optical filtering, usually in the form of a dichromatic mirror, which reflects the excitation and transmits the Stokes shifted fluorescence. When the same objective that focuses the excitation beam onto the sample is also used to collect the luminescence in conjunction with a dichroic mirror, the configuration is know as epifluorescence. Though the confocal principle is based on epifluorescence, it is specifically defined by particular suppression of out of focus light through the addition of a confocal pinhole. When placed at the focal point of fluorescence the pinhole aperture spatially filters out all light emitted from outside of the excitation volume. Figure 1 illustrates this effect using the simple example of light focussed from the focal point of one lens onto the focal point of the other. The dotted rays represent light coming from out of focus fluorescence, this is often the result of absorption of scattered excitation light, which causes fluorescence from impurities or other fluorophores outside the excitation volume, whilst the solid rays emanate from the correct image plane. The image from the out of focus beam converges at a different spatial position to the focussed image such that the aperture the rejects the unwanted fluorescence, whilst some unfocussed out-of plane light will pass through the pinhole, the majority is blocked resulting in efficient attenuation of background signal.

The pinhole aperture determines the absolute depth of field of the confocal image[2], consequently in three dimensional imaging, selection of the aperture diameter is particularly important. Smaller pinhole size gives increasing axial resolution, though this is at the expense of transmission

through the pinhole and increases difficulty in alignment. Due to the limited number of photons available from a single molecule if depth discrimination is not important it is often more efficient to use a slightly larger pinhole to increase transmission and hence improve the signal to noise of the system.

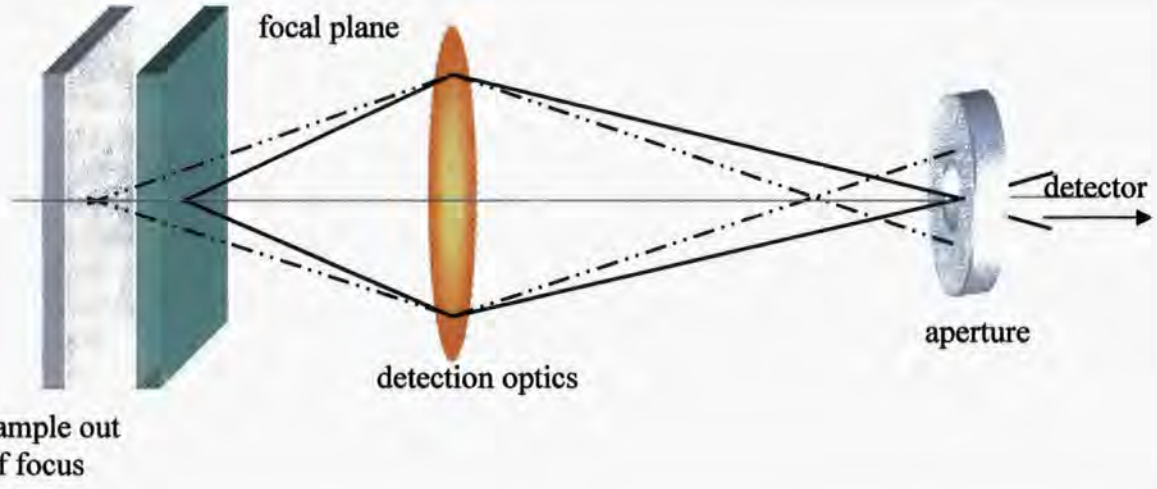

Figure 1: *The principle of confocal detection:* a pinhole aperture is placed at the conjugate focal plane of the imaging optics, only light that comes from near the optical axis and the focal plane is focused onto the aperture. Light originating from points off the optical axis or out of the focal plane is predominantly blocked.

The confocal schematic used in this investigation is shown in figure 2. The system works by directing collimated laser light onto a dichromatic beamsplitter, which reflects the excitation beam onto an infinity corrected high numerical aperture microscope objective. The excitation beam is then focussed down onto a sharp diffraction limited spot at the sample plane whose size is defined by the wavelength of the light and the numerical aperture (NA) of the objective. The sample fluorescence and scattered laser light are collected by the same objective, travel back through the objective and are separated by the dichroic beamsplitter, which transmits the fluorescence and rejects the excitation. The fluorescence then passes though a second filter to remove any laser light that may have been transmitted through the dichroic and is focussed down onto the confocal aperture, which is positioned, directly in front of the detector. In the case of this investigation, the active area of the detector acts as the pinhole due to the reduced need for

axial resolution. The single photon avalanche photo-diode (SPAD) is then linked through to a single photon-counting module, which correlates the photon arrival time with the excitation pulses of the laser to produce a time resolved histogram of the photoluminescence.

A confocal image is created by scanning the sample stage over the sample plane using a computer-controlled piezo-stage, building up the image one pixel at a time. This is in contrast to other single molecule scanning experiments, which employ a laser scanning technique involving a series of mirrors which move the excitation beam across the sample[3]. An important advantage of specimen scanning is that the optical arrangement is stationary and so off-axis aberrations such as coma and astigmatism are inherently absent giving superior imaging and high optical efficiency. It is of course not without disadvantages, despite good image quality, scan speed in specimen scanning is low, typically 10 to 150 lines per second at most, furthermore, when looking at larger samples, for example living specimens, there is concern that mechanical resonance within the specimen causes it to move relative to the stage resulting in distortion and potential rupture. These concerns are however, thought to be minor compared to the benefits of specimen scanning for single polymer chain applications.

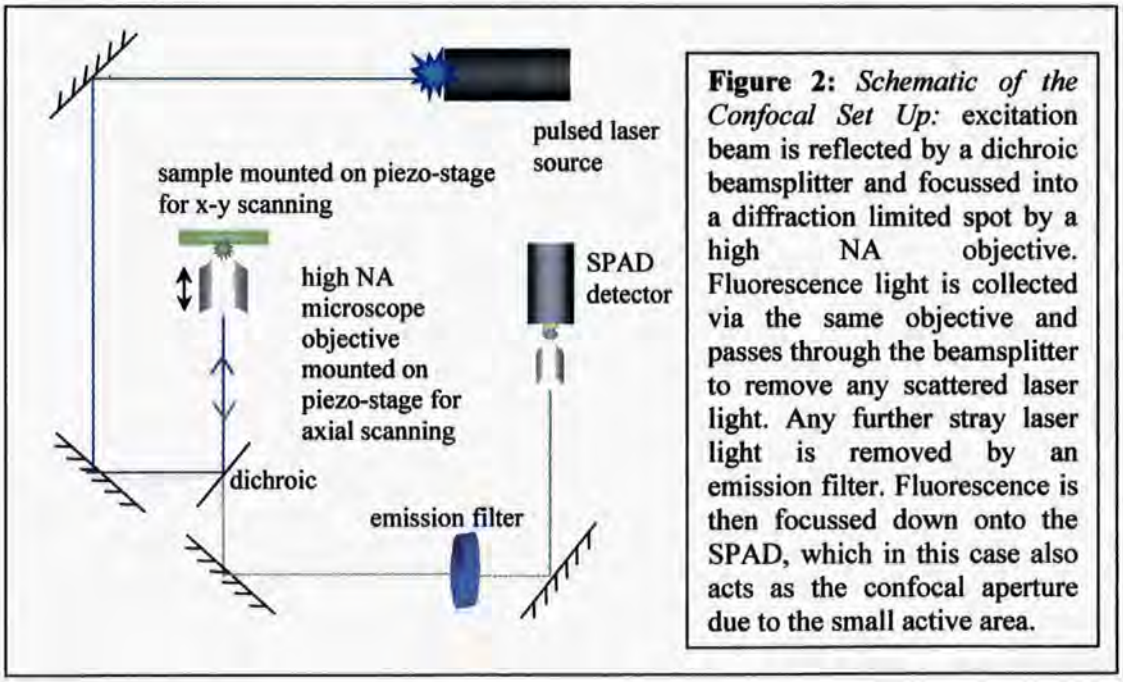

Figure 2: *Schematic of the Confocal Set Up:* excitation beam is reflected by a dichroic beamsplitter and focussed into a diffraction limited spot by a high NA objective. Fluorescence light is collected via the same objective and passes through the beamsplitter to remove any scattered laser light. Any further stray laser light is removed by an emission filter. Fluorescence is then focussed down onto the SPAD, which in this case also acts as the confocal aperture due to the small active area.

5.1.2 Reflections in Optical Systems

Reflections are common in any optical system; originating from sample scatter, lens surfaces, filters, lens holders or any number of other passive design elements. Particularly problematic are those components that have highly reflective surfaces such as neutral density filters and detector elements, which often cause back reflection of the excitation beam onto the sample and/or multiple reflections along the optical pathway.

Reflections are particularly important in time correlated single photon counting causing distortions to the effective instrument response function (IRF). As long as the reflections are the same for the recorded fluorescence and the IRF, the result is simply that the recorded curve appears distorted. Nonetheless, because of the difference in excitation and emission wavelengths this is often not the case leading to noticeable errors in lifetime measurements and numerous other experimental readings. Back reflections are particularly troublesome as they are often picked up by the microscope objective and re-focussed onto the sample stimulating a second emission event that is not correlated with the laser. If back reflection is a problem in the optical set-up, neutral density filters can be substituted for absorptive filters. Unlike ND filters, absorptive filters do not need collimated light and so they can be placed at an angle to the beam to divert any back reflection away from the optical path. In practice, any design must meet a compromise between reflections and efficiency; reflected light can be directed away from the optical axis by tilting the critical part or by placing it in a non-collimated part of the beam, but it must be decided whether the changes that such adaptations incur (IRF broadening etc..) can be tolerated or not.

5.2 Experimental

5.2.1 Experimental Set-Up

The confocal optical set-up for this investigation is shown in figure 3. This section will describe in specific terms the instrument specifications and capabilities of the experiment.

Sample

Polyfluorene has emerged as a particularly promising candidate for efficient blue light emitting LEDs[4-11]; it has a good photo luminescent quantum yield, is thermally stable and is easily dissolvable in a variety of solvents[12]. It has been selected for its interesting photophysical properties, which can be measured once the system is working whilst its PLQY and stability are useful for locating and measuring molecules during calibration.

Excitation

The excitation source is a *PicoQuant* 390nm diode laser pulsed at 65 picoseconds. At the maximum frequency, 40Hz, the optical power is 1mW ± 10%. The 390nm laser was chosen for its well-collimated beam and suitability for polyfluorene excitation.

Dichroic

The dichroic edge filter is a *Semrock Brightline* dichroic beamsplitter. It is positioned at a 45° angle to the excitation beam in order to reflect it into the microscope objective and allow the transmission of the fluorescence. It has < 5% transmission below 400nm and greater than 90% transmission above 400nm.

Objective

The excitation beam is focussed using a Plan Achromat microscope objective, Numerical Aperture 0.65, magnification x40. The working distance for a Plan Achromat with NA 0.65 is 0.56mm from the coverslip, which for the particular objective used is 0.17mm thick.

The depth of field of an objective lens gives the axial range through which the objective can be focussed without significantly reducing the image sharpness; within this region, the image is considered to be in focus. Depth of field is determined by a combination of wave optics at high numerical aperture and at lower numerical aperture by the geometrical optical depth. Equation 1 gives the total depth of field:

$$d_{tot} = \frac{\lambda n}{NA^2} + \frac{n}{M \cdot NA} r_{detector} \qquad \textbf{Equation 1}$$

Where

n: refractive index of the imaging medium i.e. air, oil.

$r_{detector}$: resolution of the detector

M: magnification of the objective

Using equation one, a detector resolution of 268* nanometers, the refractive index of air as 1 and an excitation wavelength as 390nm, the depth of field of the microscope objective is:

$$d_{tot} = 0.93\mu m$$

The microscope is therefore expected to be in focus at a distance of 560 ± 0.93μm from the coverslip.

* See section 7.1 for calculation of confocal resolution.

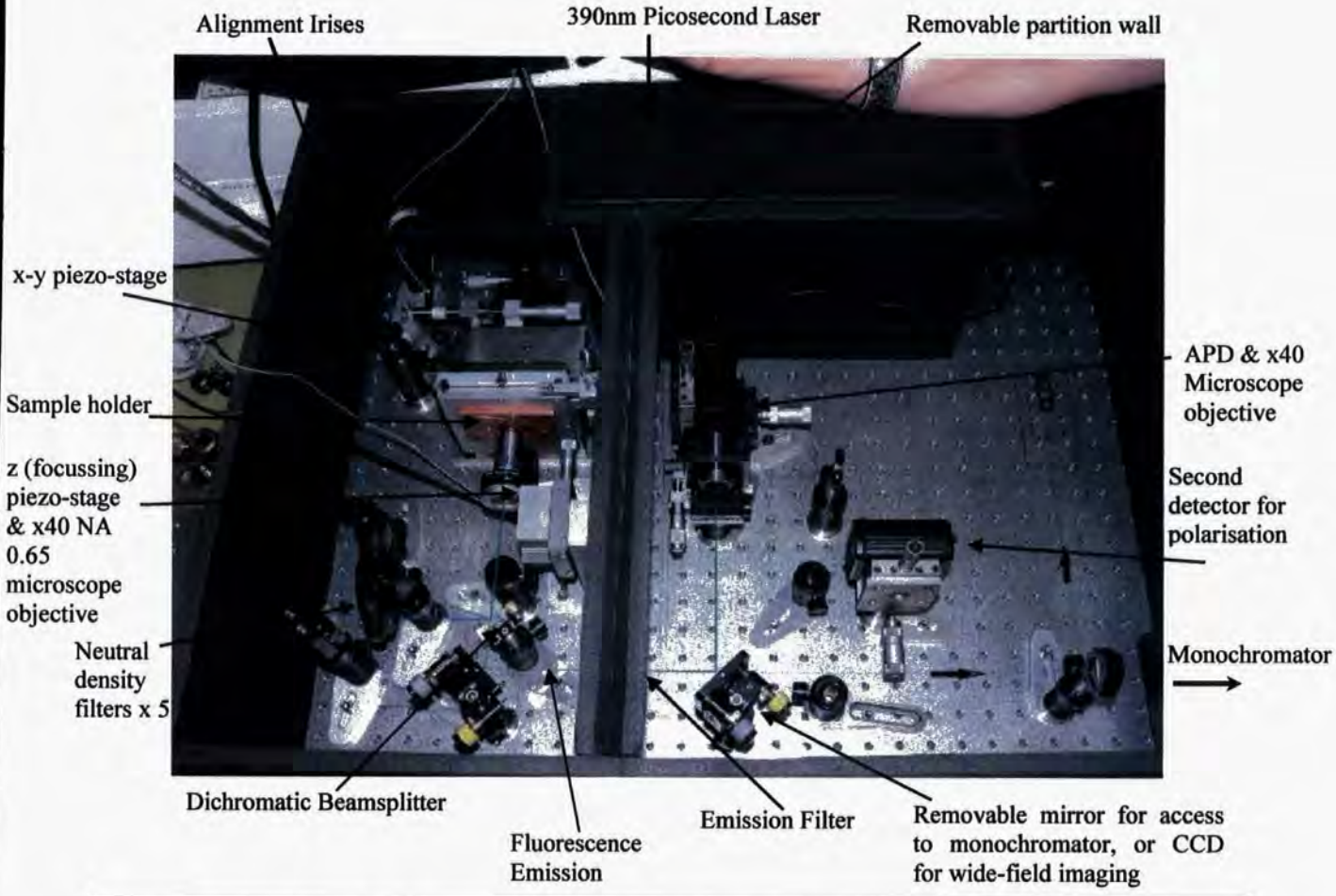

Figure 3: The confocal microscope set up for lifetime and imaging experimentation. The design also allows for the inclusion of a polarising beamsplitter cube between the two detectors. Whilst empty post holders correspond to the lenses required for wide-field imaging and for focussing the fluorescence beam onto monochromator for spectral measurements. These two modes are accessed by removing the final mirror and directing the luminescence either onto a cooled CCD (marked) or by focussing it onto the monochromator and cooled CCD (off to the right).

Emission Filter

The emission filter is interchangeable so that the appropriate transmission function may be selected according to the emission spectrum of the sample under investigation. All filters are *Semrock Brightline* filters purchased from *Laser 2000,* the *Brightline* filters are made with a single piece of glass coated with hard thin-film glass coatings, this makes them durable and resistant to shifting and laser damage. Single molecule spectroscopy suffers severe image degradation if the optical components become dirty, and so filters that are hardwearing and cleanable have been specifically chosen.

Collection Objective

The collection objective is identical to the excitation objective [NA 0.65, magnification x40 coverslip thickness 0.17mm]. The choice of a high NA objective to focus the emission is intended to increase detection efficiency; producing a very tight focal spot the maximum amount of fluorescence is delivered to the $20\mu m^2$ active area of the detector, reducing the amount of wasted photons.

Exterior light

The entire experiment is surrounded by a protective box to exclude external light. It was quickly obvious that good SNR is difficult to achieve even in normal darkroom conditions where LEDs on the laser and other electronic components can pollute the signal. Exclusion of background light is fundamentally important for single molecule spectroscopy where emissions are so low, and so the protective box was designed. It is partitioned into three compartments, which are explained below.

Because the laser requires numerous cable connections and in some cases ventilation for the cooling system, the laser is housed separately so that the cables can leave the box and the lid can be removed to allow air circulation without exposing the remaining optics to exterior light. The sample is housed separately from the detectors to form a "light-lock" between the laser compartment and the detector chamber. Any scatter from mirrors, the sample itself, and light that has escaped through from the laser compartment is confined to this area, keeping the detection chamber light-tight. The passage between the detection and sample compartments is a slot into which the emission filter fits tightly so that only fluorescence can pass through.

The box is designed so that each compartment is accessible via separate lids for reasons of practicality, allowing adjustment of the stages and sample whilst the detectors are still running. This is useful both during alignment and when manually locating molecules which can now be done without the signal being dominated by external light. Another useful design feature is that the partition wall is removable; this makes alterations of mirrors and other optics much more practical, allowing adjustments without having to remove the entire box. The partition wall slides into a deep track to ensure it is light tight at the edges and has a foam base to make it sit well with the optical bench. Cable holes are sealed using washers and brushes and finally, any scattering between optics and the box has been reduced by coating the box with ultra low-reflectivity (99% matt) black paint – *Mankiewitz.*

Detector

There are essentially two types of detectors that are used within single molecule experimentation, two dimensional array detectors and single element detectors. The two dimensional (CCD) array detector is widely used in wide-field spectroscopy whilst single element detectors are more common place in confocal systems[13], nonetheless both have the same requirement for high quantum efficiency and low background levels to conform to the tight signal to noise requirements of single molecule spectroscopy.

The detector used in this investigation is an *id Quantique id100-20* Single Photon Avalanche Photodiode; a single element detector. The SPAD has been developed following recent improvements in semiconductor photo-detection; it achieves ultra-sensitive detection at low intensity, has excellent quantum efficiency and dark counts as low as 20 dark counts per second[1].

The SPAD is essentially a *p-n* junction with a reverse bias set above the breakdown voltage producing an electric field high enough to sustain flow of an avalanche current triggered by the incoming photon flux[14]. The avalanche current continues until it is quenched by lowering the current below the latch current, in the *id100-20* this is achieved using an active quenching circuit; fast transistors triggered by the breakdown pulse quickly lower then reset the bias voltage, giving it very good time resolution. In order to reduce thermally generated dark counts and ensure fast single photon timing the single photon avalanche photodiode is designed with a characteristically small active area, $20\mu m^2$ for the *id Quantique*. In other fields, this is sometimes seen as a disadvantage however in confocal experimentation the image plane can easily be made to under-fill the detector chip. The small active area can even be used as a confocal aperture in place of the pinhole when accurate pinhole definition is not important. Discussions of the effect of pinhole size demonstrate that this is true when the image plane is 2D since the pinhole has the greatest advantages for sectioning along the excitation axis rather than along the image plane[2]. In this investigation into conjugated polymers, the image plane is assumed to be 2D at single molecule level, such that the *id Quantique* was chosen specifically to use the small active area as the pinhole, as well as the good specifications it offers in terms of time resolution and noise.

The specifications of the *id100-20* are described in by the manufacturer and illustrated in the figures above. Whilst the Quantum Efficiency peaks at 500nm with 35% it is considerably lower at the peak emission of the isolated polyfluorene, which lies at ~405nm. Nonetheless, drawbacks in quantum efficiency are compensated by excellent time resolution and low dark counts of 40ps and 20c/s respectively.

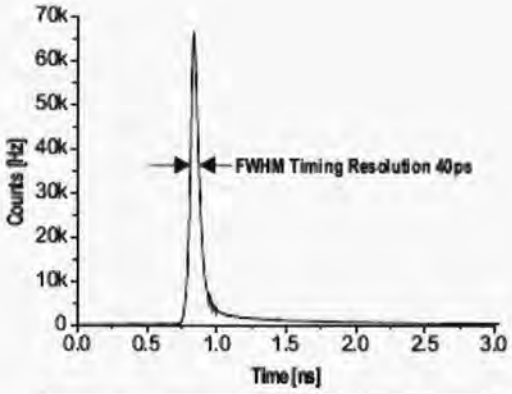

Quantum Efficiency:..... ≤ 35 %
Time Resolution:.....40ps
Dark Count Rate:.....20Hz
Dead Time:.....45ns
Maximum Count Rate:.....20MHz
After pulse Probability:.....3%

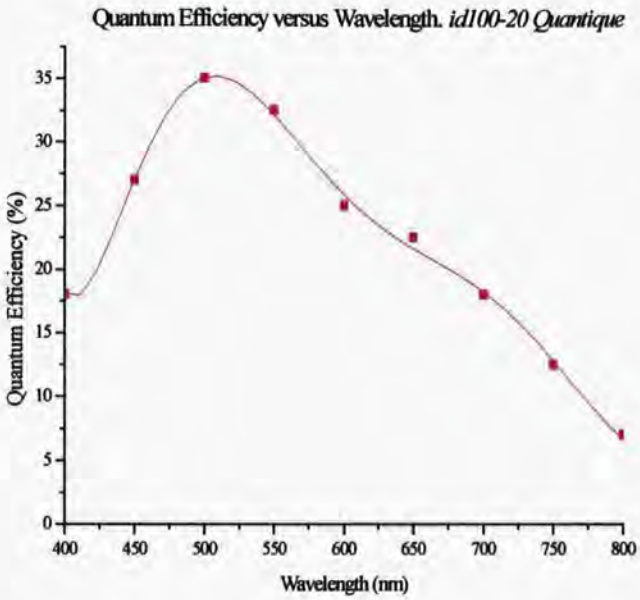

Figure 4: *Clockwise from top left*: Time resolution, Quantum efficiency and other specifications for the *id Quantique id100-20* used in this investigation[1].

5.3 Alignment

5.3.1 Instrument Response Function (IRF)

Having fixed the necessary optical components into their approximate positions the laser was aligned. Initial experiments were made using the ladder type MeL-PPV II due to the initial inavailability of the 390nm diode laser. During this time, a pulsed 475nm diode laser was used and MeL-PPV was used as a sample accordingly. In fact, the 475nm excitation source was not ideal for the MeL-PPV exciting right at the tail of its absorption spectrum and both a change in polymer and laser were made some months later when the 390nm diode laser became available. The alignment techniques used for both lasers were very similar although the 390nm laser did not need to be collimated externally.

In order to measure the degree of alignment the instrument response function was used as a reference. The instrument response function is an important feature in photon counting, and alignment is principally aimed at making the measured instrument response function as close to the actual instrument response function† as possible.

The IRF was measured by placing a mirror in the confocal sample plane and removing the emission filter. Using the adjustable mirror mounts, the beam path was moved first so that it was parallel to the optical bench. This was done by adjusting the laser first close to the point of reflection and then at a point as far as possible from the point of reflection to reduce small angle effects on the beam.

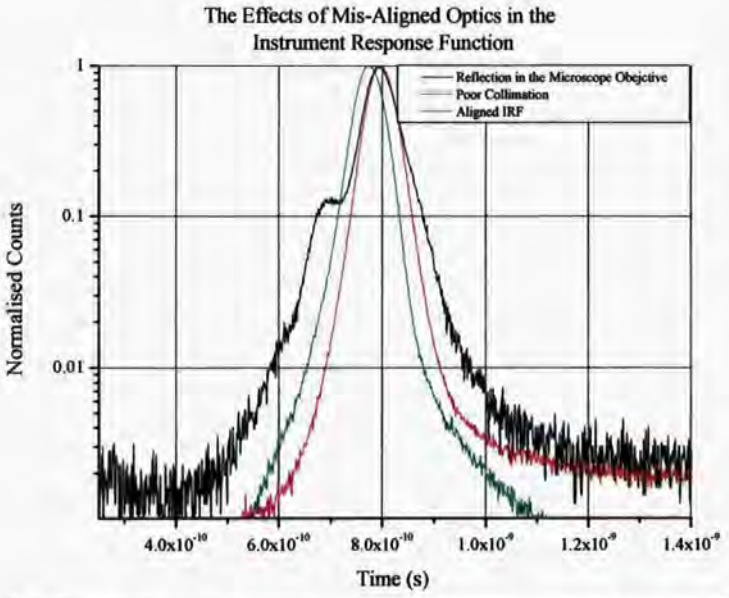

Figure 5: The least obtrusive effect of miss-alignment is elongation of the beam path resulting in a shift in the IRF. The black pulse is thought to be a result of reflections inside the microscope objective causing the excitation beam to be reflected before it reaches the sample. This can come about through the objective being slightly off axis or being skewed in relation to the beam

Once the beam was parallel, the microscope objective was positioned so that the excitation beam was incident at the centre of the objective lens. This was found to be a fundamental part of the alignment. If the objective does not lie accurately on the optical axis then severe reflection of the beam occurs inside the tube causing pre-pulses and distortion of the leading edge of the pulse with the effect shown in figure 5. In fact, most of the primary causes of pulse shape defects were attributed to the microscope objectives, both

† Specified by the manufacturer

sample and detection. The light must be as close to the optical axis and as well collimated as possible to prevent reflections and interference. A summary of three of the most common problems of pulse shape are explained below and are illustrated in figure 6. The last pulse has no pre or after pulses and its shape is almost symmetrical; a pulse with such characteristics reflects a well-aligned system. It should be pointed out that these issues refer to problems arising *after the sample focus has been optimised* i.e. it should be set to give a maximum intensity reading before looking at the issues below.

1. Reflection: the pulse in the top left-hand corner of figure 6 is a typical after-pulse. This is usually caused by a reflection from the ND filter passing all the way back to the primary mirror and then being reflected back again onto the sample. This problem can be resolved by tilting the ND filter so that it is just off 90° to the optical path. It was found that tilting the filter too much could distort the excitation pulse, giving rise to a 'vignetting' effect as the pulse travels through different thicknesses of glass across its diameter. Therefore, by positioning an iris closely surrounding the excitation beam, a very small tilt will be sufficient to remove the reflected beam from the optical path, as the back-pulse is then blocked by the iris edge.

2. Pre-Pulse: this is not entirely understood, however, it is thought to be a result of the excitation axis and the objective axis being mis-aligned causing reflections within the complex lens system of the objective. Alternatively, if the sample is an oblique angle to the objective rather than at 90°, it could be that the laser is back scattered onto the silver objective outer and then reflected back onto the sample before the arrival of the next laser pulse causing further emission that manifests itself as a pre-pulse.

3. Stretch: this can usually be resolved by carefully lining up the active area of the detector with the focus of the detection objective. If they are well aligned, then broadening is usually caused by the focal point of the detection objective falling short of the actual detection chip. Adjustment of the sample focus is also sometimes necessary.

When aligning the optics for this investigation despite carefully checking the beam path and position of the objectives, the IRF was consistently distorted. It was eventually discovered that the mountings built in the mechanical workshop for the objectives were not holding the objectives flat. This was corrected using a pressure sensor, which runs over the objectives on the top and sides to measure their flatness. Following the necessary adjustments, the IRF improved considerably and the final pulse was achieved, making a valuable point that *all* components (not just the optical parts) should be rigorously checked during alignment.

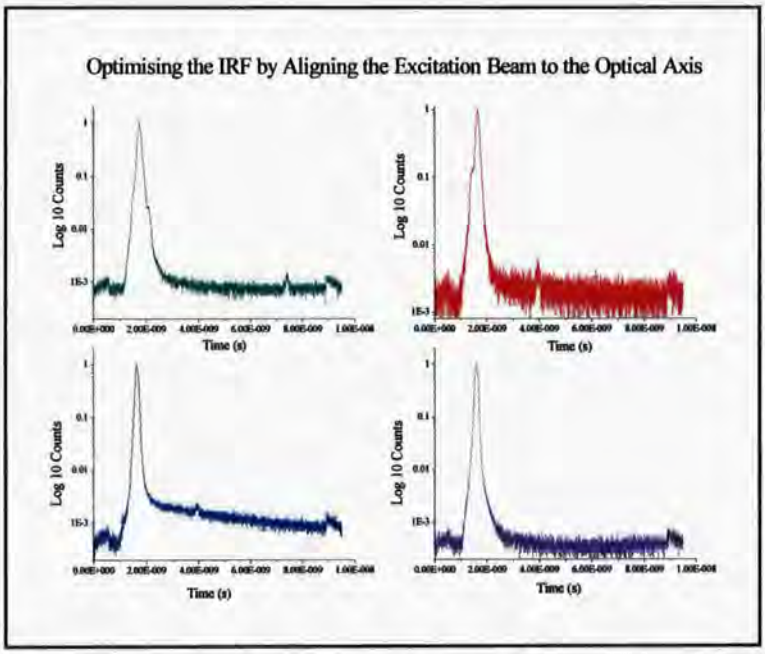

Figure 6: Problems with the IRF shape, numerous forms of reflections can cause pre-pulses and after-pulses whilst poor alignment at the detector end can cause stretching of the pulse shape. A well-aligned pulse is shown in the bottom right hand corner.

Even the best IRF measured through an optical system will often be larger then the actual laser pulse width. Each optical piece contributes to broadening of the IRF and there is a considerable amount of glass involved in the two objective lenses, which contributes to pulse broadening. In addition, the specifics of the detector can cause changes in the recorded pulse, for example, the SPAD used in this investigation suffers from broadening at count rates exceeding 1 x 10^5 counts per second making an ND filter

necessary. The optimised IRF is therefore usually broader than the desired value but should be reproducible, reliable and minimised for the experiment.

5.3.2 Focussing

Earlier calculations (section 5.2.1) of the focal distance give a value of 0.56mm from the coverslip and a depth of field equal to 0.93μm. Distances on this scale are difficult to achieve manually and leave little scope for error. What is more, without a method of calculating the distance between the objective and the sample plane accurately, much of the alignment must be done by guesswork by hand, which is usually inadequate. To overcome this issue, control software has been written to position the objective at the focal distance. Rather than producing an absolute distance calculation, by using a piezo-stage scanner, having manually positioned the objective to the approximate focal position, the objective is stepped along the optical axis over a distance of 100μm using increments defined by the user. At each point, the luminescence from the sample is recorded in order to identify the intensity maximum, a process that assumes that when the laser is focussed maximum power flux on the sample plane will produce maximum emission.

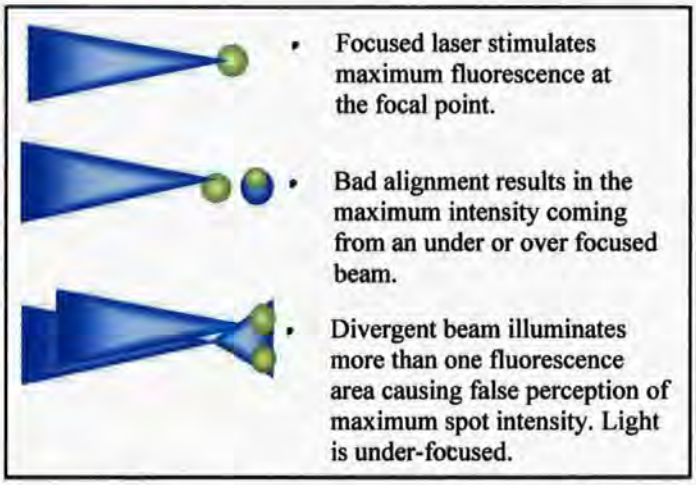

Figure 7: The effect of incorrect focal position. Maximum intensity does not always correspond to a correctly focused beam, in cases b and c the system is distorted by the presence of nearby fluorescent species and/or a mismatch in the position of the optical axis in relation to the target molecule.

This method works well for concentrated films; however, it has been noted from experiments where only a few fluorophores are present that using this method the intensity maximum can be

recorded at out of focus positions. The proposed physical situations behind this problem are shown in figure 7 whilst empirical findings to this effect are shown in figure 8.

Experiments have made it increasingly clear that difficulties arise when the subject of the image does not lie on the optical axis, and the accuracy required to resolve this issue manually is very difficult to achieve, particularly where single molecules are concerned. In the following sections, a scanning program used to build up images is described; briefly, it incorporates the focussing program mentioned above along with x-y scanning over a $45\mu m^2$ to build up a topographical intensity picture. This can be used here to solve the problem of off axis focussing; by running this scanning program twice - first to locate the molecule and second to take the measurement, off axis effects can be considerably reduced. Using a rough guess at the molecule position, the first scan can be relatively crude in terms of pixel size and objective position, having the sole purpose of producing a molecule co-ordinate for the second scan, which is then used to set the molecule in line with the optical axis ready for the desired photophysical experiment.

This technique is satisfactory given that the experiment is still in the early stages of development, and using robust target molecules such as fluorescent microspheres (see later) it has produced good results. Nonetheless, it is thought that this relatively slow method will prove to be inadequate for single polymer molecule investigations.

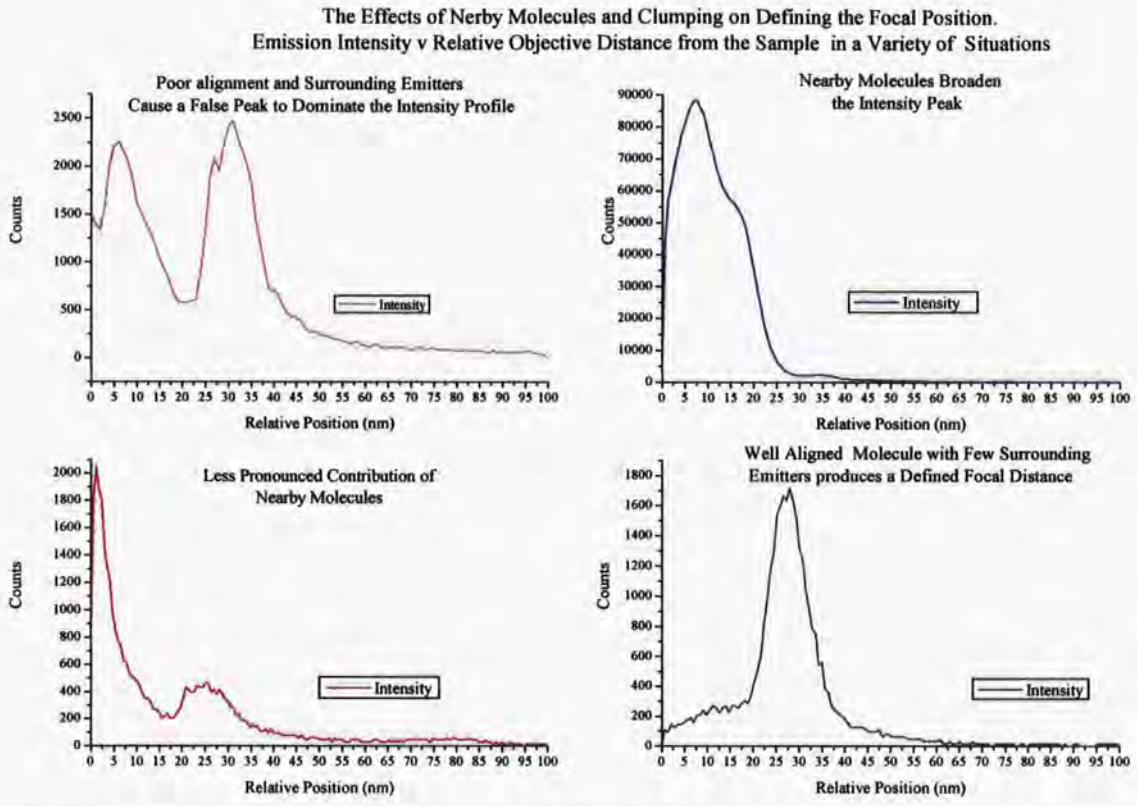

Figure 8: The implications of nearby molecules for focussing based on maximum intensity. Additional maxima are evident in the intensity-distance profile; this is often not a significant problem for this method as in the two left hand graphs. Nonetheless, in the top right figure the worst case scenario is illustrated, here a combination of the molecule being out of alignment with the laser and being surrounded by several other close emitters, combines to make the maximum intensity appear at the 34μm where it was actually found to lie on the first peak at 5μm. The bottom left graph is in correct focus but has been included to demonstrate that were the estimated position a few microns further forward a false position would be detected in the secondary maximum at 25μm. Bottom right is a well-isolated, well-aligned microsphere focus.

The finite emission lifetime of single molecules (governed by photo destruction) limits the total number of emitted photons which are available for both locating the molecule and for the subsequent spectroscopic measurement. The relatively high emission rate required for such photon hungry spectroscopies calls for two principal criteria to be satisfied. Firstly, the molecule should be carefully centred in the excitation volume to give the maximum signal to background ratio, and secondly the time and total number of photons required to do this should be minimized. Manual positioning, done by adjusting the *x-y* piezo-stages or techniques similar to the current method are simply too slow and waste many valuable photons, meaning that a significant number

of molecules are destroyed during the process. In this situation when a molecule *is* eventually found, it is likely to be specifically quite stable and long-lived, thus representing only a small subset of molecules from a larger distribution. Furthermore, it is often the molecules in those less stable environments, which display the most interesting dynamics: spectral jumps or transitions into dark states for example[15]. A final additional consideration is that manual positioning is very tedious and time-consuming, and is difficult to perform on a large number of molecules. Rapid automated positioning is seen to be essential for successful spectroscopy of volatile molecules and will bring the advantage of producing large numbers of data sets, which can be analyzed statistically.

Unfortunately, time constraints have meant that an automated system has not yet been produced, though thought has been given to a possible structure, which is suggested here for future reference. (Reference may be made to chapter 6 for clarification of the scanning system) A program should be built that incorporates the steps already used at present, but with the added advantages that automation brings in terms of speed and precision. Taking two stages, searching and optimisation, the system should scan in the normal imaging mode until the counts rise above a set background threshold. At this point, the step width should reduce and move into the optimisation routine. Here the stages are scanned in the y direction, measuring the peak decay value at each point (this is faster than using raw counts)[‡]. Whenever the measured intensity decreases, the step direction should be reversed, by repeating this over a number of cycles in the x and y direction and then averaging the result, the molecule may be located, despite the effects of noise. If the result of the average is above a pre-set threshold level, the position may then be fixed ready for spectroscopic measurements, otherwise where noise has stimulated the optimization routine or if photo destruction occurs, the loop terminates and resumes the search

[‡] An idiosyncrasy of the single-photon counting module, explained more specifically in chapter 6.

routine. This is thought to be the most efficient way of moving in on a fluorescent entity whilst conserving as many photons as possible for subsequent measurements.

With the focussing and basic alignment considerations in place, the next stage of testing will focus on lifetime measurements, thereby determining system performance in terms of detectable intensity range and accuracy of lifetime readings whilst establishing any as-yet un-noticed problems in the system.

5.4 References

1. *idQuantique, id100-20 product information.* 2006. http://www.idquantique.com/products/files/id100-specs.pdf.
2. Wilson, T., *The role of the pinhole in confocal imaging systems.*, in *Handbook of Biological Confocal Microscopy*, J.B. Pawley, Editor. 1995, Plenum Press: New York. p. 167-182.
3. Liang, S.A. and X.D. Dong, *Progress in single molecule detection.* Chinese Journal of Analytical Chemistry, 2006. **34**(3): p. 421-426.
4. Scherf, U. and E.J.W. List, *Semiconducting polyfluorenes - Towards reliable structure-property relationships.* Advanced Materials, 2002. **14**(7): p. 477-+.
5. Leclerc, M., *Polyfluorenes: Twenty years of progress.* Journal of Polymer Science Part a-Polymer Chemistry, 2001. **39**(17): p. 2867-2873.
6. Liu, B., et al., *Blue-light-emitting fluorene-based polymers with tunable electronic properties.* Chemistry of Materials, 2001. **13**(6): p. 1984-1991.
7. Bernius, M.T., et al., *Progress with light-emitting polymers.* Advanced Materials, 2000. **12**(23): p. 1737-1750.

8. Cadby, A.J., et al., *Film morphology and photophysics of polyfluorene.* Physical Review B, 2000. **62**(23): p. 15604-15609.

9. Grice, A.W., et al., *High brightness and efficiency blue light-emitting polymer diodes.* Applied Physics Letters, 1998. **73**(5): p. 629-631.

10. Kreyenschmidt, M., et al., *Thermally stable blue-light-emitting copolymers of poly(alkylfluorene).* Macromolecules, 1998. **31**(4): p. 1099-1103.

11. Pei, Q.B. and Y. Yang, *Efficient photoluminescence and electroluminescence from a soluble polyfluorene.* Journal of the American Chemical Society, 1996. **118**(31): p. 7416-7417.

12. Tammer, M., R.W.T. Higgins, and A.P. Monkman, *High optical anisotropy in thin films of polyfluorene and its affect on the outcoupling of light in typical polymer light emitting diode structures.* Journal of Applied Physics, 2002. **91**(7): p. 4010-4013.

13. Moerner, W.E. and D.P. Fromm, *Methods of single-molecule fluorescence spectroscopy and microscopy.* Review of Scientific Instruments, 2003. **74**(8): p. 3597-3619.

14. Becker, W., *Advanced Time-Correlated Single Photon Counting Techniques.*, J.W. Castleman, J.P. Toennies, and W. Zinth, Editors. 2005, Springer. p. 217.

15. Xie, X.S. and J.K. Trautman, *Optical studies of single molecules at room temperature.* Annual Review of Physical Chemistry, 1998. **49**: p. 441-480.

6. Time-Domain Lifetime Measurements

Temporally resolved photoluminescence measurements allow the observation of many dynamic molecular events that remain hidden in the steady state. Though they often involve complicated and expensive equipment due to the nanosecond time-scale of fluorescence, the benefits of time resolution are significant, and many important phenomena have come to light since the development of time resolved techniques, notably much conformational information along with decay dynamics, quenching and resonance energy transfer, few of which can be accurately observed through the steady state[2].

This section will describe the principles of time-resolved decay measurements and specifically Time Correlated Single Photon Counting (TCSPC). Calibrating the TCSPC module to the confocal microscope constitutes an important part of the experimental construction, not only is it necessary to optimise the SPC performance, but lifetime measurements can also be used to highlight any remaining mis-alignment or other deficiencies in the design. Reflections and aberrations caused by inaccurate optical set-up or bad experimental procedure readily affect the time resolved luminescence curves and may be frequently identified by certain characteristic faults in the fluorescence decay. This is in fact a useful indication of the type of optical alterations that are required when the experiment is not working correctly, which in other circumstances are often very difficult to identify.

Following careful adaptation of the SPC settings to refine the instrument response function, decays obtained from the confocal microscope will be compared to decays taken using an established (ensemble) time resolved system in order to measure performance and accuracy. Once results can be produced confidently, following chapters will go on to use the single photon counting module to measure the lifetimes of dilute polymer films.

6.1 Fluorescence Decay [3]

Excitation of a fluorescent sample stimulates an excited state population that will immediately begin to relax back to the ground state through a combination of radiative and non-radiative decay mechanisms. This is described for the ideal situation of a delta-like laser pulse in equation 1.

$$\frac{dn(t)}{dt} = -(k_{rad} + k_{nr})n(t) \qquad \textbf{Equation 1}$$

Where:

$n(t)$: number of excited molecules at time t.

k_{nr}: non-radiative decay rate

k_{rad}: radiative decay rate.

The decay from the excited state is a random process and results in a characteristic exponential intensity decay over time. Since the total fluorescence emission is proportional to the number of excited molecules, the exponential decay can be described in terms of time dependant intensity $I(t)$ such that:

$$I(t) = I_0 \exp\left(-t/\tau\right) \qquad \textbf{Equation 2}$$

Where:

I_0: intensity at time zero.

τ: inverse of the total decay rate $(k_{rad}+k_{nr})^{-1}$

Using this relationship the fluorescence lifetime τ, which is the inverse of the total decay rate, can readily be calculated from either a ln scale plot of the time resolved photoluminescence or, from the time it takes the intensity to fall to $1/e$ of the initial value.

In practice this description is often too simplistic; frequently, due to various energy transfer processes there will be more than one decay mode present in many fluorescent samples. Multiple exponential decays are often observed in the solid state where more than one fluorophore is present, an effect that is particularly pronounced in polymeric materials where conformational variation and the effects of donor-acceptor systems increase the number of decay routes. Such configurations require multiple exponential descriptions such as that of equation 3.

$$I(t) = \sum_i \alpha_i \exp\left(\frac{-t}{\tau}\right) \qquad \textbf{Equation 3}$$

Where:

α: decay amplitude.

Clearly, any curve can be described by a series of exponentials and so whilst multi-exponential fits do have a place, it becomes difficult to draw conclusion from many-exponential fits as the weighting of each component can vary widely (in relation to each other) whilst still producing the same fit. Otherwise said, persistence in fitting a curve with 5,6,7... exponentials does not yield a great deal of physical information, here it is perhaps useful to note the multi-exponentiality and conduct other measurements to investigate further.

6.2 Time Correlated Single Photon Counting (TCSPC)

TCSPC is a digital technique, which counts photons that are time-correlated in relation to the excitation pulse.

In traditional systems a pulsed laser or flash lamp is used to excite the sample and stimulate fluorescence emission. The module records the time delay between excitation and the onset of fluorescence in one of two ways which both use a Time to Amplitude Converter (TAC). The TAC is effectively a voltage ramp that is either triggered by the excitation synchronisation pulse (SYNC) or the following fluorescence pulse. Then, depending on the configuration, the voltage rises linearly until either the next fluorescence photon or sync pulse is detected (whichever triggered the ramp the other will stop it: i.e. sync trigger-fluorescence halt). When the ramp is halted, a signal is sent through to a Multi Channel Analyser (MCA) with a voltage directly proportional to the time between the laser pulse and the excitation detection. The MCA then converts the signal into a time channel using an analogue to digital converter (ADC) and adds the result to a frequency histogram of counts versus time to produce a luminescence decay curve[4].

Most modern SPC modules favour the modified method of a fluorescence trigger rather than using the excitation pulse, which was the original triggering sequence. The reason for this is that the TAC is one of the main rate-limiting components in modern TCSPC, taking several microseconds to discharge and reset, and whilst in older experiments using relatively slow repetition rate flash lamps the excitation-fluorescence sequence is quite sufficient, the use of modern high repetition laser sources can overload the TAC through continuous start pulses. This can be avoided by using the fluorescence decay as the trigger mechanism, in the reverse mode the TAC is then only activated if an emitted photon is detected, making the system much more efficient and reducing overload problems.

Because of the finite width of the laser and the instrument response, the raw decay curve produced using TCSPC is a convolution of the excitation pulse and the real fluorescence decay. In order to separate these two entities, global analysis of the instrument response function and the measured decay curve is used to give a fitted function that represents the true decay.

Alternatively, if the initial fast component of the decay is not important, the measured fluorescence lifetime can be considered from times greater than the instrument response function.

The time accuracy of the single photon counting technique is determined by the transit time spread of the single photon pulses in the detector and the trigger accuracy in the electronic system. As a result, the timing resolution can in fact be superior to the half width of the detector IRF, which in some avalanche photodiodes can be as large as 500ps.

As in any counting method, the accuracy of the measurement is defined by the standard deviation of the number of collected photons for each time channel. Because all detected photons contribute to the decay, SPC typically has a very good signal to noise at a given intensity and measurement time. Another advantage of single photon counting is that noise emanating from current leakage, gain instability and stochastic gain mechanisms does not appear in the measured luminescence histogram because it does not relate to the TAC, giving further improvements in the SNR compared to other signal processing methods.

Photon counting is of course not without drawbacks and in the single photon counting method the effect of photon pile-up is an important shortcoming. Photon pile up can happen when using very intense samples and describes the situation where the time between two or more photons arriving is shorter than the time it takes for the detection impulse to be sent to the MCA and for the voltage ramp to recommence. The result is that the fast decay component of the luminescence is under-represented because the photons are lost in the dead time of the TAC. By using the pulse inversion technique mentioned earlier, the Becker and Hickl TCSPC module used in this investigation has very short dead time and can record up to 1×10^6 photons per second. This is an impressive time resolution compared to other SPC modules and makes the system very useful for fast image scanning.

6.3 Optimising the System

In order to optimise the timing resolution, the parameters of the constant fraction discriminator (CFD) and the time to amplitude converter (TAC) should be adjusted to meet the specific requirements of the system. The instrument response function was used to monitor improvements in the system and the optimum settings were chosen for reproducibility rather than the time resolution alone. In order to avoid ground loops which can induce high noise currents, all components were connected to a distribution board which was then connected into a single socket.

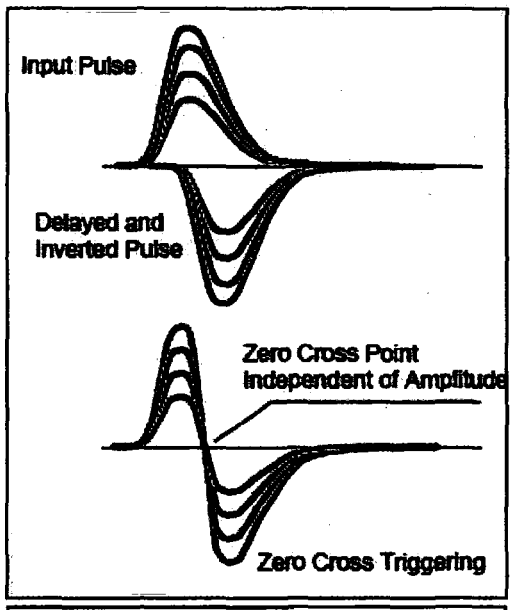

Figure 1: In order to match the CFD as closely as possible to the detector pulse, the trigger point is set at the zero cross of the sum of detector pulse and the inverted pulse. [1]

CFD: The constant fraction discriminator strongly influences time resolution and is one of the most important parts of the SPC electronics. The purpose of the CFD is to measure the arrival time of the photoelectron pulse and transfer it to the subsequent electronics. Although seemingly simple, in practice correlating the CFD with the temporal location of the detector pulse is often a complex task, suffering significant complications due to pulse height variations.

To understand this effect consider that the CFD associates the arrival of a pulse when a signal of a value x, which lies above a certain threshold, is detected. If there is then any variation in pulse amplitude between a group of temporally identical pulses, this method will record a spread in the measured arrival time, with large pulses crossing the threshold early and small amplitudes pulses crossing it later.

The method of circumventing this problem is to minimise the contribution of the pulse height distribution. This is achieved by breaking the signal up into two parts, the pulse and an inverted pulse delayed by ~ 1 pulse width. These pulses are then recombined by summing the input pulse with the delayed inverted input pulse. The zero-cross point is then used as a trigger as shown in figure 1. Since the crossover point of the two pulses is independent of pulse amplitude, this method minimises any jitter in the temporal domain caused by amplitude jitter of the detector. False triggering is further reduced by the use of a low threshold discriminator which rejects pulses that are smaller than a certain limiting value. Adjusting this limit changes the effective CFD time window and it follows that for smaller time windows the effects of random noise along with any systematic after or pre-pulses are reduced.

The CFD threshold and zero cross voltages were adjusted to give the best possible combination of time resolution and reproducibility.

6.3.1 TAC Parameters

The time to amplitude converter (TAC) is used to determine the temporal position of the detected photon within the SYNC train. The TAC is effectively a voltage ramp which is triggered by an incoming photon and stopped by the following SYNC pulse (or vice versa). In this way a voltage that is linearly proportional to the time between photons is produced and converted to give a temporal value. The settings on the front panel control the gradient and length of the TAC voltage ramp, which adjusts the time scale of the recorded luminescence. Whilst the CFD parameters are usually set for a given excitation source and electrical set-up (cables, connectors etc..) the TAC parameters can be adapted to the fluorescence characteristics of the sample, for example some samples with long lifetimes require a longer time range whilst other faster fluorophores can be recorded sufficiently using a much smaller time window. The TAC settings consist of three

variables, the range, the off-set and the gain. The range and gain control the voltage ramp characteristics and should be set to display the emission of the fluorophore whilst the offset can be used to alter the area over which values are recorded. The TAC characteristic is slightly non-linear at the edges of the time window and an important use of the offset is to move the very beginning and end of the TAC window out of the recording range. The area of non-linearity can be seen at end of the time window in figure 2; it appears as a small step in the fluorescence decay. Whilst altering the gain parameter can be used to magnify the time axis it is not an essential adjustment unless the range is at a minimum, although it has been found during the optimisation, that high gain does gives slightly improved temporal resolution.

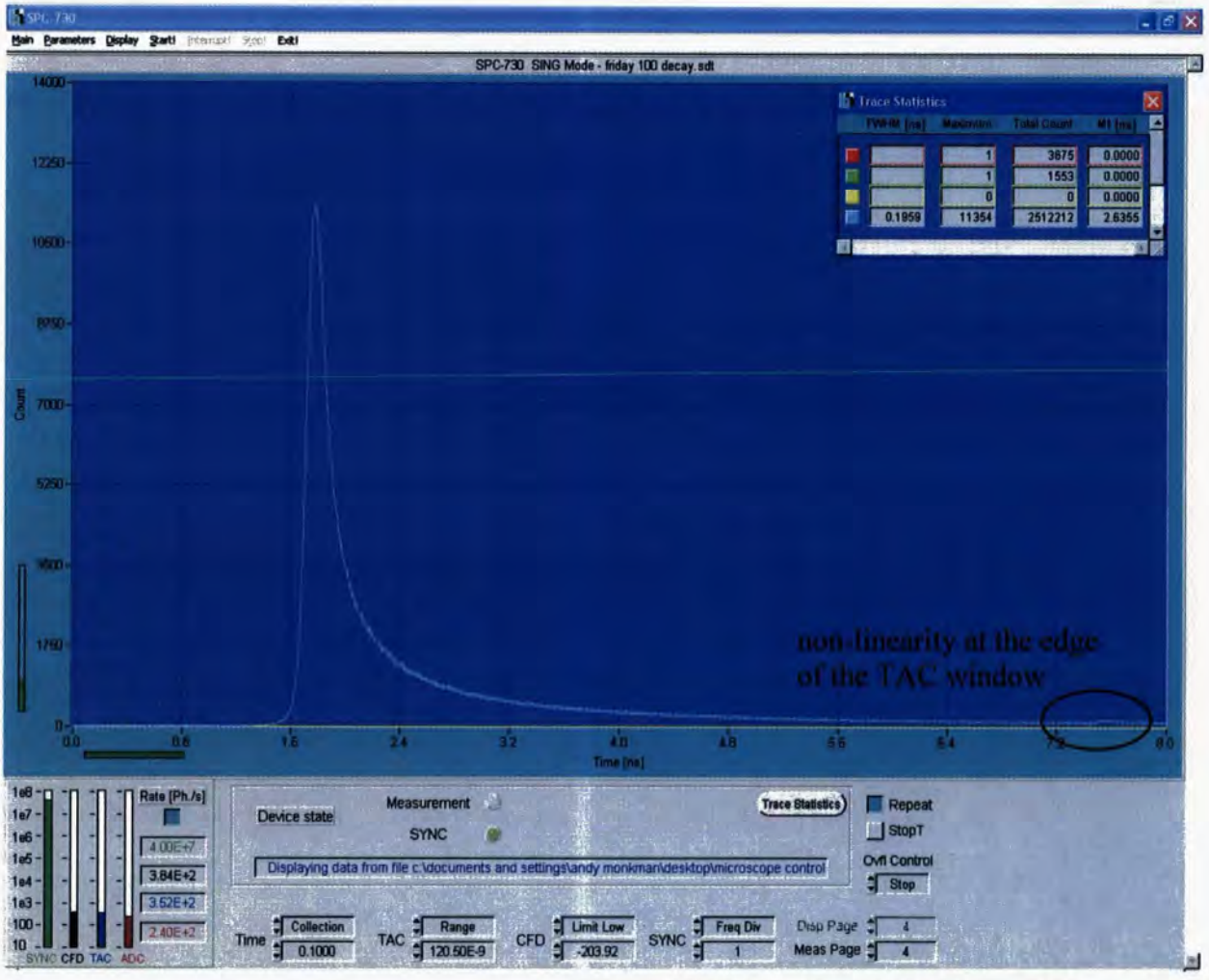

Figure 2: Single Photon Counting. The single photon-counting module should be adjusted to suit the specifics of the experiment, factors such as cable length, excitation source, detector type and sample characteristics all affect the parameters seen at the bottom centre of the panel. These should be adjusted to give good time resolution as close to the time resolution of the detector or the laser pulse, whichever is larger. To this effect the CFD settings are particularly important as they govern the synchronization between the incoming photons and the excitation pulse.

Having set the TCSCP parameters to give the optimum time resolution, lifetime measurements were tested using films of concentrated polyfluorene and of fluorescent microspheres in PVA.

Lifetime Measurements 6.4

6.4.1 Sample Preparation

OF 2/6 was dissolved at 1% into toluene (*Romil*) and stirred at room temperature for 5 hours. The solution was then spun cast at 2500rpm onto clean quartz discs and stored in an inert environment when not in use.

Films of fluorescent microbeads were prepared using *Plum Purple* fluorescently labelled polystyrene microspheres purchased from *Bangs Laboratories*. Microspheres were mixed into a PVA matrix at 1% and spun at 1300rpm onto clean quartz or sapphire substrates.

6.4.2 Experimental

Samples were mounted in front of the microscope objective and the focus was set using the maximum intensity technique described previously. The fluorescence lifetime of many polymers in the solid state varies widely depending on sample preparation, for example choice of solvent and host have been noted to affect decay kinetics quite considerably[5], furthermore solid state lifetimes are notoriously complex making them difficult to describe quantitatively[6]. As a result of this in order to assess the accuracy of this experiment, qualitative assessment of decay curves has been used to compare those decays taken from the confocal system and those taken using a single photon counting experiment already in use in the department. This system uses a *PicoQuant* picosecond pulsed (65ps) diode laser to excite a bulk portion of the film; it is

established in measurements of lifetimes for both films and solutions which have been verified in comparison to known values. The excitation area of the film is greater in the confocal set up and the IRF is slightly different in shape, so a perfect match in decays is not expected though the general decay time and shape is expected to be similar, if the confocal SPCM is working correctly.

Lifetime decays taken for a film of OF 2/6 in PMMA at 1% are shown in figure 3 for both the picosecond SPCM and for the confocal microscope.

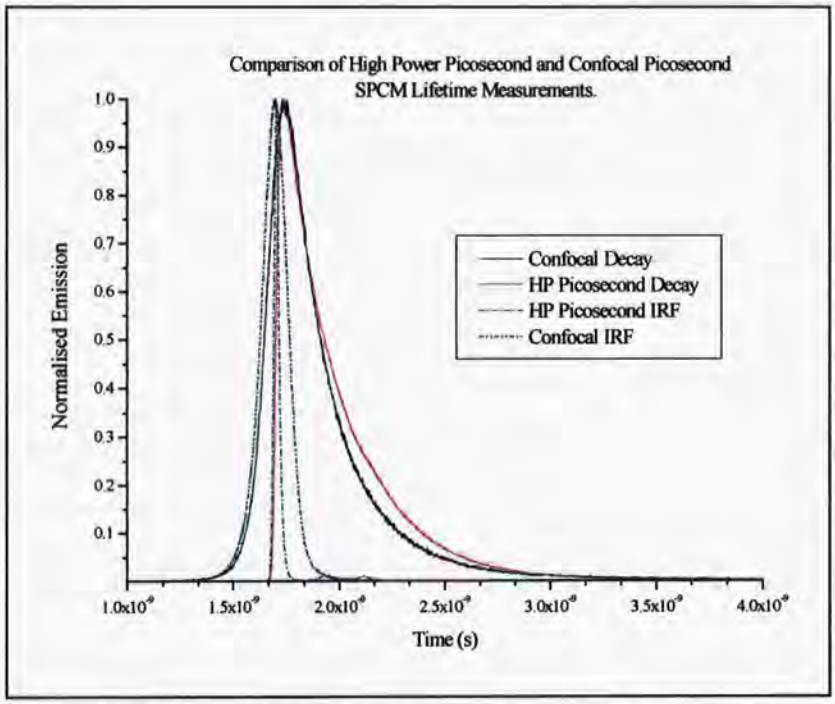

Figure 3: Comparison of the time-resolved photoluminescence of OF 2/6 in PMMA 1%, using the confocal microscope and a femtosecond SPC module. Both decays are multi-exponential and have significant fast components that occur on the time scale of excitation. The femtosecond IRF is naturally considerably narrower and has a different shape to the confocal scatter, giving rise to small differences in the decay curve.

The measured curves are notably similar, though there is a slight difference between the two decay shapes, this is as expected and is attributed to the different instrument response functions of the two systems. Other small dissimilarities in the luminescence tail are attributed to the increased excitation area of the high power system, which does not focus the excitation source onto the sample, and the inevitable difference in the part of the film presented to each laser. With these considerations in mind, the time resolved luminescence curves are considered to be in excellent agreement.

In order to test the accuracy of the confocal SPCM over longer time decays, the lifetime of a fluorescent microsphere has been recorded. Spheres were chosen with a known lifetime of ~ 4.7 ns and measured, this time solely on the confocal SPCM yielding single exponential fluorescence decay with a lifetime of 4.62ns-figure 4 navy trace. These results are taken as strong evidence that the system is functioning correctly up to lifetimes of ~5ns.

Although the issues surrounding the definition of the focal distance have already been discussed, a further important feature has been identified in the course of recording lifetime decays. Where in earlier discussion false focussing was presented as an issue only at very low concentrations, here at all concentrations a problem region has been identified. Specifically, setting the focus too close to the sample can lead to a large distortion of the decay that manifests itself in a fast initial decay of considerable amplitude. It is very noisy, but is otherwise similar in appearance to the scattered beam though with a small decay tail, presumably a remnant of the real fluorescence. Due to the similarity also of very concentrated sample decays with the scatter because of their very fast initial decay components, the problem remained undetected until low concentration films and long lived microspheres were studied, whereupon the true long decay tail was distinguishable from the strong rapid decay of the distortion.

The source of the problem was identified as an effect of poor focus (and not of poor sample preparation for example) by comparing two decays taken from the microsphere film. One was taken with the objective well focussed, whilst in the other the focus was moved forward until the fast decay effect became obvious. The results are shown in figure 4, where the correct decay is clear and in good agreement with all specifications whilst the decay recorded of the same film at the close objective position shown in light blue is clearly very noisy and not representative of the real fluorescence decay. Importantly for positions just off the correct focal position there is no real distortion just reduced intensity: the distortion occurs at a specific position.

The region where the distortion suddenly becomes apparent is located close to the sample at a small *local* intensity maximum. This poses a problem for the definition of the focal point when using the computer controlled program which seeks the intensity maximum over 100μm and identifies it as the focus. Because the global and local maxima that correspond to the real and false focus respectively are greater than 100μm apart, if the local maximum is in that 100μm range it will be associated with the correct focal position due to the absence of the global maximum.

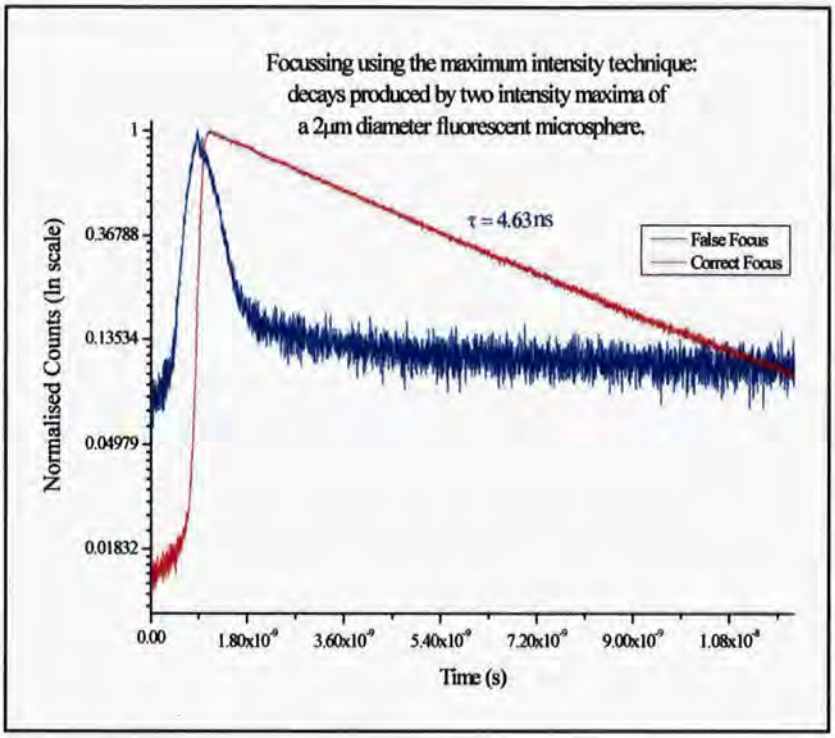

Figure 4: Focusing by maximum intensity can yield an incorrect focal position. If the objective is too close to the sample, a new local maximum occurs, resulting in a low level, noisy trace dominated by scatter (blue trace) The two curves shown are of the same bead when in focus (red trace) and when out of focus but at the local maximum close to the sample.

The reason for this phenomenon is not entirely clear, though, owing to the fact that this peak itself is only observed at a specific position, it is tentatively suggested that it occurs as a result of the excitation image plane correlating with the back of the sample substrate. At this position scattered light from the sample face is efficiently focussed back into the objective resulting in a scattered signal that is uncharacteristically high, and, importantly, high enough to pass through the emission filter. Avoiding the region of the false focus is important, as such two values are noted below, giving the best manual position region for locating the true focus, and importantly the region to avoid. Using these values the computer can then scan successfully over 100μm to locate

the global maximum, a point which will vary from sample to sample due to substrate and film variation.

Correct focal region ~ 10.5155μm

High Scattering at ~ 11.537μm

This is a relative measurement for the system in its current state, and, if the objective stand should be moved in the course of any future adjustments it should be re-evaluated. The local intensity peak is readily identifiable and is in fact quite useful for signalling that the focal position has been missed.

6.4.3 Experimental Calibration Conclusions

The system has been aligned to produce a repeatable IRF of 100ps at FWHM. This is 27ps broader than the pulse width specified by the laser delivery report manual however this considered to be acceptable when the broadening effects of the optical parts are taken into account. The specific alignment of light passages into the microscope objectives has been identified as a major potential source of IRF distortion and should be given particular care during any future alterations.

Focussing has also been noted as an important part of spectroscopic measurements and must be done with a considerable degree of accuracy to ensure valid results. The focal distance of the objective lens has been calculated to be 0.73mm ± 0.93μm without coverslip, though current methods of locating the focal distance rely on intensity measurements. Assuming that the focussed excitation beam will deliver the highest excitation flux to the sample the position where maximum luminescence intensity is observed used to infer the correct objective displacement. Though manual positioning can be used to approximately locate this point, for accuracy, due to

the small depth of field, a computer controlled routine has been written to scan the objective over 100μm from the manually set position to set the optimum objective-sample separation accurate down to 0.5μm. With the caveat that the sample is sufficiently concentrated that molecule alignment is not necessary, this method has been tested and found to be both practical and accurate. The only error posed for this technique lies in bad initial positioning of the objective by the user. A misleading scattering effect has been identified to produce a small local intensity maximum close to the sample yet out of the 100μm scanning range of the global maximum. Consequently if the user sets the initial position by this point the system will not be in focus. In order that this does not pose future problems, the danger region has been specified as has the approximate correct initial micrometre setting for the objective.

In dilute films alignment of the target molecule with the optical axis is of the utmost importance for setting the correct objective distance. Currently this is achieved by performing an x-y intensity scan over the rough area containing the molecule in order produce an accurate molecule position value for the subsequent spectroscopic measurement. Adequate at the time being, the time consuming nature of this method is predicted to pose a problem when single polymer molecules are under investigation because of bleaching effects. A solution has been suggested in the form of an automated search algorithm that will locate the molecule rapidly and conserve photons for the subsequent measurement.

The performance of the confocal system concerning lifetime measurements has been tested. By comparing the lifetime of OF2/6 in PMMA on both this system and on a more established standard SPC module it has been determined that the confocal system is recording accurate lifetime measurements. As the decay of concentrated OF2/6 is very rapid, a longer lived species was tested to check the performance of the system at long lifetimes. Fluorescent microspheres with a known lifetime of τ = 4.7ns were examined, results were found to be in excellent

agreement with this value giving a lifetime of $\tau = 4.62$ns. In view of these findings the system is now seen to be functioning sufficiently to be used for lifetime investigations and it is now intended to develop scanning confocal imaging, to act in support of lifetime measurements at single molecule level.

6.5 References

1. Becker, W., *Advanced Time-Correlated Single Photon Counting Techniques.*, J.W. Castleman, J.P. Toennies, and W. Zinth, Editors. 2005, Springer. p. 317-326.
2. Michalet, X. and S. Weiss, *Single-molecule spectroscopy and microscopy.* Comptes Rendus Physique, 2002. **3**(5): p. 619-644.
3. Lakowicz, J.R., *Principles of Fluorescence Spectroscopy.* 2nd Edition ed. 1999, New York: Kluwer Academic/Plenum Publishers.
4. Becker, W., *Advanced Time-Correlated Single Photon Counting Techniques.*, J.W. Castleman, J.P. Toennies, and W. Zinth, Editors. 2005, Springer. p. 217.
5. Lee, Y.J., D.Y. Kim, and P.F. Barbara, *Effect of sample preparation and excitation conditions on the single molecule spectroscopy of conjugated polymers.* Journal of Physical Chemistry B, 2006. **110**(20): p. 9739-9742.
6. Meskers, S.C.J., et al., *Relaxation of photo-excitations in films of oligo- and poly(para-phenylene vinylene) derivatives.* Chemical Physics, 2000. **260**(3): p. 415-439.

7. Scanning Imaging

Scanning in modern confocal microscopy is most commonly achieved either by laser scanning or by specimen scanning. In laser scanning, the angular position of the excitation beam on the back of the microscope objective is adjusted through varying the angle of reflection from the dichroic filter. As the illuminating beam moves across the microscope objective, a lateral displacement on the sample occurs. Whilst in specimen scanning the excitation beam remains fixed, with the specimen scanned laterally in the focal plane of the objective lens.

Specimen scanning has many important advantages over laser or beam scanning, not least that the experimental set up is much simpler to implement and run. Importantly in specimen scanning, off-axis optical aberrations such as coma and astigmatism, which occur in beam scanning, are largely minimized or absent as a result of having a constant axial illumination. Furthermore, since the microscope is only used at one part of its field, the field curvature is not important. Other notable advantages include the fidelity of contrast and resolution across the scanning area, moreover, the field of view is not limited by the objective aperture but is determined by the amplitude of the scanning stage.

7.1 Resolution [3]

Optical resolution is an important consideration in any imaging system, and, as with conventional microscopy, confocal microscopy has inherent resolution limitations stemming from a number of fundamental physical factors. Defining the smallest detail that can be imaged or the minimum discernable separation between two points, the resolution of a system improves as the resolving power and numerical aperture of the objective lens increase and as the wavelength of excitation light decreases. Fine-tuning these parameters allows optimization

of the number of spatial frequencies that are imaged and hence gives increased sharpness and resolution, (Abbe Theory[4])

Figure 1: As two point sources of equal intensity approach, they can be resolved at distance up to the resolution limit, which occurs when the central maximum of one Airy Disc coincides with the first minimum of the other. [2]

Ultimately, the resolution of the confocal system is defined by the point spread function (PSF) of the focal spot. The PSF, which results from diffraction of the incoming light at the edges of the aperture, results in a point source being blurred into a 3D light distribution. For an ideal aberration-free lens this is determined solely by the wavelength of the light, the NA of the lens and by diffraction. In the plane orthogonal to the excitation beam, Fraunhoffer diffraction through the circular aperture results in a characteristic Airy Disc pattern. In the axial direction, the PSF is significantly elongated and can be calculated from classical theory to be a factor of 3.3/NA larger than the lateral PSF. In order to describe the lateral resolution of the confocal system it is useful to consider the Rayleigh criterion, which defines the minimum separation of two points such that they are resolved into separate entities. In terms of the Airy pattern this criterion is achieved as two point sources converge to the point where the central maximum of one coincides with the first intensity minimum of the other as illustrated in figure 1. This minimum separation is equal to the Airy radius and is expressed as r in equation 1.

$$r = \frac{1.22\lambda}{2NA} \qquad \text{Equation 1}$$

The Airy Radius.

The Airy radius is commonly used as the limit of resolution in wide-field microscopy though in confocal microscopy the resolution limit must account for both the focus of the excitation

and detection objectives: in this case, the primary consideration is the effect of combining two PSFs. Defining for convenience the PSF as the probability of a particular photon being incident at point *(x,y)*, the confocal PSF is the probability product of the excitation and detection point spread functions on the detector:

$$PSF_{confocal} = PSF_{exc}(x,y) \cdot PSF_{det}(x,y) \qquad \text{Equation 2}$$

The result of this product is a narrower PSF with a significant reduction in the intensity of the side lobes compared to the wide field PSF, figure 2.

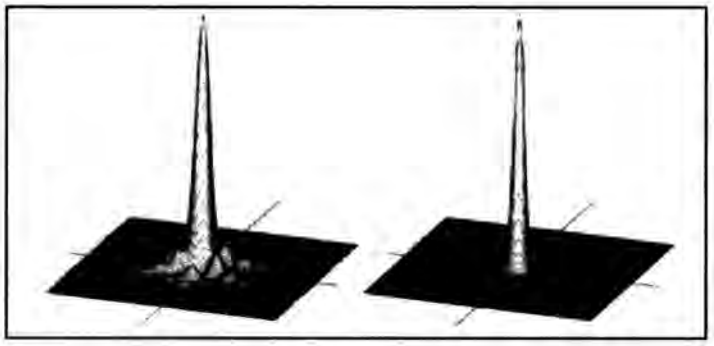

Figure 2: Wide-field (right) and Confocal (left) Point Spread Functions. Confocal imaging offers considerable improvement in the detection point spread function; side lobes are significantly reduced and a sharper central peak is observed. [1]

The second important difference between the confocal and standard case is spatial position of the PSF. Due to the difference between the excitation and detection wavelength, the spatial co-ordinates of the point spread functions are displaced, this means that the Rayleigh Criterion is invalid because it relies on the position values of the Airy pattern. To circumvent this problem whilst maintaining the convenience of Equation 1, the full width at half-maximum (FWHM) is generally used as a reasonable approximation to the lateral resolution, *r*. For a Gaussian Shaped PSF the lateral confocal FWHM is determined by the square of the excitation PSF:

$$FWHM_{conf} \approx \frac{1}{\sqrt{2}} FWHM_{exc}$$

Taking into account that the longer detection wavelength has the effect of reducing the resolution, the lateral confocal resolution is approximated by:

$$FWHM_{conf} \approx \frac{1}{\sqrt{1+\beta^2}} \frac{1.22 \cdot \lambda_{exc}}{2NA}$$ Equation 3

Confocal Resolution

Where $\beta = \frac{\lambda_{exc}}{\lambda_{det}}$.

Using Equation 3 the resolution of the confocal system described here for polyfluorene emission at 420nm is approximated to:

$$FWHM_{conf} \approx \frac{1}{\sqrt{1+\left(\frac{390}{420}\right)^2}} \frac{1.22 \cdot 390 \times 10^{-9}{}_{exc}}{2 \times 0.65}$$

=268 nm (3s.f)

7.2 Pinhole Size

Pinhole size is an important feature in any confocal design, it rejects out of focus light and dramatically improves the axial resolution of the system, though has a lesser effect on the lateral resolution. Studies by Wilson [5] investigated the response of a confocal microscope to a thin fluorescing layer as a function of pinhole size and β. His findings showed that axial resolution improves with decreasing pinhole size. This phenomenon introduces the question of the minimum pinhole size that will achieve an acceptable balance between signal to noise and resolution, to this effect Wilson noted that axial resolution does not improve considerably for pinhole apertures less than the radius of the first zero of the Airy disc.

If the optimum pinhole size is then taken as one Airy diameter, the actual pinhole size should match the size of the magnified airy disc as projected onto the detection pinhole. For a magnification factor of 40x and emission wavelength of 420nm the pinhole aperture d_p should be set such that:

$$d_p \leq M\frac{1.22\lambda_{det}}{NA}$$

$$d_p \leq 40\times\frac{1.22\cdot 420\times 10^{-9}}{0.65}$$

$$d_p \leq 31.5\mu m$$

Despite dramatically improving the optical sectioning capabilities of the microscope it is worthwhile to note that for lateral resolution the benefits are significantly less. Only at tiny pinhole sizes is there any noticeable gain in resolution by which point intensity will have fallen to 95% of the maximum [6]. This is clearly a disadvantage in terms of signal collection and so the use of a pinhole can be much more liberal if axial resolution is not important. This is the case in 2D single molecule spectroscopy so in this investigation and the pinhole size is set by the active area of the detector without the capacity for adjustment. In this way out of focus light is largely blocked whilst the majority of emitted photons are detected.

7.3 Digitisation

Each real-life picture that is taken using the confocal scanning technique requires digitization in order to convert the real life image into an accurate digital representation. This necessity for digitization stems from the inherently discrete nature of any imaging process; the image is read at a number of discrete spatial steps and displayed as a discrete function of intensity.

Digitization should give the most detail possible within the limits of practical experimentation. In this section digitisation considerations and settings will be explained and calculated for both the spatial and intensity domains.

7.3.1 Spatial Digitisation

Following Nyquist's sampling theorem an object should be sampled with at least twice the highest frequency of the sample in order to avoid aliasing and artefacts. In the case of the confocal microscope, the Nyquist frequency is not determined by the infinite detail of the specimen but by the PSF of the system: half the confocal FWHM.

For excitation at 390nm, detection at 420nm, NA = 0.65 the maximum resolution is 268nm (above) hence Nyquist sampling / pixel size $\leq$ 134nm.

7.3.2 Intensity Digitisation[7]

To determine the number of intensity levels required to represent the acquired image the minimum detectable difference in the intensity domain is used. This quantity is related directly to the noise of the detection process and the detection system - defined principally by Poisson Noise and the noise within the detector such as dark counts, read out noise, thermal noise etc... The combination of these factors results in the minimum intensity resolution r_{int}

$$r_{\text{int}} = \sqrt{N_{Pois} + N_{\text{det}}} \qquad \text{Equation 4}$$

It can be seen from equation 4 that as the number of detected photons increases, the intensity resolution falls, furthermore the resolution is not evenly spaced in terms of detected photons. For a given maximum signal N_{max} the number of meaningful intensity levels is:

$$N_I = 2 \cdot (\sqrt{N_{\max}} - \sqrt{N_d})$$

Whilst the number of grey / colour levels required to represent N_I intensity levels is:

$$N_G = \frac{N_{\max}}{\sqrt{N_d}} \qquad \text{Equation 5}$$

7.4 Stage Control Software

A control program has been designed to run the scanning stages and record the fluorescence lifetime and fluorescence intensity. Although current investigations only run using one detector, the program is built to record fluorescence lifetimes from two detectors when connected, so that polarisation dependant studies can be carried out in future. The programme is written using *National Instruments LabVIEW* software.

The *LabVIEW* program integrates control sub programs that are supplied along with both the SPCM and the PI stage control, using them to produce lifetime and image information. The program performs initialisation, scanning and lifetime measurements sequentially and saves the data produced to file for analysis. The sequences will be explained here in order and are shown in detail in the appendix. The numbers referred to within the description are indicated on figure 3.

1. Initialisation of the Single Photon Counting Module.

This performs a number of operations that are not directly visible by the user but are required to run before any measurements can be taken. This stage connects the program up with the SPCM and reads in the operating parameters from an initialisation file, re-calculates parameters depending on hardware restrictions and sends the parameters to the SPC control register. It checks that the SPC hardware is operating correctly and will send out an error message if any problems are detected.

Once this is complete the memory is then configured for the particular module type to set the number of detector channels and the ADC resolution, which can be from 64 to 4090. (ADC resolution defines the number of points per decay curve). This makes sure that when the lifetime information is read in to the memory it is configured to match the number of points and number of curves that it receives. The details of the memory configuration are displayed on the front panel at point 1.

2. Initialisation of the PI Stage Control.

Again this process is required as the initial communication with the stage control. It opens up an interface so that the user can specify the type of connection – RS-232 or GPIB and the port number. This system uses a GPIB on port 4. It also has options for the number of systems and setting the time out. These do not need to be altered and should be set to 1. Once this has been completed it checks the presence of the three axes, reports back and turns the system online. The indicators at point 2 show if the axes are functioning and gives their status. If they do not read back properly check the connectors and make sure the power switches next to the input cables are on. It then moves each axis to 0.0μm and is ready to be used.

3. Focussing.

A dialogue box will appear and ask the user to choose a step width for the stage controlling the objective lens. This value is set in microns and can be any value between 0.01μm and 100μm. Before you start the program the position of the x-y plane during focussing must be entered, it might be chosen for example to be at the centre of the subject, the position values, in microns should be entered at point 3[1] and can range from 0 to 45μm in each plane. The input values are then read into the PI system which will position the sample and then scan the objective forward over 100μm at the input step width. At each step the SPC module reads the ADC reading and writes it to an array. Once the objective scan is complete, the program converts the array index to a position and plots the intensity as a function of position shown in the top left corner of figure 3. Simultaneously the maximum intensity position is selected from the array and is sent to the PI controller which moves the objective to that position. The z-axis is now fixed for the rest of the experiment.

The focal position should have been set by hand to an approximate focus before running the experiment, if for any reason this is sufficient and fine focussing is not required enter 100μm as the step width and the program will perform only one step and reset the objective to zero.

The time taken to focus the objective is extended considerably by the time needed for the SPC module to read the rates values, if the program runs too fast, the rate value for the ADC cannot be collected and the error *"Rates Not Ready"* is displayed. A time delay has been incorporated into the measurement stage to avoid this problem however it does make focussing slow and the use of an ND filter during this process should be considered to avoid bleaching the subject molecule.

[1] There must always be a value in each box; if the point of focus is not important, arbitrary values should be entered.

Once focussing is complete the user is prompted to save the focussing information to file, this can be bypassed by clicking *cancel* in the save dialogue. The program will then display a warning saying the file has not been saved and offer to *continue* or *stop,* clicking continue sets the program to run as normal.

4. Lifetime Measurement and Image.

The active area should be set before the focussing stage is complete in the *from* and *to* boxes at point 4 as the stages will be set to these positions immediately upon completing the focus stage. The step width in μm and collection time are also set here and define the pixel size and dwell time. When these parameters are input the *Go* button should be pushed down to start readings.

Measurements are taken directly by the SPC module; the lifetime is measured and displayed on the front panel in the lower left graph. The signal from the lifetime is then passed through a filter which smoothes the curve and displays another smoothed lifetime in the top right hand corner. Whilst the raw lifetime is available for lifetime analysis, the smoothed curve is used to build up the image profile by recording the maximum intensity of the decay. At each position the maximum count value is taken and put into an array. When the scan reaches the maximum y value it leaves the measurement loop and is moved one step in the x-direction, the y scan repeats and the intensity maxima are recorded into a new line of the array. In this way a 3 dimensional intensity profile is constructed.

The reason that the lifetime is smoothed is to reduce the impact of noise which distorts images at low intensity. This distortion often occurs when there is no luminescence decay when because of scattering and system noise etc.. there are often a number of counts still recorded. Due to Poisson noise over the whole time range occasionally these counts include

a single high count. This rogue reading would then be counted in the same way as a small decay curve if the raw maximum were taken. By averaging over a number of counts, noise peaks are reduced whilst real decays are preserved. In this way the image background is flattened allowing molecules to be more easily identified.

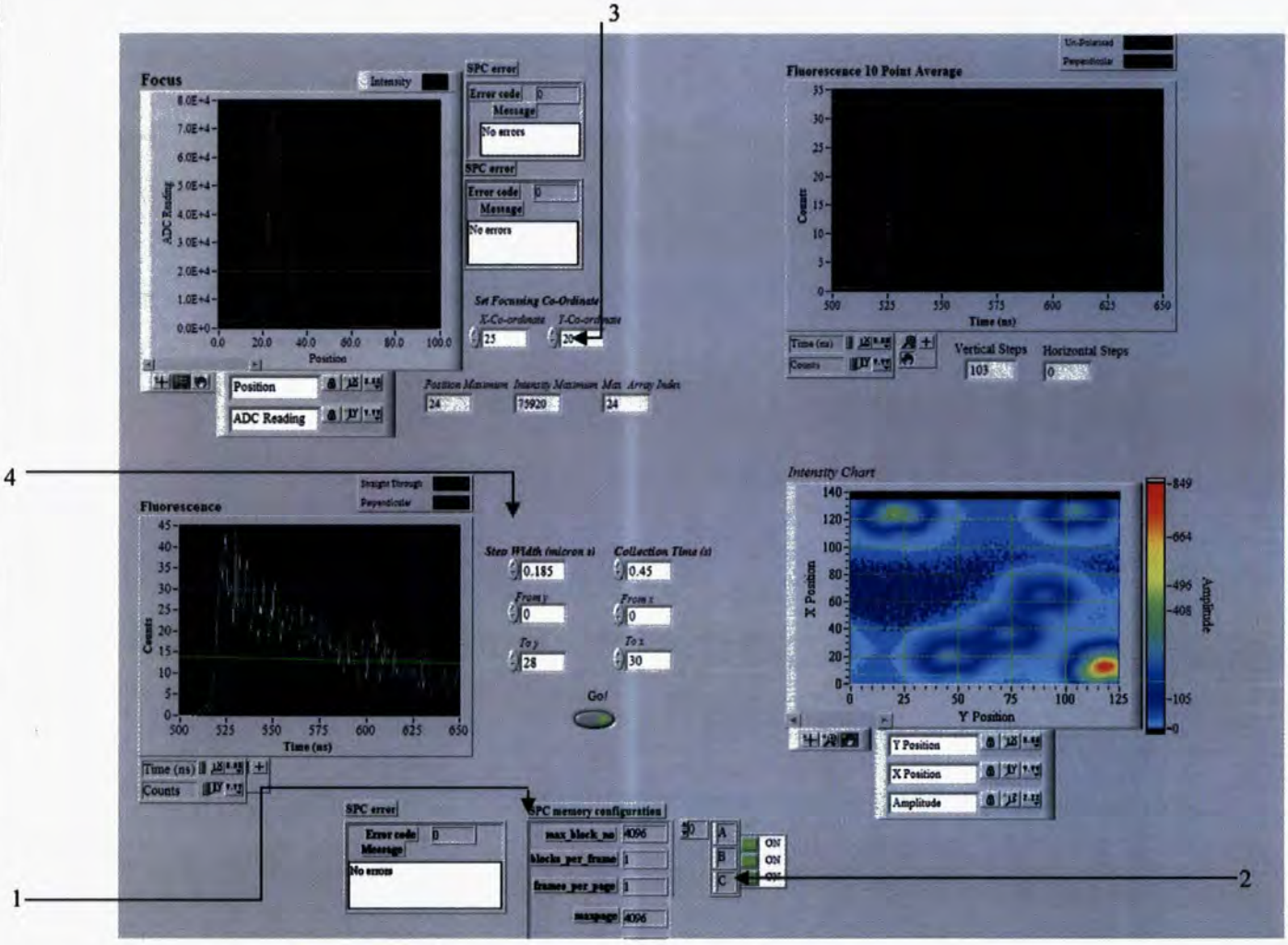

Figure 3: Labview Control Front-Panel. The program focuses the laser by stepping the objective towards the sample over 100μm and recording the ADC reading at each point (top left). The scanning parameters set by the user are then used to control the movement of the piezo-stages in the x–y plane, as the stages scan the fluorescence lifetime is recorded at each point (bottom left) and a smoothed lifetime is calculated (top right). The maximum from the smoothed lifetime is put into an array for each pixel, once the scan is finished the intensity array is converted into an image of the active area (bottom right).

The reason that this method is used rather than simply taking a reading from the ADC is that the rates values from the ADC take a number of seconds to update; this is too long to be spending at each pixel when scanning for single molecules as they will begin to bleach and

high resolution scans would take too long to complete. The lifetime reading is a much faster measurement to take; the minimum dwell time is limited by the step response time of the PI servo to 0.35s per pixel.

By conducting a position check at the end of each y and x line scan the program registers that the scan is complete when the read back has reached the final x-y position values entered at point 4. This comparison has a small margin of error built into it to accommodate fluctuations in the position read back and to account for the possibility that the step width chosen is not a multiple of the chosen line length, so it would stop for example if the final position was 40 and the read-back was 40±0.2. When running fast scans it is advisable for the user to go into the program and alter this error buffer to about half the step width as when the system is moving quickly it is possible that it will step over the maximum error and consequently never receive the stop command, in which case it will keep trying to increase in that dimension and the programme will need to be started again.

5. Building the image and end.

Once the entire area has been scanned the array containing the intensity maxima from the smoothed lifetimes is converted into an intensity image seen in the lower right corner. A dialogue box prompts the user to save the array data in ASCII format so that analysis can be carried out. The system then switches offline.

7.5 Results

Samples were mounted on a 50 x 50 μm^2 closed loop scan bed (*Physik Instrumente*) A digital instruments controller was linked to the stages and operated by a *labview* program. The speed

appears brighter than the blank disc scan. There are a number of spots visible in figure 4 with sizes ~450-500nm these are thought to be possible polymer molecules.

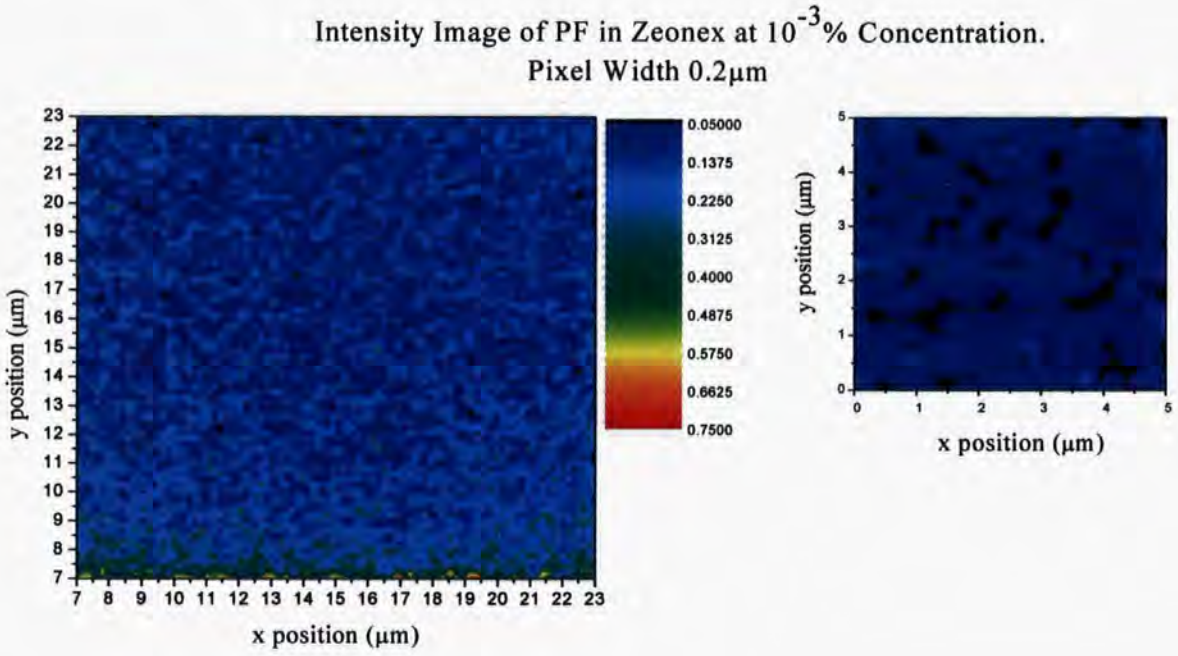

Figure 4: Intensity scan over a film of OF2/6 in a zeonex host at 10^{-3}% concentration w/w. The inset is a scan over a small area of a blank quartz substrate to give a background comparison. The two images have the same intensity scales. The fluorescence image shows distinct areas of emission though their size ~0.2μm (1step) and low emission is more indicative of background fluctuations rather than emission from a molecule which should appear no smaller than the wavelength of emission ~400nm. Though some of the lager bright areas are of the correct order in size, the signal to noise ratio is poor and it is unclear as to whether these are indeed polymer molecules, background emission or impurities.

Trying to set the system up for imaging using polymer films is difficult for a number of reasons. Firstly the size of the molecules under investigation allows little space for error in the system set up; unless all aspects of the experiment are accurately defined, individual polymer chains are not expected to be visible. Secondly it is not known whether or not the molecules are isolated in the films and how many molecules are expected per unit area of the film so the size of the subject is undefined. Thirdly the polymer molecules are short-lived in the dilute films made here, meaning that numerous scans can not be taken over the same molecule for the purposes of refining the focus collimation etc…

In response to the problems experienced with the PF films it was decided that imaging of evaporated AlQ_3 would allow easier calibration of the imaging parameters. By evaporating AlQ_3 at a low rate onto a quartz disc only a few molecules would affix to the surface. In this way scattering through the film and changes in the refractive index between the fluorescent molecule and the host polymer are eliminated and it is expected that much clearer isolated AlQ_3 molecules will be observed.

7.5.1 AlQ_3 Imaging

AlQ_3 was evaporated onto quartz discs at a rate of 0.1 Å/s for 5 seconds in order to deposit a sub-mono-layer film onto the quartz surface by Chiang, Chien-Jung. Scanning over $40\mu m^2$ with a step width of 0.36μm a scan was taken to establish any evidence of fluorescence. The result is displayed in figure 5.

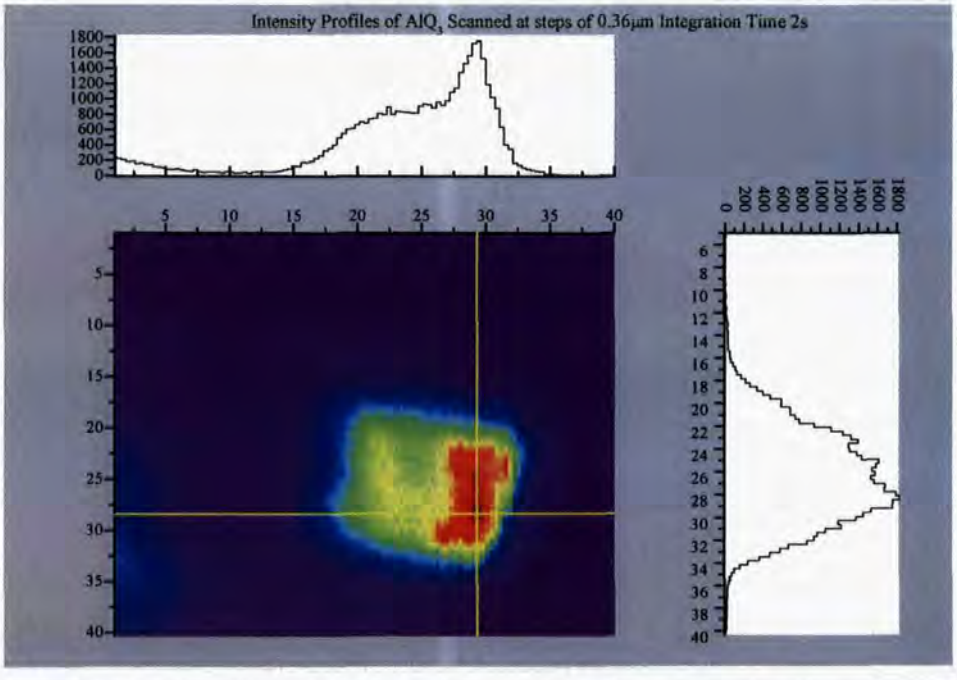

Figure 5: Intensity profile of AlQ_3 evaporated onto a quartz disc. Peak emission is 800 counts per second the background is ~10 counts per second. The blob like appearance suggests that the excitation point is not focused correctly on the AlQ_3 and the presence of two distinct emission peaks suggests a pair or group of molecules.

Clearly distinguishable is an isolated fluorescence patch with an area of roughly 15μm^2. Within the bright area are two clear hot spots one larger, which appears to contain two unresolved peaks. With the initial intention of zooming in on the area of fluorescence and taking a more detailed scan at the resolution limit, a second image was taken using the focal co-ordinates as those at which the highest intensity spot occurs. The resulting image did not yield the expected detail of the fluorescence spot but an area of little emission with no clear surface topography. To check that the sample had not changed or been destroyed, a second experiment identical to the initial scan approximately 48hours later was taken. The result is shown in figure 6.

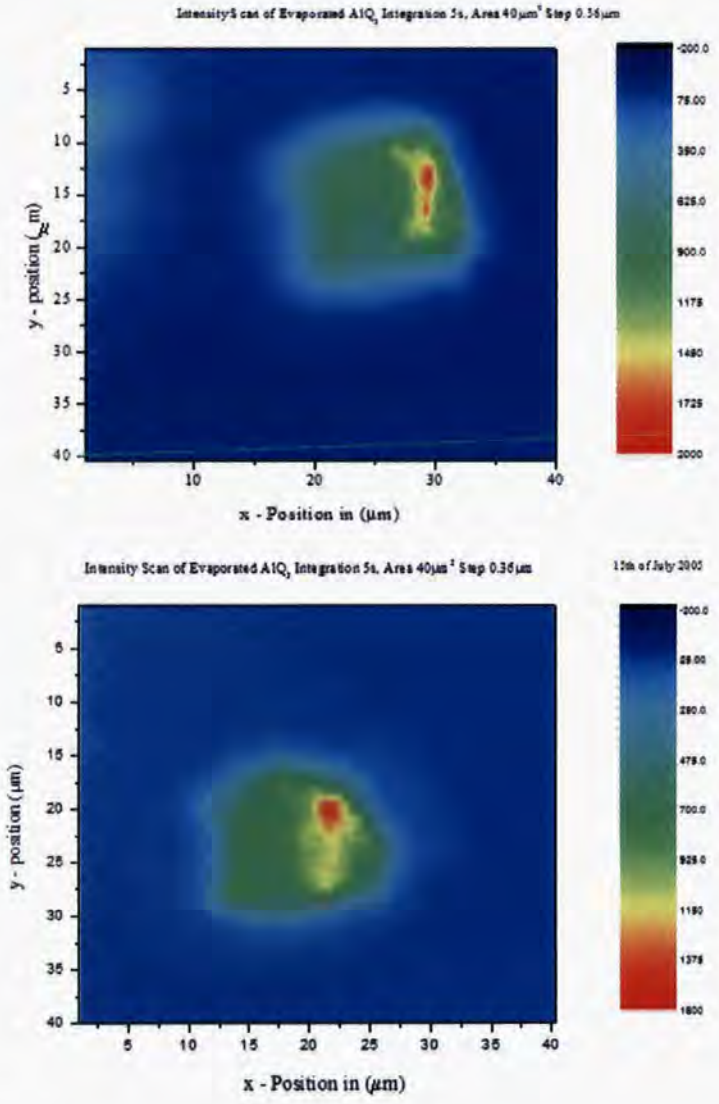

Figure 6: Intensity Scan over the same area of 40μm^2 top, initial scan below scan under identical conditions 48 hours later. The area of fluorescence has clearly displaced and changed in shape over a distance of ~ (8,13) μm. This could be an the result of external factors - expansion in the quartz substrate, vibration of the system, temperature fluctuations or a consequence of intermolecular attraction, vibrational energy of the molecules.

The change in intensity distribution points towards either merging of the two initial emitters or, a reduction in fluorescence of the sample. A further point to note is the effect of the focal point, which is different for each image.

There is clearly a shift in position and fluorescence topography of the image over a scale of ~10 microns. The overall maximum intensity is reduced in the second scan, and it seems that the two

areas of fluorescence have merged, although this apparent change could be a result of the focus of the objective, which is different between the two images. Any effects brought about by sagging or movement of the scanning stage can be ruled out as the position sensor on the piezo control records actual not relative position, and as the stage position was identical for both scans the movement is thought to be a result of either the entire sample or of the individual AlQ_3 molecule. Movement of the substrate is not thought to be the cause either, since if the disc were slipping in its mounting the movement would only be noted on occasion as would be a random effect. As it is, molecular position has been consistently observed to decrease in several similarly made AlQ_3 samples suggesting that the explanation lies in movement of the molecule in relation to the substrate over time. This is not unlikely especially upon taking into account the heating effects of the laser and the fact that the AlQ_3 is not fixed by a host or covering layer.

Movement of the sample clearly requires addressing if any optical sectioning or repeated images of a single spot are required. Particularly important for sharp images is the definition of a focal co-ordinate, so that the correct focal distance is selected. It had been hoped that a layer of Zinc Selenide could be evaporated over the AlQ_3 molecules to fix them in place, however, evaporation of the Zinc Selenide layer was not possible using our evaporating oven and so it was decided to take on a different molecule for imaging.

7.5.2 Fluorescent Microspheres

Having made initial imaging attempts with AlQ_3 it was clear that a more standard subject molecule was required to characterise the microscope accurately. With a view to this a batch of polystyrene microspheres with fluorescent labelling were purchased from *Bangs Laboratories, Inc.*

Fluorescent microspheres have a known size and spectrum and are easily isolated and immobilised; this makes them ideal for use as a standard for confocal imaging. The aim of imaging the microspheres is to improve spatial resolution and to detect any problems of alignment in the system.

7.5.3 Sample Preparation

Uniform dyed microspheres of 1.94μm diameter were purchased as a starting point for image calibration. The microspheres are polystyrene labelled internally with *"Plum Purple"* fluorescent dye. Microbeads were supplied at 4.07% solids and were diluted 100 times in ultrapure deionised water, resisitivity: 18 MΩ for imaging purposes. To embed and immobilise the microspheres the 1:100 solution was mixed 1:1 with PVA (Aldrich) dissolved in de-ionised water at two concentrations, 1% and 5%. The PVA-Microbead solutions were then sonicated for half an hour[2] to give a good dispersion in the PVA and to separate aggregates.

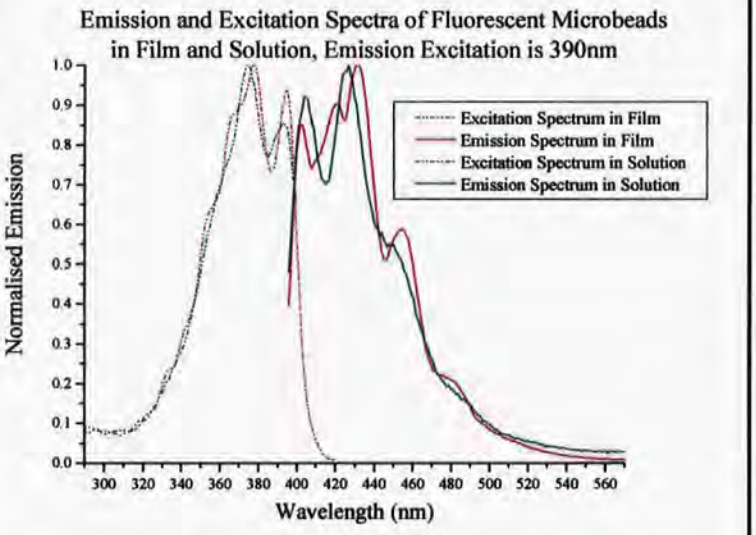

Figure 7: Emission spectrum of fluorescent microspheres, internally labeled with "Plum Purple" dye. (Purchased from *Bangs Laboratories, Inc)*. Peak emission at 420nm, peak absorption at 365nm.

Once the microbead solutions were well mixed films were made by spin coating at 1300rpm for 240s onto clean quartz discs.

[2] To avoid aggregation the temperature of the beads was kept below 8°C during sonication by adding ice to the bath.

The spectrum of the microbeads in PVA was taken at an excitation wavelength of 390nm and is shown in figure 7 for beads in the PVA solution and in film. The beads clearly absorb strongly at the wavelength of the laser used here and have a suitable emission spectrum.

Before imaging was attempted on the confocal system, an optical microscope was used to examine the spin coated disc. The image shown below in figure 8 is taken at x200 magnification and clearly illustrates the presence of several well separated circular beads.

The central part of the bead is ~2μm in diameter as expected whilst the dark perimeter is due to mismatching refractive indices between the PVA and the beads.

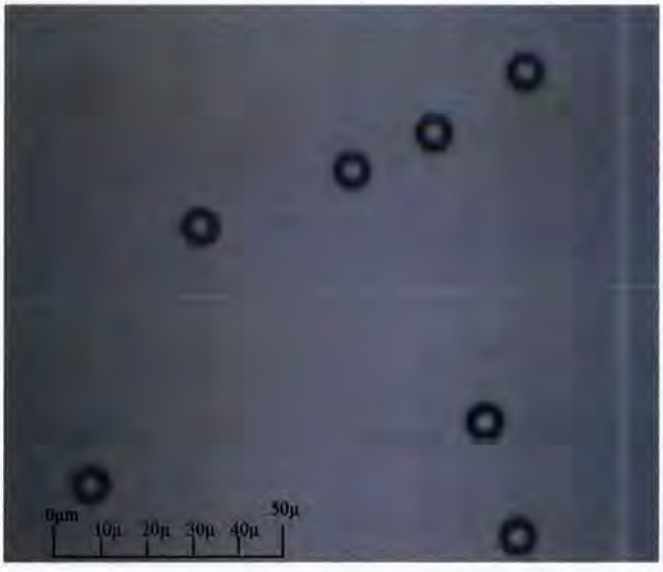

Figure 8: Optical Microscope image of the Fluorescent Microbeads x200 magnification. The central area of the dark ring is the microbead measuring 2μm in diameter; the dark periphery is caused by mismatched refractive indices between the bead and the PVA host. The total object size is 10μm diameter.

Although the end-point confocal image profiles would ideally represent a clear Gaussian function of intensity versus space, it is not expected that such a result will be achieved. There will always be slight broadening of the image at its edges due to the PSF of the excitation point, accounting for 0.27μm spread in the case of imaging a perfectly aligned 1 dimensional subject. Secondly the microbeads are three dimensional objects; if the excitation is focussed on the tip of the sphere, by the time it has scanned to the edge of the 2μm sphere it will be 1μm further from the bead edge than at the centre, this is beyond the depth of field for the objective and so the image will be slightly out of focus. Thirdly the PVA host forms a thick matrix for the beads, this is likely to cause broadening due to mismatches in the refractive index between it and the bead as seen in the optical

microscope image, whilst there is also the possibility of wave-guiding of the excitation pulse through the host matrix, which is expected to broaden the apparent size of the object, and wave-guiding of the emission, which is expected to raise the background levels when imaging bright objects.

Images were taken using the confocal scanning laser system. The first step in imaging was to manually locate and focus on a bright spot in the film and take a rough scan over that area. This was done with a fast scan speed and a step size of 1μm to give a location of the bead within the scanning area. Following the initial scan the area immediately containing the beads was scanned again, quickly and at the same step width to check that the bead positions were constant and that fluorescence was still detectable. In the first scans it was very obvious that the beads were not sufficiently immobilised with significant motion over the course of minutes. These beads had been put into a host of PVA and water at 1%. To stop motion of the beads new samples were made in a host of 5% PVA to water which was tested in the same way and found to be sufficient.

When testing the bead immobilisation problems of bleaching became apparent, with the count rate dropping considerably over two scans of the same bead, from 180 cps to 22 cps for example then bleaching in the third attempt. To overcome this problem a neutral density filter was put in the excitation path and tilted off axis to avoid reflections. It was found that photobleaching is considerably reduced if the emission is limited to below $5x10^4$ cps. With the ND filter in place a new area was scanned- figure 9. Following the initial rough scan scanning it was assumed that the beads would not have moved and the program was run a second time this time at high resolution focussing on the position of the lower right molecule. The step width of the objective is set to1μm and the x-y scanning step width is 0.14μm, the resolution limit.

As in the optical microscope image there is a bright central area of 2μm surrounded by a larger ring that extends approximately 3μm beyond the bead edge. The intensity per objective displacement is also shown in figure 9 to illustrate how the system defines the focal point. Focussing is only done once the molecule / bead has been approximately located to get the best focus possible, and is set at the point of maximum emission.

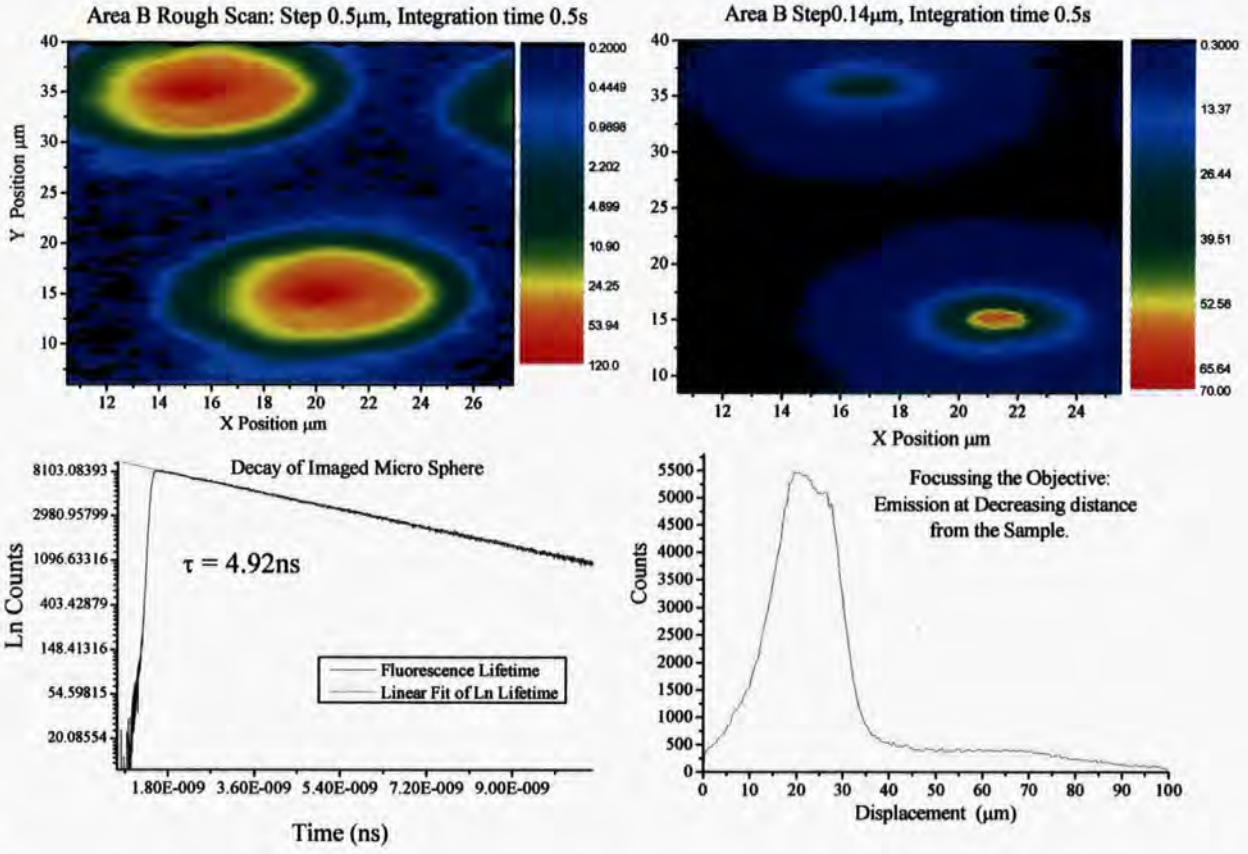

Figure 9: Images of fluorescent microspheres. Clockwise from top left: *Rough Scan:* used to see if there are any spheres in the field of view and provide the focusing position. *Secondary Scan:* Detailed scan of the two beads focused on the bottom right sphere, the central peak is roughly 2μm in diameter surrounded by a larger ring of lower intensity thought to be due to the mismatched RI between the bead and the PVA seen in figure 5. *Focus:* The focal point is set by positioning the stages so that the bead is on the optical axis and then recording the luminescence intensity as the stage is scanned forward at 1μm intervals over 100μm. *Lifetime:* the lifetime is recorded for the lower right microsphere. The decay follows a single exponential and is fitted with a lifetime of $\tau = 4.92$ ns.

As is the final objective of the experiment following the location of the microsphere, the ND filter was removed and the fluorescence lifetime was recorded from the imaged microsphere,

which was positioned on the optical axis using the piezo stage. By a linear fit to the natural logarithm of the fluorescence decay the lifetime has been calculated for the fluorescent microspheres:

$$\tau = 4.92\text{ns}$$

This is in excellent agreement with the manufacturers specifications and clarifies that the subject of the image is a microbead and not dust or impurity.

The intensity profile of the scanned spheres at the highest resolution is shown in figure 10. The symmetry of the intensity profile is good indicating that the optical elements are well aligned. The width of the profile however is several microns wider than the 2μm due perhaps to a badly focussed objective either at the detector or the sample.

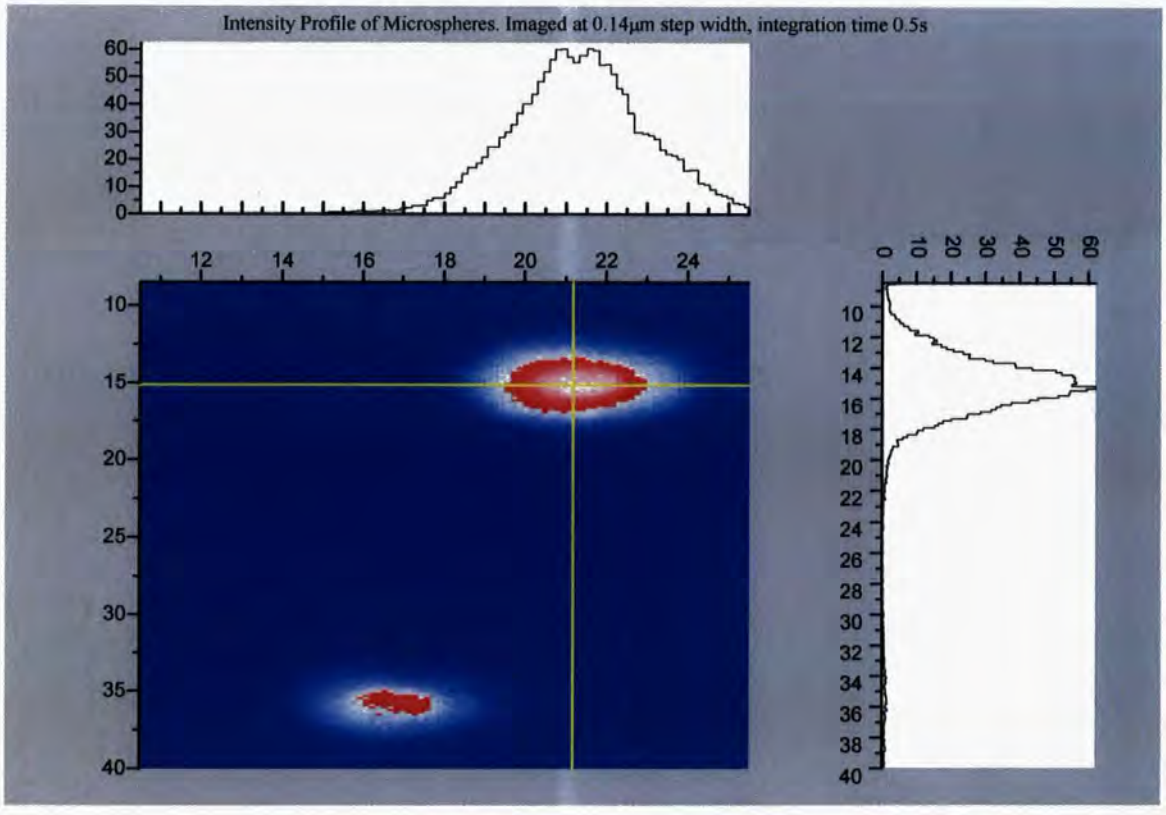

Figure 10: Intensity Profile of the beads imaged in figure 6. The profiles are almost symmetrical, indicating good alignment. FWHM = 3.54 μm. The intensity profile drops to 1% of the maximum emission at a radius of 5.24μm.

7.5.4 Further System Optimisation

In order to improve the intensity profile the focus of the detection objective was adjusted. A bead was located and line-images were then taken before and after adjustment to observe any effects on the profile. The adjustments were made by maximising the luminescence intensity, and from figure 11 it can be seen that in doing so significant improvements were made. Whilst both profiles have the same central peak of 2μm the improved peak does not suffer from the same distortion at the base; the intensity drops off much faster giving a sharper image. The improved peak still exhibits some broadening and is slightly non-symmetrical this is attributed to bad alignment of either the excitation beam on the sample or of the fluorescence on the detector or both whilst the broadening is thought to be due to scattering within the thick PVA film.

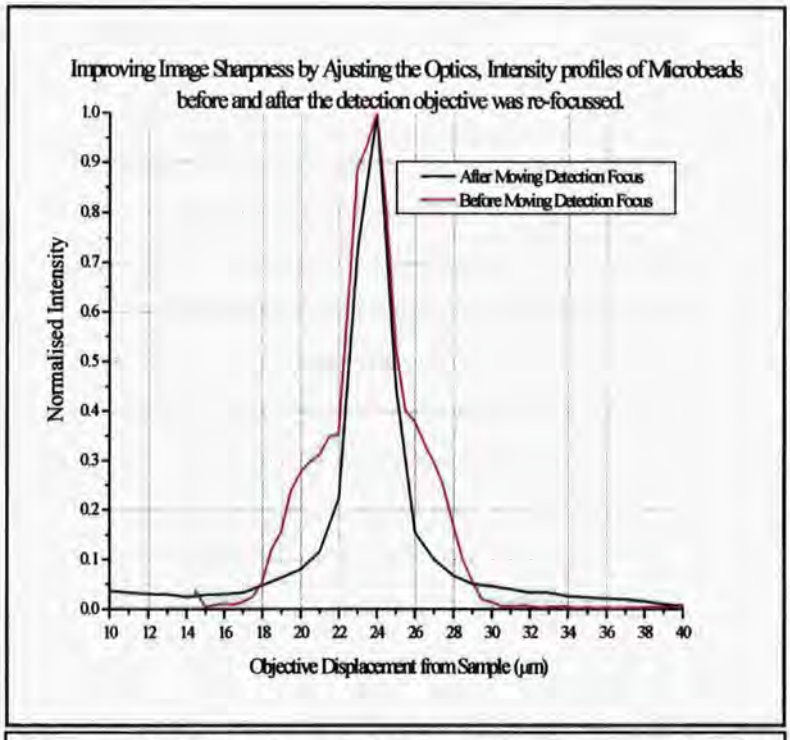

Figure 11: Improving spatial resolution by changing the detection objective. The first profile has a broad base profile which is absent once the detection objective has been improved. After re-focusing, the profile is more symmetrical though there is still a broad faintly emissive tail.

Any method used to measure changes in image sharpness involves a great deal of re-excitation of the same bead (an alteration is made and the bead is re-imaged to observe the effect) making bleaching a problem, for example even with the ND filter in place, the molecule of figure 11 bleached after the experiments displayed were taken. Repetition over the same spot is however an important way of empirically quantifying alignment. Once a bead has bleached it does mean that a new bead must be located with a similar intensity, and then all the processes of centring and

focussing on the bead are conducted afresh. During these processes it is quite likely that the bead will experience a large drop in luminescence even with the ND filter in palace, and a new bead should again be found. This makes quantitatively comparing images a difficult task and at all times it is important to be aware that changes in the image quality will be incurred not only by adjustment of mirrors, lenses and focussing of the detection objective: 'external parameters', but also by variations in the 'internal parameters' of centring and fine focussing when moving between beads.

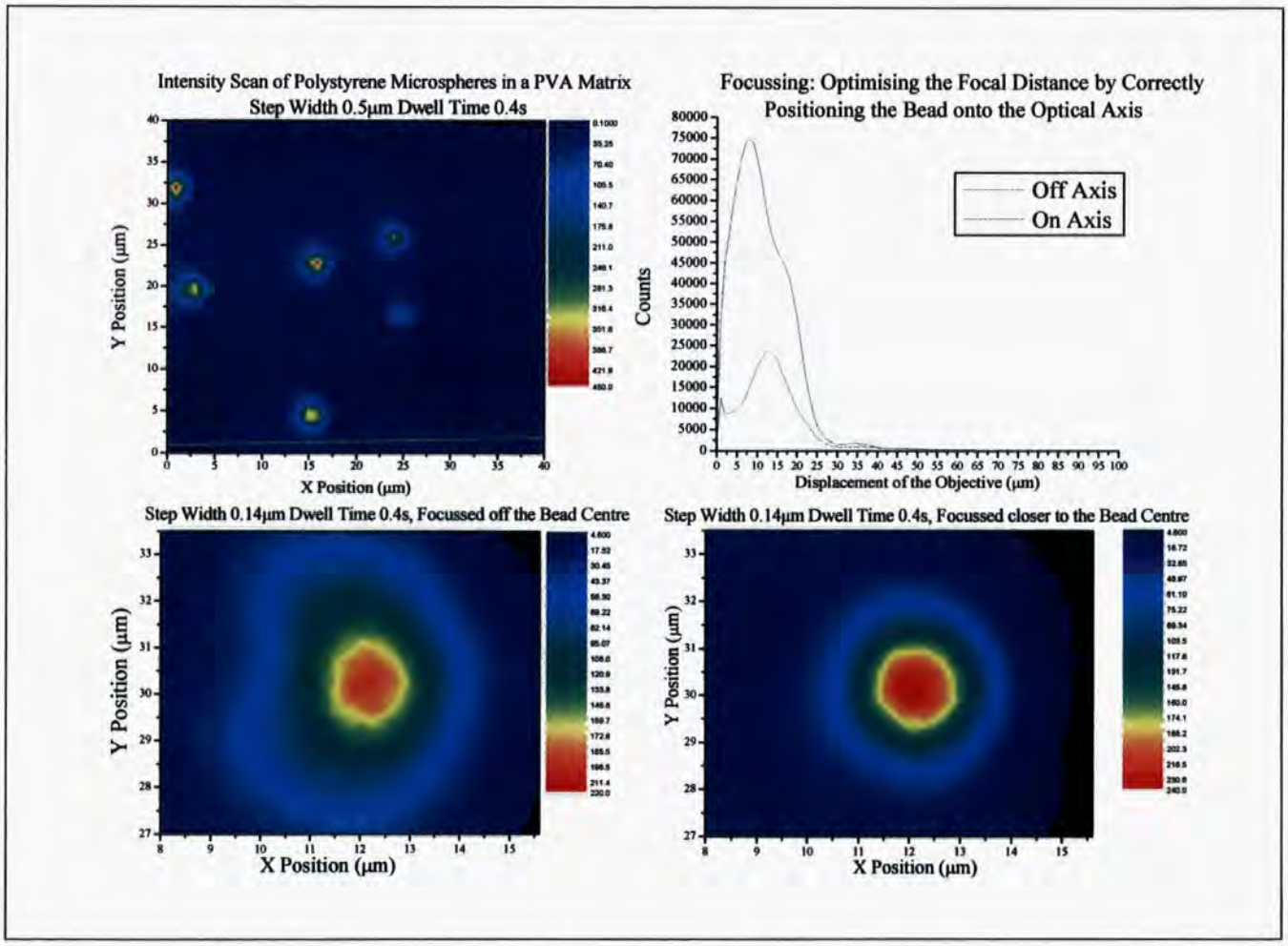

Figure 12: Aligning the bead with the optical axis during focusing. At the correct x-y position during focusing, the intensity is maximized and the image quality is improved. Off-centre focusing causes distortion of the image shape.

7.5.5 Focal Position

It was found that when locating and focussing on a bead, the focal position in the x-y plane is particularly important. Figure 12 shows the progression of images made over a fresh group of microbeads. A rough scan was made to locate the molecules showing a cluster of beads with approximately symmetrical bead images. Though when a bead was singled out and focussed on at high resolution the image was much distorted, displaying a sickle shaped image of the bead. This was initially thought to be a problem of alignment of the optical path; however, since these effects have been largely unseen in previous images an identical scan was taken this time with an adjusted point of focus to sit more precisely on the centre of the bead. The effect of getting the focus on the centre of the bead is evident: in the final scan the profile is vastly improved.

Following adjustments of the optical parts the resolution is considered to be optimised for the current sample of microbeads in PVA. There are still questions over the broadening of the intensity profile greater than the PSF of the excitation point (figure 11) however, it is expected that this broadening is due to wave guiding and scattering of the excitation beam inside the thick host film accompanied by scattering from the back of the quartz disc. To eliminate these effects from the investigation a set of microbeads with the same dye labelling but of 0.5μm diameter have been purchased. Films of fluorescent microspheres have been prepared in the same way as the 2μm beads though the PVA host concentration has been reduced to 1%. The reduced film thickness is hoped to reduce the scattering around the bead seen in previous images. The diameter of the 0.5μm beads is close to the diffraction limit of the experiment and so the ability to image these beads sharply is seen as an important bench-mark.

Figure 13 is an image of the 0.5μm beads in PVA 1%, taken using an optical microscope, here it can be seen that as with the 2μm bead films, a dark perimeter round the bead is still evident. As

expected with the more dilute PVA host, the periphery is less pronounced measuring 1.2μm deep as opposed to ~2μm in the 5% films, though in the optical microscope images the bead itself is in fact only discernable by these dark rings. It is expected that fluorescence imaging will give greater contrast, exciting the beads directly rather than simply using background illumination. The scanning images of the 0.5μm beads are shown in Figure 14

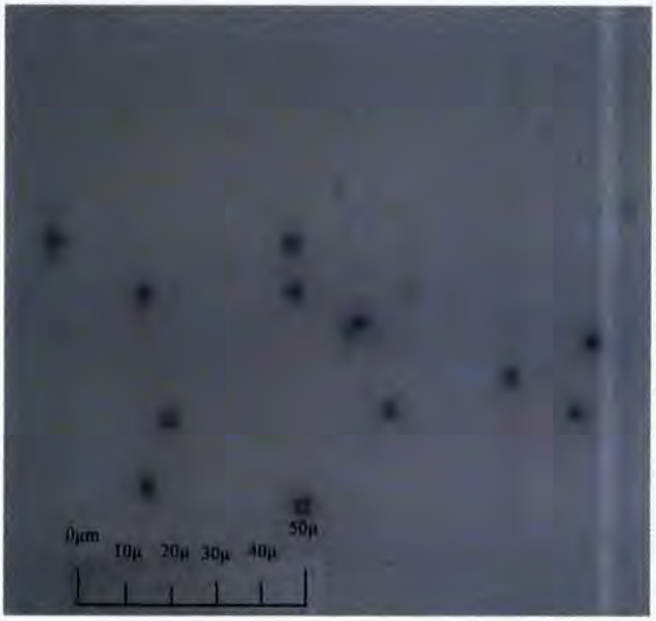

Figure 13: Optical Microscope image of the 0.5μm Fluorescent Microbeads x200 magnification. At this diameter, the bead is almost completely concealed by the dark perimeter. The depth of the ring is however notably smaller than in figure 5. The dark periphery is caused by mismatched refractive indices between the bead and the PVA host. The total object size is ~4μm diameter.

Although a number of adjustments were made to try to further optimise the image quality it was not possible to improve on the image shown in figure 14, which records the beads as before with a surrounding fluorescent ring again attributed to scattering of the excitation beam inside the PVA host, whilst the central diameter measures 0.869μm on average. Accounting for the spread in size caused by the PSF of the excitation beam – 268nm, the maximum acceptable size for this region is 0.768μm.

Clearly something is reducing the resolution of the system; poor focussing and host effects have been eliminated through numerous images taken with different films and focal distances, and given that careful alignment of the optical parts has been rigorously refined using many independent methods, IRF, lifetimes, images…it is not thought to originate here either. The only suggestion that can be put forward for this lack of resolution is that the excitation beam is slightly elliptical rather than perfectly circular and more importantly it is not particularly well defined at the edges; it has an irregular speckled surround of low intensity light. Of course this

will certainly affect the resolution of the confocal PSF, and is very likely to be the cause of the problem since all other aspects have been optimised as far as possible. Although it will be difficult to change the shape of the excitation beam, the hazy area around the edge is more simply eliminated. To do this a 5μm confocal pinhole has been purchased along with two 8cm focal length lenses. These will fit into the experiment as it stands, and by focussing the excitation beam onto the 5μm aperture the blurry area at the edge of the beam should be blocked allowing only the central bright portion through which can then be re-collimated using the second 8cm lens.

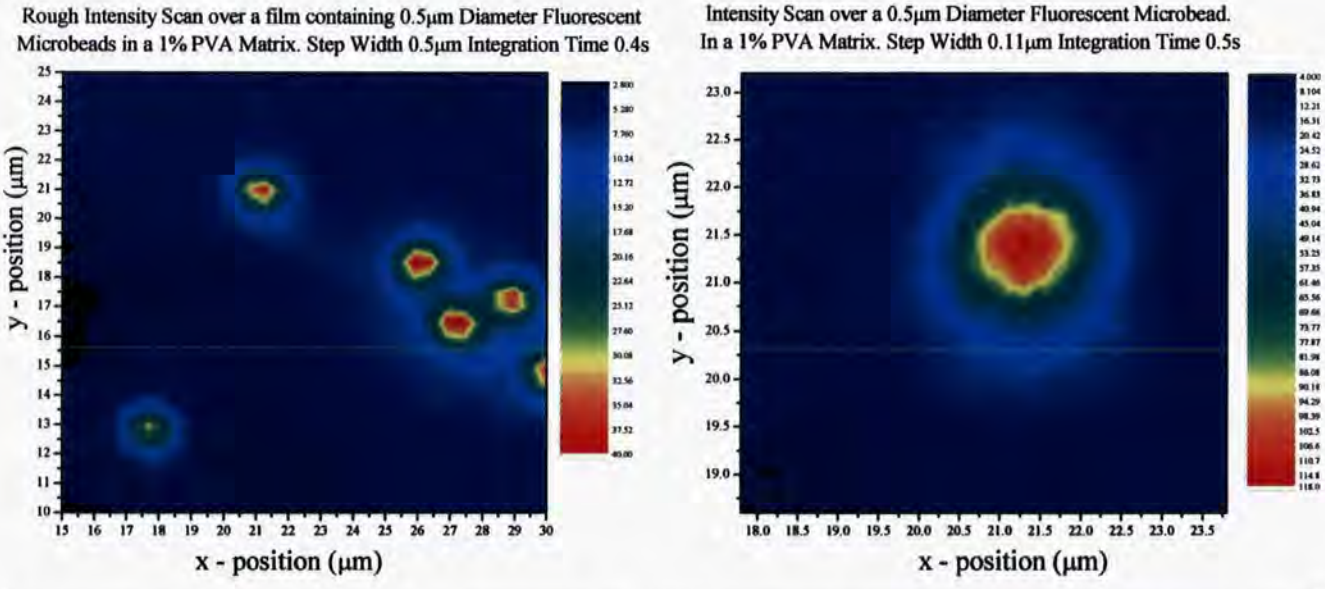

Figure 14: Images taken of 0.5μm diameter fluorescent microspheres. Similar to the 2μm images, an area of weak emission surrounds a bright central spot of fluorescence. Whilst the high resolution image shown on the right is successful as in so far as its symmetrical appearance, the central region is larger than the actual bead diameter, even when the limits of the confocal PSF are considered: d = 0.869μm.

Lack of time has meant that this modification has not been implemented during the course of this work, aligning a focus onto a 5μm spot is not a quick task, though with the use of translation stages to adjust the lenses it is of course possible and should hopefully improve the system resolution considerably. Once this has been implemented a batch of 60nm fluorescent microspheres has been purchased to be used in final resolution adjustments. Their size means

they should be suitably immobilised in very thin PVA films as opposed to the thick matrices required for the 2μm and 0.5μm beads, this should reduce scattering effects considerably and if the system is functioning perfectly they should appear as bright areas limited by the size of the PSF.

7.6 Conclusions

Images taken of fluorescent microbeads dispersed in PVA have been used to consolidate the alignment of the optical system and test imaging capabilities. Following minor adjustments to the detection objective and to the beam path images are now being produced with a high degree of symmetry which is taken as evidence that the experimental alignment is now optimised.

All images of microbeads in PVA are affected by peripheral scattering though this is attributed to the scattering effects of the PVA host on the excitation beam. Beads of 2μm in films of 5% PVA have been imaged producing a profile of 2.3μm at the full width at half maximum. This is in agreement with the actual bead size within the limits of the confocal PSF- 268nm.

Following the successful images of 2μm beads, the position dependant fluorescence intensity of 500nm beads dispersed in PVA was measured. Here because the beads were smaller the thickness of the PVA host was lowered to 1% to reduce excitation scattering within the host. This measure successfully reduced the depth of the peripheral ring from ~2μm to 1.2μm.

Although many attempts have been made to improve the image resolution by adjusting the focus of both the sample and detection objectives and by carefully checking the collimation and alignment, images of 0.5μm beads are consistently larger than the upper limit defined by the resolution of the system of 0.768μm. The reason for this lack of resolution is thought to be due to

the shape of the excitation beam, which is elliptical rather than circular and is poorly defined at the edges. There has not been time to solve this problem during the course of this report, though it is thought that the use of an excitation pinhole will provide significant improvements to image quality. To this effect a 5μm confocal pinhole and two 8cm lenses have been purchased.

Unable to image 500nm beads it is evident that the confocal microscope is as yet not accurate enough for single polymer molecule imaging. Nonetheless, significant progress has been made towards this goal, with the current resolution lying at ~ 600nm. It is thought that the incorporation of the excitation pinhole will give the resolution of the system the final improvements it needs, wherein it will then be possible to spatially discriminate between molecules, and accurately position them for spectroscopic measurements. Many of the initial steps for other spectroscopic measurements have already been made and are described in the appendix, the optical set up for focussing light onto a cooled CCD for wide-field images has already been successfully tested, and a recently repaired monochromator has been incorporated and calibrated along with a cooled CCD to produce time resolved spectra.

The system is though to be very close to producing exciting results, pending the improvement of the resolution and the development of an automated positioning program, spectral measurements of single molecules can then begin almost immediately and work on positioning and perfecting the optics for wide field imaging can be carried out. With these capabilities in place along with the already tested capacity for lifetime measurements the system will certainly be a valuable multifaceted spectroscopic device. It will permit the investigation of phenomena at the forefront of polymer photophysics, allowing this group the exciting prospect of dynamic observation of polymers and other luminescent materials at the ultimate level of the single molecule.

7.7 References

1. NT-MDT and http://www.ntmdt.ru/SPM-Techniques/Basics/3_SOM/3_2_Confocal_Microscopy/text231.html, *Scanning Optical Microscopy*. 1998.
2. http://micro.magnet.fsu.edu/primer/anatomy/numaperture.html, *Microscope Objectives Numerical Aperture and Resolution*. 1998.
3. Müller, M., *Introduction to confocal fluorescence microscopy*. 2006, Washington: SPIE- The International Society of Optical Engineering. 42-49.
4. Hecht, E., *Optics*. Third ed. 1998: Addison Wesley. 694.
5. Wilson, T., *The role of the pinhole in confocal imaging systems.*, in *Handbook of Biological Confocal Microscopy*, J.B. Pawley, Editor. 1995, Plenum Press: New York. p. 167-182.
6. Centonze, V. and J. Pawley, *Tutorial on practical confocal microscopy and the use of the confocal test specimen.*, in *Handbook of Biological Confocal Microscopy.*, J.B. Pawley, Editor. 1995, Plenum Press: New York. p. 549-568.
7. Müller, M., *Digitization*, in *Introduction to confocal fluorescence microscopy*. 2006, SPIE- The International Society of Optical Engineering: Washington. p. 63-69.
8. Bohmer, M., et al., *Time-resolved confocal scanning device for ultrasensitive fluorescence detection.* Review of Scientific Instruments, 2001. **72**(11): p. 4145-4152.

Appendix

Labview Program

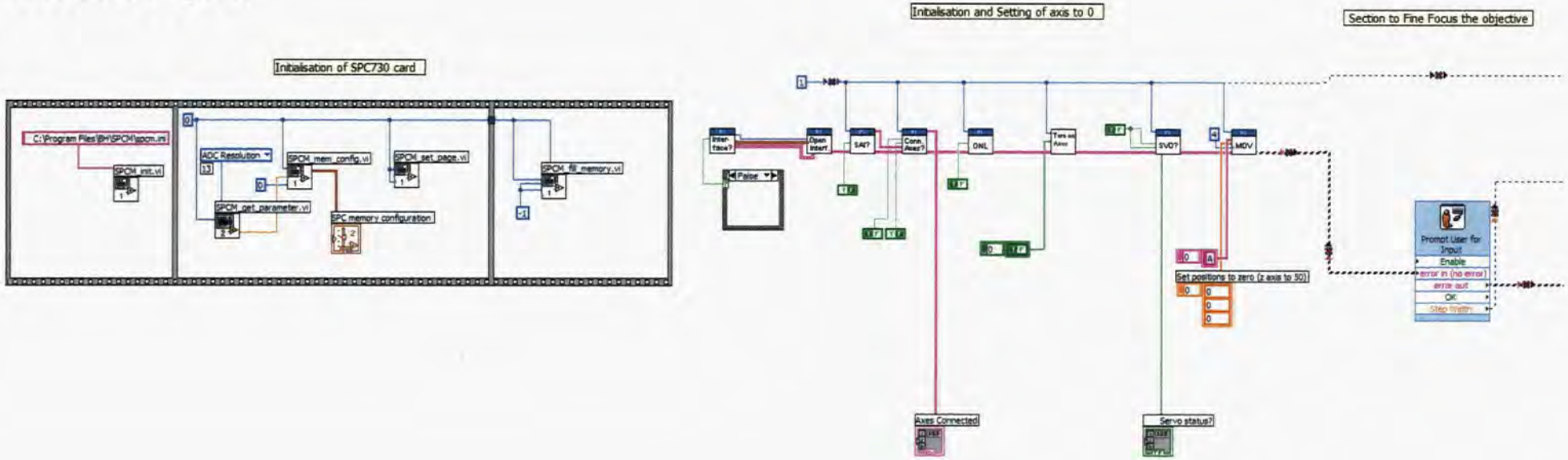

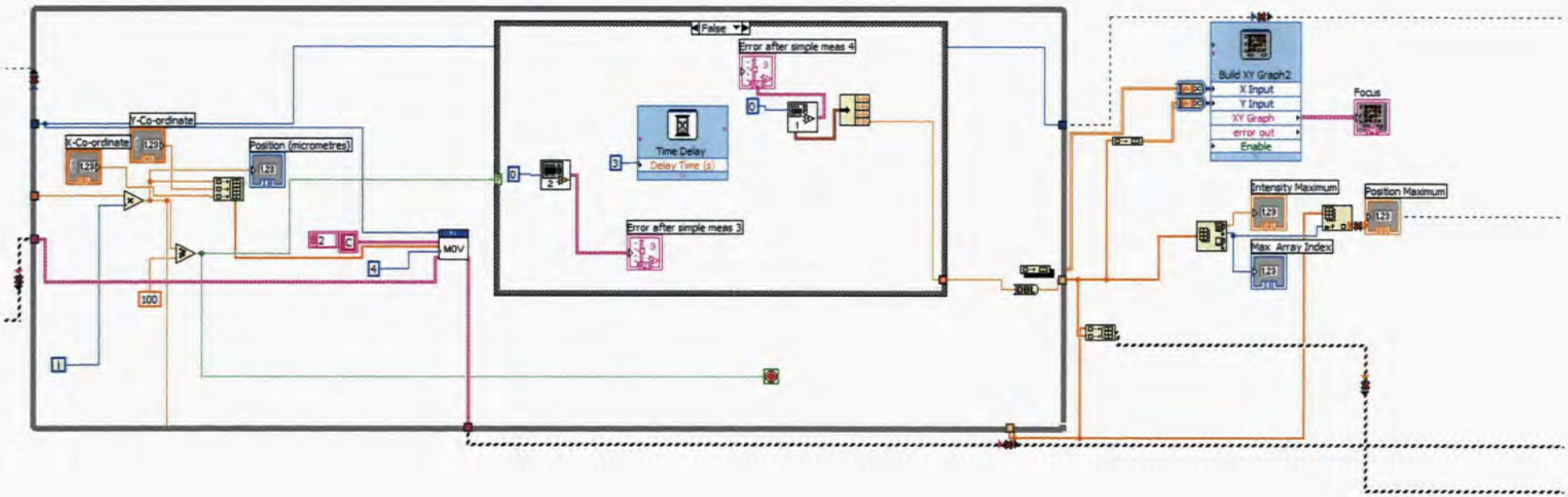
False
Error after simple meas 4
Time Delay
Delay Time (s)
Error after simple meas 3
Y-Co-ordinate
X-Co-ordinate
Position (micrometres)
MOV
100
Build XY Graph2
X Input
Y Input
XY Graph
error out
Enable
Focus
Intensity Maximum
Position Maximum
Max. Array Index

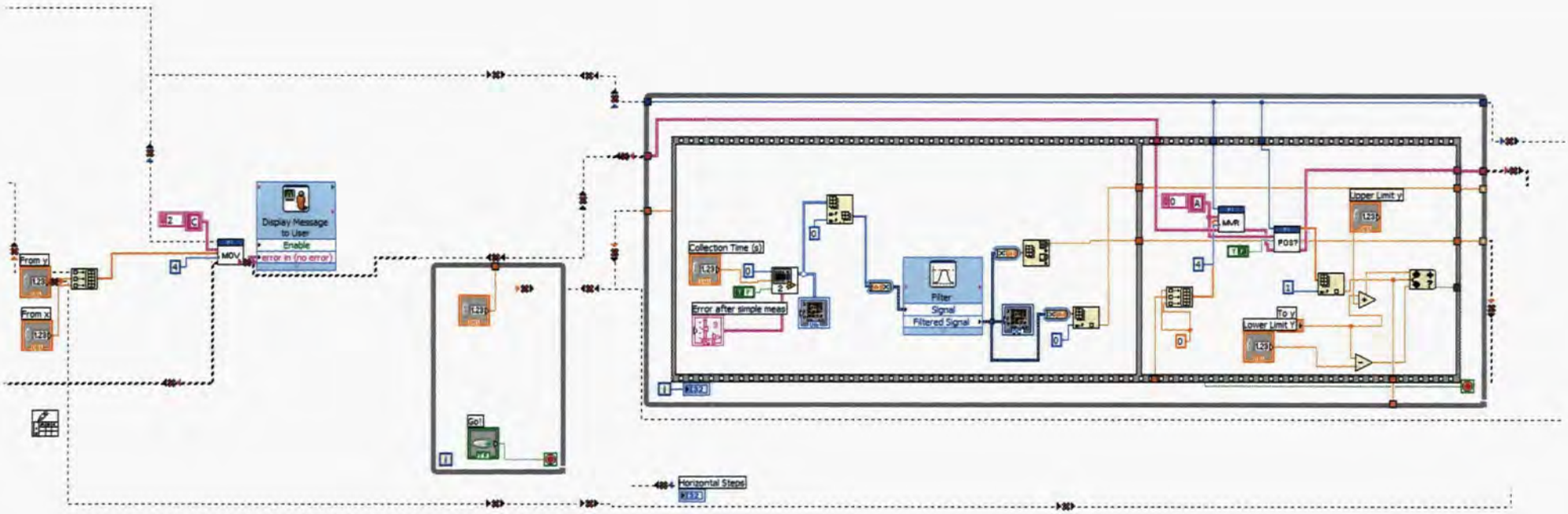
From y
From x
MOV
Display Message to User
Enable
error in (no error)
Go?
Collection Time (s)
Error after simple meas
Filter
Signal
Filtered Signal
MVR
POST
Upper Limit y
To y
Lower Limit Y
Horizontal Steps

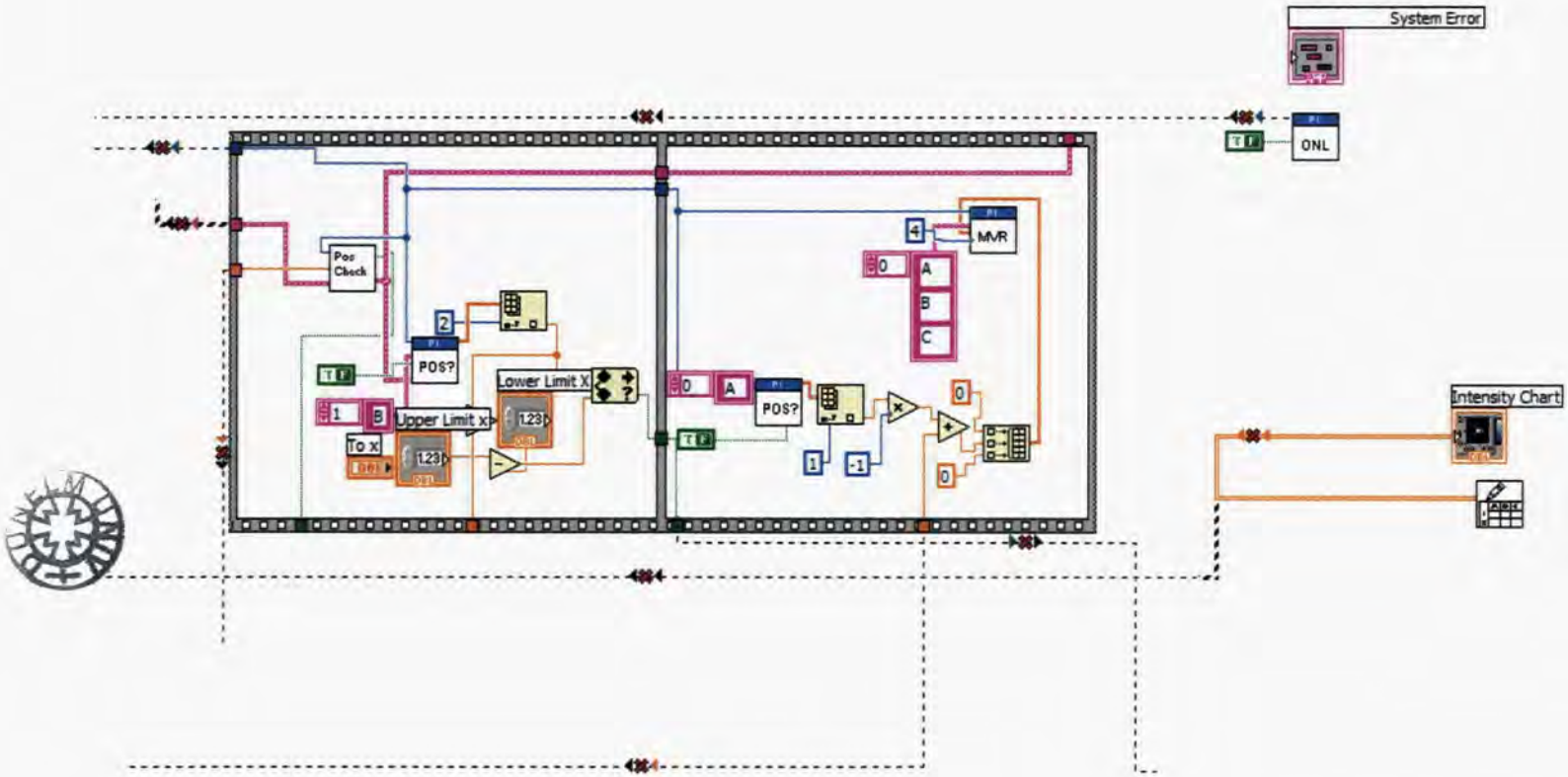

NB. In the images above, some wires appear 'broken', in the *LabVIEW* program, wires are complete, they appear broken here due to the transferal from *LabVIEW* to *Word*.